Investigating Variability in Marine Mollusk Carbonates Using Infrared Spectroscopy and Radiocarbon Analysis

by

©Marisa Dusseault

A Dissertation submitted to the School of Graduate Studies in partial fulfillment of the requirements for the degree of

Master of Science

Department of Physics and Physical Oceanography

Memorial University of Newfoundland

August 2021

St. John's Newfoundland

That I had come perhaps a hundred million years too late did not distress me; it was enough to have come at all.

THE SENTINEL

Abstract

Marine bivalve mollusks are complex hierarchical calcium carbonate ($CaCO_3$) materials that are frequently used in archaeological studies and in chronologies that are used to study marine environment and climate change. Radiocarbon (^{14}C) analysis of these materials is central to most of these studies. I study the variability of ^{14}C signatures within marine bivalve mollusk shells from British Columbia, Canada by considering both the raw, uncalibrated fraction of modern carbon measurements and the calibrated age ranges. I use infrared (IR) spectroscopy as a method to screen for diagenesis - contamination or alteration of the original shell $CaCO_3$ - prior to radiocarbon analysis, and as a method to investigate the natural variability in the composition and structure of the shell $CaCO_3$. Using IR spectroscopy, I show that in three archaeological samples of the butter clam (*Saxidomus gigantea*) from Sechelt, British Columbia, only one shell contained contaminating calcite. However, analysis of the relative IR peak intensities showed a consistent difference between the inner nacreous aragonite layer and the outer crossed lamellar aragonite layer for all three shells. This consistent difference is likely correlated with that natural variability in aragonite microstructures. Three other archaeological shell samples from Deep Bay and Comox, British Columbia, were analyzed for ^{14}C at three different locations within each of the shells. One sample displayed a variation in fraction of modern carbon within the shell while the others did not. I highlight that ^{14}C measurements are meaningless without

an understanding of date calibration and the choices that must be made when calibrating marine and mixed marine-terrestrial samples. My results are a starting point for developing best practices for ^{14}C dating marine shell samples and for more focused studies on the links between crystallinity, diagenesis, and ^{14}C.

Acknowledgements

My supervisor and I respectfully acknowledge the territory in which this research and analysis was conducted as the ancestral homelands of the Beothuk, and the island of Newfoundland as the ancestral homeland of the Mi'kmaq and Beothuk. We would also like to recognize the Inuit of Nunatsiavut and NunatuKavut and the Innu of Nitassinan, and their ancestors, as the original people of Labrador. We strive for respectful relationships with all the peoples of this province as we search for collective healing and true reconciliation and honour this beautiful land together.

We acknowledge that we are working with materials from the traditional territory of the Coast Salish and Shishálh people of British Columbia.

I would like to thank my supervisor, Dr. Kristin Poduska, for endless support, guidance, and knowledge, and Dr. Meghan Burchell in the Department of Archaeology for her insight into the consequences of this work in archaeological settings and her expertise in sclerochronology. The mentorship you both have provided me with is valuable beyond words.

A massive thank you to Carley Crann, Sarah Murseli, Carolyn Dziawa, and the staff at the Lalonde AMS laboratory at the University of Ottawa for their training during my visit in 2018 and for their correspondence afterwards.

Thank you to Bryn Tapper for his help and guidance in producing high-quality maps.

To the Poduska lab group and the Burchell lab group: your community has provided me with endless support and a place to explore new ideas and paths for my research. For this I am so grateful.

Thank you to NSERC and the School of Graduate Studies at Memorial University for their financial support, which allowed me to focus my energy into my research.

To my family, thank you for always encouraging me to be curious and for instilling in me a value for the pursuit of knowledge. To my friends and cohort, thank you for all the laughs and Treats coffee we shared - both early morning and late night. These moments mean the world to me!

Table of Contents

List of Tables

List of Figures

List of Abbreviations and Symbols

AMS	accelerator mass spectrometer
$CaCO_3$	calcium carbonate
Cal BP	calibrated years before present
cm^{-1}	inverse centimeters, energy unit used in IR measurements
DIC	dissolved inorganic carbon
DiSe-7	sample name for shells from the Deep Bay archaeological shell midden
DkSf-20	sample name for shells from the Comox archaeological shell midden
DOC	dissolved organic carbon
F14C	fraction of modern carbon
IR	infrared
IntCal13	2013 atmospheric calibration curve
KBr	potassium bromide
Marine13	2013 marine calibration curve
Ox-II	Oxalic Acid - II
PDB	Pee Dee Belemnite radiocarbon standard
POC	particulate organic carbon
R	global marine reservoir offset
ΔR	local marine reservoir offset

ν_1	IR vibration mode corresponding to the $CaCO_3$ in plane symmetric stretch
ν_2	IR vibration mode corresponding to the $CaCO_3$ out of plane bending
ν_3	IR vibration mode corresponding to the $CaCO_3$ in plane asymmetric stretching
ν_4	IR vibration mode corresponding to the $CaCO_3$ in plane bending
1σ	67 percent probability range
2σ	95.4 percent probability range

Glossary

biomineralization	the biologically driven process of the formation of calcium carbonate and other minerals in the exoskeleton (shell) of mollusks
bivalve mollusks	any species that has a hinged, two-part external covering, such as clams and oysters
β-chitin	the principle component of the organic matrix in bivalve mollusk shells
crossed lamellar	thin, elongated crystals
crystalline domain	a region within a solid that perfect three-dimensional periodicity of its atomic arrangements
diagenesis	any process that alters the shell structure or chemistry after the cessation of shell growth
nacre	thin platelets of crystals
ontogenetic age	age since birth
periostracum	the uppermost portion of the shell that is formed primarily of organics and does not preserve well in archaeological contexts
remineralized	inner portion of the mollusk shell that do not display growth lines
sclerochronology	the study of growth lines, their physical features and chemistry, in hard tissues of animals

Chapter 1

Introduction

Marine bivalve mollusk shells are frequently radiocarbon (^{14}C) dated to determine the ages of coastal archaeological sites and to build coastal chronologies around the world. Apart from archaeology, these materials are also studied across other disciplines including materials science, earth sciences, and biology. Mollusk shells are primarily composed of calcium carbonate ($CaCO_3$) making them a great candidate for ^{14}C dating. However, the complex ^{14}C variation within the shells can cause problems for building confidence in and interpreting ^{14}C dates [1, 2]. One way to build confidence in the ^{14}C measurements is to search for and detect signs of diagenesis, meaning contamination or alteration of the original shell $CaCO_3$. However, this can be challenging because in addition to variation in ^{14}C, these materials may also display natural variations in their degree of 3 dimensional order (crystallinity), crystal structure, and composition of the $CaCO_3$ [3].

The variability in ^{14}C and the structure and composition of the $CaCO_3$ have not previously been studied for the shell of the mollusk species *Saxidomus gigantea*, more commonly known as the butter clam. This species is abundant in shell middens in British Columbia and is frequently studied by archaeologists to determine past

shellfish harvesting practices [4–6]. The confidence that archaeologists and researchers from other disciplines place in ^{14}C measurements depends on the ability to identify all factors that may affect these measurements. There are environmental elements to consider, and there must be a level of trust that the $CaCO_3$ is pristine and free from contamination or post-depositional alteration.

To identify post-depositional alterations that may affect ^{14}C measurements, it is crucial that ^{14}C variation is studied in conjunction with other methods that can help ensure the $CaCO_3$ is pristine: free from $CaCO_3$ not produced by the original growth of the shell. If this is not done, the result can be unexplained intrashell variation which can reduce confidence in the ^{14}C measurements, therefore impacting interpretations of past cultures. Rigorous studies of these intrashell variations are necessary to build confidence in the ^{14}C measurements obtained from *S. gigantea*.

While screening for diagenesis is a common practice, mollusk shell samples are not often the subject of studies that combine considerations of shell growth patterns, detecting diagenesis, and intrashell ^{14}C variability, all of which are crucial for building confidence in calibrated ^{14}C dates from archaeological marine mollusk shells. There are very strong studies that address each of these concerns by themselves, but these studies often lack a more comprehensive discussion of the interplay between these factors, especially in archaeological samples [1,2,7,8]. For example, Guzman et al. [7] use IR spectroscopy to investigate diagenetic changes in the mollusk shell aragonite, but with no discussion on how these concerns may impact or influence ^{14}C measurements. Additionally, the use of IR spectroscopy in the study of marine bivalve mollusk shells has not been as prominent in archaeological studies, particularly those which also emphasize ^{14}C analysis.

On the other hand, studies on intrashell ^{14}C variability are quite abundant. Jones et al. [8] conducts a very insightful theoretical study on intrashell ^{14}C variation com-

bined with growth pattern considerations, but because it is a theoretical study, it lacks the discussion around the effects of diagenesis in intrashell ^{14}C measurements of archaeological shells. Similarly, experimental intrashell ^{14}C studies are not often combined with a rigorous analysis of diagenesis in these samples either [1, 2].

Although studies that center on diagenesis in marine bivalve mollusk shell $CaCO_3$ have been conducted in relation to ^{14}C measurements, these often do not focus on natural (not anthropogenic) forms of diagenesis, nor do they consider the combined effects of diagenesis and intrashell ^{14}C variation. For example Milano et al. [9] study changes in mollusk shell $CaCO_3$ using Raman spectra as the samples are heated in a similar method to that of prehistoric cooking practices. However, studies like that of Milano et al. [9,10] that investigate natural (not due to heating or cooking by humans) diagenetic changes in shell $CaCO_3$, let alone in *S. gigantea* from British Columbia, are sparse.

Here I perform one such rigorous study by analyzing the ^{14}C variation in marine mollusk shells and investigating changes in the structure of the shell $CaCO_3$ using a materials analysis technique, infrared (IR) spectroscopy, that probes the vibrational modes of the mineral. Combining these two types of data will help me to explore which variations in composition and structure of the $CaCO_3$ are important for building confidence in the ^{14}C measurements, and which variations in the ^{14}C measurements are linked to the marine and environment and which are linked to contamination.

What follows in this chapter is the necessary background information on the structure of marine bivalve shells and on the use of infrared spectroscopy and ^{14}C analysis in the study of marine bivalve shells. I conclude this chapter by describing my approach to using these methods to study the shell of the marine bivalve mollusk *Saxidomus gigantea* from British Columbia.

1.1 Shell Structure and Chemistry

In this section, I outline the basics of the structure of the shell of *S. gigantea*, focusing particularly on the portions of the shell that are of interest for our ^{14}C and infrared spectroscopy analysis.

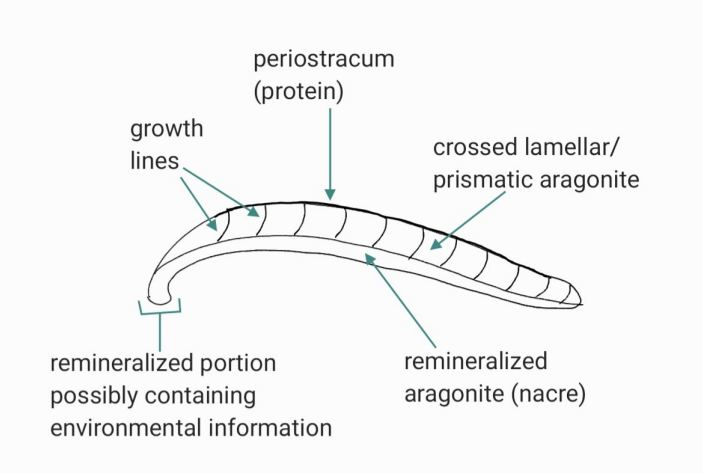

Figure 1.1: Schematic of a cross section of a typical bivalve mollusk. The length of the shell sketched is about 7 cm. The growth lines labelled are present in the crossed lamellar layer and signify the annual winter growth lines that are visible by eye in the shell.

Most marine bivalve shells are composed of $CaCO_3$ in the form of either calcite or aragonite [11–13]. Calcite and aragonite are polymorphs of $CaCO_3$, meaning they have the same chemical formula, but different crystal structures; calcite forms a trigonal lattice while aragonite forms an orthorhombic lattice. Marine bivalves form one or both of these polymorphs by means of a process called biomineralization, where the $CaCO_3$ is deposited by the organism at specific times (i.e. seasons) throughout the mollusks lifetime [14]. Biomineralization is a biologically driven process, controlled by different protein molecules [15].

Biomineralization is an active field of research in itself [16–18]. Many biomineralization studies focus on analyzing the aragonite and calcite microstructures - the

Figure 1.2: Photo of the cross section of *S. gigantea* shells with growth lines visible, the inner remineralized layer (white in colour) is distinct from the crossed lamellar layer (brown in colour). Photo used with permission from Dr. Meghan Burchell. The portions of the shells picture here are 2 mm in length.

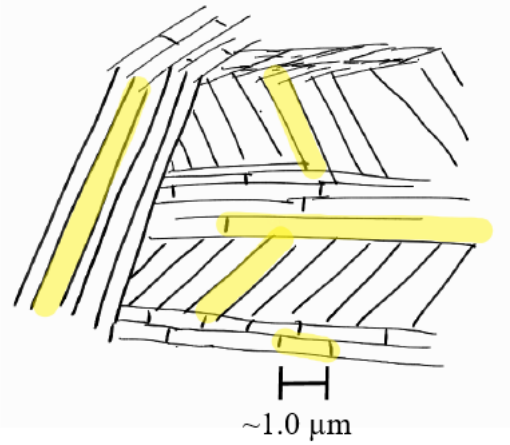

Figure 1.3: Schematic of the crossed lamellar aragonite microstructure. A few lamellae, elongated crystals of aragonite, are indicated with the yellow highlight and are separated by a thin organic matrix which is not visible by eye.

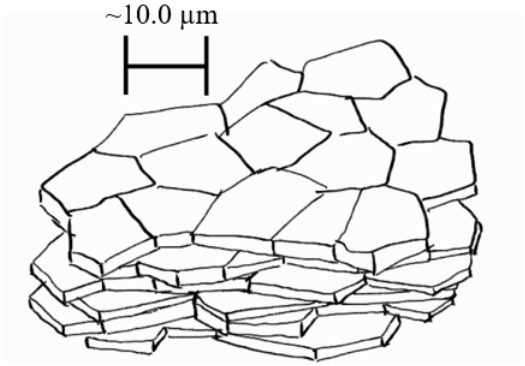

Figure 1.4: Schematic of the nacre microstructure present in the inner layer of *S. gigantea*. The nacre platelets are separated by a thin organic matrix which is not visible by eye.

organization of these crystals on the order of μm - in bivalves and gastropods. Marine bivalves can biomineralize a variety of microstructures and these may vary from species to species. Some of these microstructures include: prismatic, lamellar, nacreous, and foliated to name a few [19]. Studying these microstructures can provide a glimpse into the evolution of the biomineralization process [20,21]. Studies have shown trends in the aragonite microstructures extending all the way back to the Cambrian period [18].

These studies also have consequences for how we understand the effects of environmental conditions on biomineralization processes and the crystallinity and crystal structure of biogenic aragonite and calcite [22, 23]. Both theoretical and experimental studies have contributed to the biomineralization field by investigating lattice distortions of biomineralized aragonite and calcite [23–25]. Crystallinity is particularly insightful to study in biomineralization contexts because amorphous calcium carbonate is known to be a precursor to other ordered phases of calcium carbonate in mollusks and other marine organisms that form aragonite and calcite [26].

Because there is so much variability in the shell structure and types of microstructures formed from species to species, the remainder of this discussion will focus on *S. gigantea* specifically. For the purpose of this work I identify three distinct components of the shell of *S. gigantea*: the inner remineralized layer, the outer crossed lamellar layer, and the periostracum (see Figure 1.1).

The crossed lamellar layer is composed of rod-shaped aragonite crystals (lamellae) with an organic matrix acting like a "glue" that holds the lamellae together (see Figure 1.3) [14, 27]. The growth lines in the crossed lamellar layer are visible by eye and are formed during periods, usually annually, of slowed growth. These growth lines are more rich in organics than the intermittent periods of more rapid growth. By counting the growth lines, it is possible to determine the ontogenetic age (age since birth) of

an individual [4, 6, 28]. The study of the growth lines in the shell of marine bivalves is called sclerochronology. Considering the growth patterns and ontogenetic age of the mollusk becomes valuable when sampling the mollusk shell for ^{14}C in areas that biomineralized at different times as these details are necessary to determine the length of time over which the shell $CaCO_3$ was biomineralized and can thus be useful when considering uncertainties or constraints on the ^{14}C dates.

As the shell of the mollusk grows and biomineralizes subsequent growth layers, the carbon in the $CaCO_3$ of the crossed lamellar layer is derived primarily from dissolved CO_2 in the seawater, referred to as dissolved inorganic carbon (DIC). It is generally accepted that the ^{14}C signal in the crossed lamellar is equal to that of the DIC, and that there is a minimal signal from metabolic carbon - carbon derived from food pathways - in this portion of the shell [29]. In other words, this means that the ^{14}C signal in the crossed lamellar layer is considered to be directly reflective of the mollusk's marine environment at the time of biomineralization.

In the samples of *S. gigantea* used in this thesis work, the inner remineralized layer is also composed of aragonite. However, this inner layer is smooth and does not contain defined growth lines in the same way that the crossed lamellar layer does. The deposition process of the remineralized layer occurs throughout the mollusks lifetime and is the result of the digestive fluids inside the mollusk dissolving and remineralizing the aragonite mineral as a smooth layer of nacre. Nacre is characterized by flat, layered platelets of aragonite (see Figure 1.4), but still has that organic glue that acts as a mortar between the "bricks" of aragonite.

For both microstructures, the crossed lamellar and the nacre, the sketches in Figures 1.3 and 1.4 show the largest possible size of the crystal domains of the aragonite in these microstructures. This does not mean that there cannot be smaller crystal domains within those microstructures, but the separation of the lamellae and the nacre

platelets by the protein matrix restricts the upper limit of crystal domain size.

The uppermost layer of the shell is a protein layer - the periostracum. This layer is present on living samples, but is often not preserved archaeologically.

1.1.1 Details on the Growth and Habitat of *Saxidomus gigantea*

The mollusk that is studied in this thesis work is *Saxidomus gigantea*. *S. gigantea* individuals can live to be 20 or more years old. More details about this species life history are documented in Hiebert et al. [30]. The shell of this mollusk is biomineralized outward from the hinge to the ventral margin. The shell is composed entirely of aragonite, with the inner shell being nacre and the outer shell being crossed lamellar.

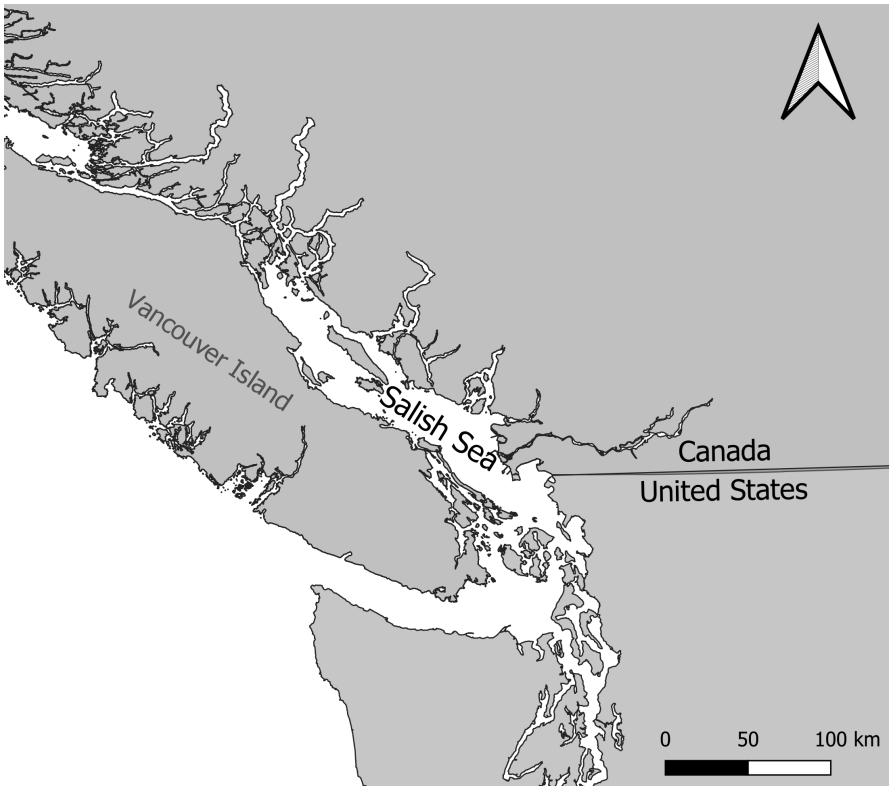

Figure 1.5: Map showing the Salish Sea, British Columbia.

The mollusk *S. gigantea* is found along the west coast of North America, from California to to Alaska. Samples used in this thesis work come from the Salish Sea of British Columbia, shown in Fig. 1.5. This species is typically found in estuaries and sheltered bays that are not exposed directly to the open ocean, which is apparent when considering the region where these samples were collected from (see Figure 1.5) [30]. This is an important consideration for understanding the origins of the carbon incorporated into the shell $CaCO_3$ and how closely the carbon signature of the shell reflects that of the marine carbon signal. While the ^{14}C signal in the crossed lamellar layer is considered directly reflective of the marine environment, because this species lives in estuarine environments it may be relevant to be critical of this assumption.

The organic rich growth lines in the crossed lamellar layer are formed during periods of slow growth in the winter [14]. The growth lines in the crossed lamellar layer of *S. gigantea*, which are visible by eye, as shown in Figure 1.2. The inner remineralized layer of the shell of *S. gigantea* is composed of aragonite in the form of nacre and, as mentioned previously, does not contain growth lines.

1.2 What Can Mollusk Shells Tell Us? - Importance to Palaeoclimatology and Archaeology

Because of the growth lines and environmental signatures in the crossed lamellar layer, mollusk shells are extremely valuable for palaeoclimatology and archaeology studies. I have thus far outlined the mineral structure of mollusks shells and the relevant biological details of the samples studied in this thesis, *S. gigantea*. In this section I will outline why these materials are so valuable and what kind of information we can learn from studying them.

Mollusk shells contain a variety of information relevant to palaeoclimatologists. The $CaCO_3$ in the crossed lamellar portion of the shell acts like a thermometer [31], an archive of oceanographic conditions [32–34], and an environmental monitor [35]. The oxygen isotopes (^{18}O and ^{16}O) and carbon isotopes (both ^{13}C and ^{14}C) are often used to unravel the information encoded in a mollusk shell. The oxygen isotopes are useful for inferring sea surface temperature and salinity at the time that the $CaCO_3$ was biomineralized [36, 37]. The variations in ^{14}C within the environmental layer of a shell can be useful for reconstructing patterns of ocean upwelling - the mixing of deep ^{14}C depleted ocean water with surface water - over time, which is often linked to wider climate events such as El Niño [2, 38]. Sometimes trace elements and clumped isotopes are also studied to more precisely reconstruct seawater conditions [39, 40]. In regions where many long-lived mollusk species are available, chronologies can be constructed using techniques of sclerochronology - the study of the internal growth lines in the shell [32, 33, 41].

While mollusk shells are incredibly useful tools for studying past climates, they also have archaeological significance. Humans across the globe have also harvested mollusks for thousands of years as a food resource, and studies of these harvesting practices can offer insights into human activities over time. Luckily for archaeologists, evidence of mollusk harvesting practices has been preserved in coastal archaeological sites across Canada and across the globe in the form of shell middens, which are large refuse dumps that contain shell remains along with other archaeological remains including both artifacts and fauna [6, 28, 42–44]. Many archaeological studies that use mollusk shells to study the activities and interactions of past humans with their environment will employ techniques of sclerochronology and palaeoclimatology. Although interpretations of oxygen isotopes can be complicated by the competing effects of temperature and salinity, when combined with sclerochronology - analyzing the isotopic

signatures of the oxygen within the growth increments of the shell - it is possible to determine the season in which the growth stopped and the mollusk was harvested [45]. This technique allows researchers to determine if mollusks were harvested only during a certain season and thus it is possible to infer if sites were occupied year round or only seasonally. Of course, archaeology has benefited greatly from the practice of ^{14}C dating shells, because this makes it possible to anchor human-environment interactions in time and build ^{14}C chronologies for coastal archaeological sites.

In both archaeological and palaeoclimate contexts, the confidence in the ^{14}C measurements depends on the ability to account for and identify environmental conditions and contaminants that may affect these measurements. Identifying all of these factors is often a challenge. This has been a concern since the advent of radiocarbon dating itself [46–49]. Any study that uses ^{14}C dates, or any other geochemical measurement, on archaeological marine shell samples relies on the shell material being pristine and unaltered after their deposition in archaeological contexts.

1.3 Why is Radiocarbon Dating Shells Difficult?

^{14}C dating of marine shells is a very useful practice, but one that comes with challenges. Marine samples, and shells in particular, face a unique set of challenges because of two key factors: 1) intrinsic variability in the ^{14}C within the shell $CaCO_3$; and 2) limitations due to sampling.

1.3.1 Sources of Intrinsic Variability

A combination of several factors produces ^{14}C variability in shells. First, marine shells are sensitive to the temporal and spatial variability in the ocean ^{14}C reservoir because throughout the mollusk's lifetime it biomineralizes $CaCO_3$ in equilibrium with

the seawater. This intrinsic ^{14}C variation stems from both variability in the marine environment, growth patterns, and diagenesis - changes in the crystal structure or composition of the shell $CaCO_3$ that occur after deposition into an archaeological context.

Variation in marine ^{14}C reservoir and upwelling

Variations and uneven mixing of the marine ^{14}C reservoir have been known since the 1960's, when ^{14}C analysis first rose to popularity. In the 1961 publication by Dr. Willard Libby [50], he notes that his initial theoretical calculations denoted that the global carbon reservoir has maintained a constant mixing time: a necessary condition for there to be a steady state of ^{14}C production and disintegration and solidified the fundamental assumption of radiocarbon dating [50]. This further implies that the mixing time of the oceans must be constant and be on a shorter timescale than that of the half-life of the carbon-14.

Libby is careful to state that a constant mixing time does not suggest that the ocean is always evenly mixed (now we know in fact that it is not). The ocean tends to dilute the total carbon reservoir because carbon gets dissolved in the ocean in the form of CO_3, HCO_3, and carbonic acid, which prevents it from mixing evenly with the global atmospheric reservoir. This has serious implications for ^{14}C dating marine samples. Ultimately, it means that researchers must consider that the ^{14}C signatures in the oceans are temporally and spatially variable. This factor affects all marine samples analyzed for ^{14}C and plays a role in possible ^{14}C variability within marine shells.

Marine upwelling is a driving factor behind the uneven mixing mentioned above. While factors like temperature and salinity are known to directly affect the oxygen isotopes in marine shells, marine upwelling directly affects the ^{14}C content. When

upwelling occurs and cold, deep, ^{14}C depleted ("old carbon") seawater mixes with the "younger" carbon near the surface, this causes ^{14}C ages at the surface to appear older and thus those of mollusk shell carbonate will appear older as well. It is important to note that upwelling patterns vary locally and may be difficult to distinguish if they are not well documented in the literature.

Other sources of old carbon can also affect the shell ^{14}C signatures. For example, limestone leaching can release old carbon into the local marine environment and shift dates older [49]. Freshwater runoff or brackish water can have similar effects on ^{14}C signals [49].

When calibrating ^{14}C measurements, nearly all of the factors mentioned above can be accounted for by the appropriate choice of marine calibration curve and local marine reservoir correction (ΔR), but this becomes more involved when mollusk shell growth patterns are considered.

Mollusk shell growth patterns

Growth patterns play an essential role in the shell's ^{14}C variability. If variations in upwelling occur during the shell's growth, the result will be a non-uniform ^{14}C profile within the shell. There is a large extent of interspecies variability in growth patterns and mineralogies (see "Illustrated Glossary of the Bivalvia [51]) which can affect the intrashell ^{14}C variability differently. Some species completely stop growing during certain seasons, which can lead the ^{14}C signature in the environmental portion of the shell to display a more complex profile [8]. For example, a species that only grows during the spring will result in the $CaCO_3$ in the shell only incorporating ^{14}C from spring upwelling [8]. Moreover, more long term trends in upwelling can also be reflected in the ^{14}C within the shell of long-live samples [33, 52].

Additionally, each portion of a marine bivalve shell - inner nacreous layer, outer

crossed lamellar layer, proteinaceous periostracum - may have unique ^{14}C signatures because their carbon content is derived from different sources. While the crossed lamellar layer primarily incorporates dissolved inorganic carbon in the seawater, the other portions may incorporate more metabolic carbon, and their signatures may not be representative of the seawater [29, 53].

Diagenesis

Diagenesis is the final factor affecting ^{14}C variability in shells. I mentioned previously that diagenesis is the totality of physical and chemical changes that occur in the shell carbonate material after its death. Many processes can contribute to diagenesis, but in marine shells the most common form of diagenesis is the dissolution of aragonite and its recrystallization as calcite, and on rare occasions, as aragonite [54]. When aragonite is dissolved and recrystallized as calcite (or aragonite), new carbon may be incorporated into the recrystallized $CaCO_3$, and thus the ^{14}C signature that does not reflect the age of the shell. [49, 55]. This process of dissolution and recrystallization is not a reflection of the environment in which the mollusk lived, nor does it reflect the growth patterns of the mollusk. Detecting which changes are due to diagenesis is necessary to prevent ^{14}C or other geochemical data being misinterpreted and leading to erroneous interpretations of palaeoenvironment or archaeological sequences. The detection of diagenesis can be difficult because it requires a substantial amount of previous knowledge about what the chemistry and structure of the mollusk shell material is in natural conditions so that it is possible to identify when it has been altered.

1.3.2 Sampling Limitations in the Study of Marine Shell ^{14}C

I have discussed where the intrinsic variability in ^{14}C within a shell can come from, but studies of marine shell ^{14}C are also limited by sampling strategies.

The requirements of accelerator mass spectrometer (AMS) ^{14}C measurements are the over-arching limiting factor in the case. For an AMS ^{14}C measurement, which is now the standard method for ^{14}C analysis, about 1 mg of sample ($CaCO_3$) is needed [56]. When the goal is to study intrashell ^{14}C variation this creates a challenge.

Let us consider a situation in which we want to analyze the difference between the ^{14}C in the protein matrix in the shell and the $CaCO_3$ in the shell. Only about 1% of the shell is protein, so extracting a protein sample large enough for an AMS measurement would require extracting protein from several shells. This completely eliminates the possibility of investigating intrashell differences in the protein.

If we would like to analyze intrashell differences in the $CaCO_3$, it is not a problem to obtain a few samples of about 1 mg, but to obtain enough material for an AMS measurement, there is no choice but to average over perhaps several years of growth in the shell. Because of limitations on sample amount, these measurements will not be at the resolution of individual growth lines in the crossed lamellar layer. This type of averaging is called time-averaging. In marine shells, this results in ^{14}C variability within each individual growth line being averaged over.

Sampling limitations restrict the ability to efficiently distinguish between different features of the shell, whether that be between the different growth lines in the crossed lamellar layer, or between the proteinaceous portion and the mineral $CaCO_3$ portion. Factor in the cost of obtaining ^{14}C measurements and this may further limit the number of measurements that can be obtained for a single shell.

1.4 Application of Infrared Spectroscopy in the Study of Carbonates - Biogenic and Beyond

Despite all the concerns mentioned above, marine shell ^{14}C is still commonly used in archaeological studies [37, 57, 58]. While some of the factors mentioned above may be beyond the control of the researcher, they should be estimated and quantified whenever possible. A thorough analysis of signs of diagenesis in the shell assists greatly in building confidence in the ^{14}C measurements. Screening for diagenesis - detecting the conversion of aragonite to calcite - before ^{14}C analysis can greatly reduce uncertainty in the ^{14}C measurement. The materials analysis method I use to look for diagenesis and to further complement the ^{14}C analysis is infrared (IR) spectroscopy. This technique has been used extensively in the study of calcium carbonates from all types of origins: geogenic, pyrogenic, and biogenic, and provides insight into the composition, crystal structure, and crystallinity of these samples [54, 59–62].

IR spectroscopy is a materials analysis method that probes the vibrational modes within the sample and provides information on both the short-range local vibrations of the atoms and the long-range lattice modes of the crystal [63]. The peaks that appear in the IR spectra of calcite and aragonite are dependent on the stretching and bending of the carbonate moiety, which is in turn affected by its location relative to the calcium ion. This technique is able to distinguish between the polymorphs of calcium carbonate and can identify more subtle differences in samples of the same polymorph by comparing relative peak intensities. For that reason, this technique shows potential for detecting the forms of diagenesis that may affect my samples: the dissolution of the aragonite and recrystallization as either calcite or aragonite.

It is quite straightforward to distinguish between the polymorphs of $CaCO_3$ using IR spectroscopy. This is valuable because the most common form of diagenesis is that

in which shells that are originally composed of aragonite dissolve and reprecipitate as calcite [54]. The detection of aragonite itself has previously been considered to be evidence of good preservation, especially with fossilized samples [64]. For some species of mollusk, such as abalone, both calcite and aragonite structures are biomineralized in the shell and IR spectroscopy has been used previously to map the interface between these two mineralogies [65].

Diagenetic processes do not always result in a change in polymorph. For example, the dissolution and reprecipitation of $CaCO_3$ can result either in the aragonite being reprecipitated as calcite, although aragonite reprecipitation has been recorded only in rare circumstances [54,66,67]. Other studies suggest that the early stages of diagenesis can be studied by looking at geochemical signatures of the shells [7, 62]. Luckily, IR spectroscopy can detect some of these signatures. For example, as ions are substituted into the calcite lattice in place of Ca^{2+}, the energies of certain vibrational modes will shift [68]. Similar effects are seen in the IR spectrum of aragonite [27]. Analyzing these energy shifts in the vibrational modes has been used as a tool for screening samples for diagenesis and for studying biomineralization processes [54, 64]. Guzman et al. [7] used IR spectroscopy alongside scanning electron microscopy (SEM), atomic force microscopy (AFM), and energy dispersive spectroscopy (EDS) to assess diagenetic alterations to gastropod (snail) shells by analyzing shifts in vibrational modes. A study by Verma et al. [62] used photoacoustic IR spectroscopy and X-ray diffraction (XRD) to investigate undisturbed nacre and nacre powder from the shell of red abalone.

Tracking changes in crystallinity using IR spectroscopy has been a valuable technique in studies of biomineralization and in archaeological contexts. The crystallinity of biogenic samples can provide information on the organism's stage of growth since amorphous $CaCO_3$ is often biomineralized as a precursor to the more ordered phases

of calcite and aragonite [26, 69]. Studies that combine IR spectroscopy with x-ray diffraction have also shown distinct differences in crystallinity among calcites formed by different processes: pyrogenic, biogenic, and geogenic [60, 61, 70–72]. In archaeological contexts, this can be useful for determining whether or not the calcite present in the archaeological record was the result of human activities. Similar results have been shown for aragonite, where biogenic and geogenic aragonites have differences in relative IR peak intensities [3, 64].

There are some intrashell studies that focus on using IR spectroscopy to investigate the variation in the $CaCO_3$ *within* the shell of marine bivalve mollusks [3, 64, 73–75]. While IR spectroscopy has been used as a screening method to determine if samples have been affected by diagenesis and are suitable for ^{14}C analysis, it can also be used as a method for studying the natural variation within the shell $CaCO_3$. I also point out that while there are many studies that utilize IR spectroscopy and other materials analysis methods to study shell, these studies are not often combined with intrashell ^{14}C analyses on samples of the same species and lack discussions surrounding variability in the marine reservoir [3,7,62]. As all these factors - diagenesis, individual variability, and marine reservoir conditions - are relevant for the interpretation, they should be considered together. Both ^{14}C and IR spectroscopy measurements are affected by diagenesis, however variations in these measurements may not always be correlated. The presence of recrystallized calcite does not guarantee a corresponding change in the ^{14}C measurement, and conversely a change in the ^{14}C measurement may not be the result of diagenesis. This is why both IR spectroscopy and ^{14}C analysis are useful for studying the full extent of variability and diagenesis in marine bivalve shell $CaCO_3$.

1.5 Summary: Approach to the Problems Outlined Above

I have outlined that marine bivalve shells are complex materials to study because of their variation in ^{14}C and their variation in $CaCO_3$ microstructures, crystal structures, and crystallinity. In this thesis work, I combine the study of intrashell ^{14}C variability with infrared spectroscopy. I use IR spectroscopy as a tool for detecting possible signatures of diagenesis, which helps build confidence in the ^{14}C measurements. I also use IR spectroscopy to study intrashell variation in the $CaCO_3$ by analyzing the relative IR peak intensities, with the aim of exploring which variations are natural and which may be due to diagenesis.

The *S. gigantea* samples used in this thesis work come from three archaeological sites in the Salish Sea of British Columbia - Deep Bay, Comox, and Sechelt (see Figure 1.6) - which were inhabited by the ancestral people of the Coast Salish and Shishálh peoples of British Columbia. The samples analyzed in this work were obtained from the archaeological collections at the Royal British Columbia Museum. The Salish Sea is an apt region to conduct this study because there are an abundance of shell middens and ^{14}C measurements on this shell material is often incorporated into site chronologies [76, 77].

In this thesis work my approach to studying *S. gigantea* includes exploring the extent of variability in both the IR spectra of the $CaCO_3$, which may be linked to crystallinity, and variation in ^{14}C. However, I approach the ^{14}C data without worrying about interpreting the archaeological significance of the calibrated ^{14}C dates. I use IR spectroscopy, a materials analysis technique that probes the vibrational modes of the $CaCO_3$, both as a method of screening for diagenesis, and as a method to explore natural intrashell variation. I analyze the extent of ^{14}C variability in shells

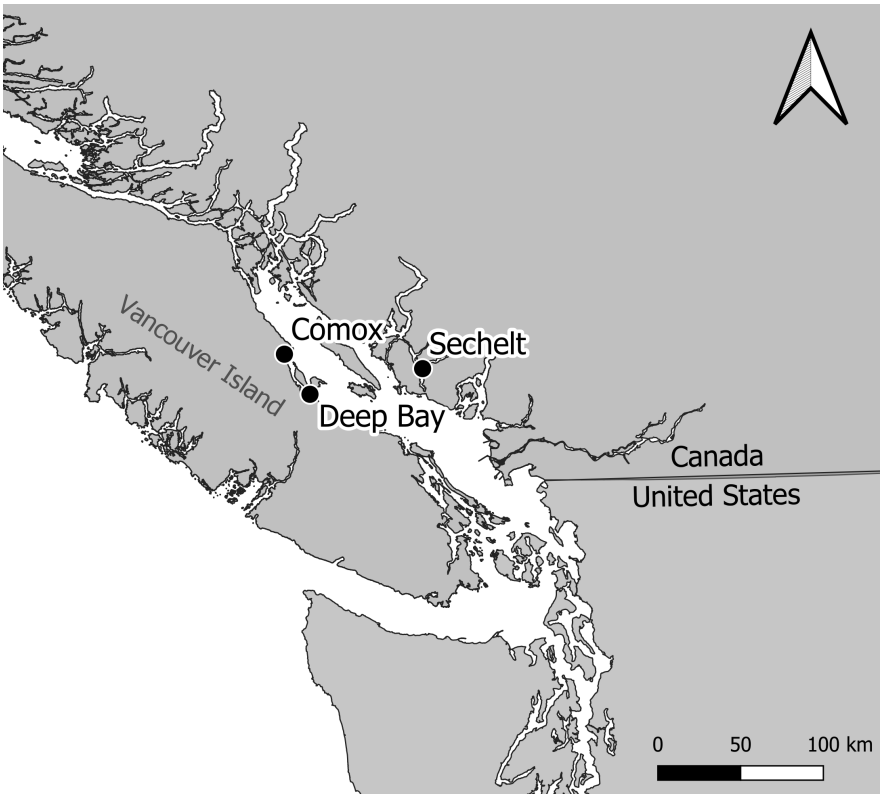

Figure 1.6: Map showing the locations where our samples were obtained. Samples from Comox (DkSf-20 samples) and Deep Bay (DiSe7 samples) are used for radiocarbon dating and samples from Sechelt are used for IR spectroscopy analysis.

of *S. gigantea* from British Columbia, by looking at both uncalibrated and calibrated measurements. Combining these two types of data will help me to explore which variations are significant, which reflect variations in the marine environment, and which may be linked to contamination.

I will answer the following research questions:

1. Is there variability in the $CaCO_3$ that is not linked to diagenesis?

2. What is the extent of ^{14}C variability in the shell of *S. gigantea*?

3. How can the infrared spectroscopy data inform our understanding of ^{14}C variability in marine shells and help build confidence in marine shell ^{14}C used in other disciplines?

The remainder of this thesis is structured as follows. In Chapter 2, I provide background on the IR spectroscopy method and explore the variation in the shell of *S. gigantea* by analyzing IR peak locations, peak shifts, and grinding curves. In Chapter 3, I discuss the theory behind ^{14}C dating and our sampling strategies. In this chapter I also report the results of our ^{14}C analysis, looking at measurements before and after calibration. Chapter 4 delves into the consequences of the IR spectroscopy measurements on interpretations of the ^{14}C data, and the possible links to environmental factors and diagenetic processes. I conclude in Chapter 5 by outlining what researchers can do to build confidence in their shell radiocarbon measurements and provide possible directions for future research.

1.6 Co-authorship Statement

Dr. Kristin Poduska and Dr. Meghan Burchell were instrumental in helping me identify the research questions and for providing expertise in research design. Dr. Poduska assisted greatly in the analysis of the infrared spectroscopy data. Dr. Burchell provided expertise in understanding the basics of the shell structure prior to and during data collection and analysis. I collected the IR data independently, and Dr. Poduska assisted in the data analysis. The preparation of the samples for radiocarbon (^{14}C) analysis was completed by myself, Dr. Burchell, and Anna Sparrow (M.A.) under the supervision and assistance of the laboratory staff at the Lalonde AMS laboratory at the University of Ottawa. The ^{14}C data collection was completed by the laboratory staff at the University of Ottawa. Both Dr. Poduska and Dr. Burchell provided guidance during calibration and interpretation of the ^{14}C measurements.

Bibliography

[1] B. J. Culleton, D. J. Kennett, B. Lynn Ingram, J. M. Erlandson, and J. R. Southon. Intrashell radiocarbon variability in marine mollusks. *Radiocarbon*, 48(3):387–400, 2006.

[2] K. B. Jones, G. W. L. Hodgins, M. F. Etayo-Cadavid, C. F. T. Andrus, and D. H. Sandweiss. Centuries of Marine Radiocarbon Reservoir Age Variation Within Archaeological Mesodesma donacium Shells From Southern Peru. *Radiocarbon*, 52(2):1207–1214, 2010.

[3] M. Suzuki, T. Kogure, S. Weiner, and L. Addadi. Formation of aragonite crystals in the crossed lamellar microstructure of limpet shells. *Crystal Growth and Design*, 11(11):4850–4859, 2011.

[4] N. Hallmann, M. Burchell, B. R. Schöne, G. V. Irvine, and D. Maxwell. High-resolution sclerochronological analysis of the bivalve mollusk Saxidomus gigantea from Alaska and British Columbia: techniques for revealing environmental archives and archaeological seasonality. *Journal of Archaeological Science*, 36(10):2353–2364, 2009.

[5] A. Cannon and M. Burchell. Clam growth-stage profiles as a measure of harvest intensity and resource management on the central coast of British Columbia. *Journal of Archaeological Science*, 36(4):1050–1060, 2009.

[6] M. Burchell, A. Cannon, N. Hallmann, H. P. Schwarcz, and B. R. Schöne. Refining Estimates for the season of shellfish collection on the pacific northwest coast: Applying high-resolution stable oxygen isotope analysis and sclerochronology. *Archaeometry*, 55(2):258–276, 2013.

[7] N. Guzmán, Y. Dauphin, J. P. Cuif, A. Denis, and L. Ortlieb. Diagenetic changes in Concholepas concholepas shells (Gastropoda, Muricidae) in the hyper-arid conditions of Northern Chile - implications for palaeoenvironmental reconstructions. *Biogeosciences*, 6(2):197–207, 2009.

[8] K. B. Jones, G. W. L. Hodgins, C. F. T. Andrus, and M. F. Etayo-Cadavid. Modeling Molluscan Marine Reservoir Ages in a Variable-Upwelling Environment. *Palaios*, 25(2):126–131, 2010.

[9] Stefania Milano, Susanne Lindauer, Amy L Prendergast, Evan A Hill, Chris O Hunt, Graeme Barker, and Bernd R Schöne. Mollusk carbonate thermal behaviour and its implications in understanding prehistoric fire events in shell middens. *Journal of Archaeological Science: Reports*, 20(March):443–457, 2018.

[10] Stefania Milano, Amy L Prendergast, and Bernd R Schöne. Effects of cooking on mollusk shell structure and chemistry: Implications for archeology and paleoenvironmental reconstruction. *Journal of Archaeological Science: Reports*, 7:14–26, 2016.

[11] G. Falini, S. Albeck, S. Weiner, L. Addadi, G. Falini, S. Albeck, S. Weiner, and L. Addadit. Control of Aragonite or Calcite Polymorphism by Mollusk Shell Macromolecules. *Science*, 271(5245):67–69, 1996.

[12] A. G. Checa, C. Jiménez-López, A. Rodríguez-Navarro, and J. P. Machado. Precipitation of aragonite by calcitic bivalves in Mg-enriched marine waters. *Marine Biology*, 150(5):819–827, 2007.

[13] J. B. Thompson, G. T. Paloczi, J. H. Kindt, M. Michenfelder, B. L. Smith, G. Stucky, D. E. Morse, and P. K. Hansma. Direct observation of the transition

from calcite to aragonite growth as induced by abalone shell proteins. *Biophysical Journal*, 79(6):3307–3312, 2000.

[14] H. A. Lowenstam and S. Wiener. *On Biomineralization*. Oxford University Press, New York, 1989.

[15] F. Marin, N. Le Roy, and B. Marie. The Formation and Mineralization of Mollusk Shell. *Frontiers in Bioscience*, 4 S(3):1099–1125, 2012.

[16] I. Almagro, J. H.E. Cartwright, A. G. Checa, E. Macías-Sánchez, and C. I. Sainz-Díaz. Evidence for a liquid-crystal precursor involved in the formation of the crossed-lamellar microstructure of the mollusc shell. *Acta Biomaterialia*, 120(15):12–19, 2021.

[17] M. S. Clark. Molecular mechanisms of biomineralization in marine invertebrates. *Journal of Experimental Biology*, 223(11), 2020.

[18] L. Li, X. Zhang, H. Yun, and G. Li. Complex hierarchical microstructures of Cambrian mollusk Pelagiella: Insight into early biomineralization and evolution. *Scientific Reports*, 7(1):1–11, 2017.

[19] S. M. de Paula and M. Silveira. Studies on molluscan shells: Contributions from microscopic and analytical methods. *Micron*, 40(7):669–690, 2009.

[20] X. Wang, L. Li, Y. Zhu, X. Song, X. Fang, R. Huang, H. Que, and G. Zhang. Aragonite shells are more ancient than calcite ones in bivalves: new evidence based on omics. *Molecular Biology Reports*, 41(11):7067–7071, 2014.

[21] L. Xiang, J. Su, G. Zheng, J. Liang, G. Zhang, H. Wang, L. Xie, and R. Zhang. Patterns of Expression in the Matrix Proteins Responsible for Nucleation and

Growth of Aragonite Crystals in Flat Pearls of Pinctada fucata. *PLoS ONE*, 8(6), 2013.

[22] S. C. Fitzer, S. Torres Gabarda, L. Daly, B. Hughes, M. Dove, W. O'Connor, J. Potts, P. Scanes, and M. Byrne. Coastal acidification impacts on shell mineral structure of bivalve mollusks. *Ecology and Evolution*, 8(17):8973–8984, 2018.

[23] S. Sinha and P. Rez. Distortions of the calcite and aragonite atomic structures from interstitial water. *Materials Chemistry and Physics*, 157:56–62, 2015.

[24] B. Pokroy, J. P. Quintana, E. N. Caspi, A. Berner, and E. Zolotoyabko. Anisotropic lattice distortions in biogenic aragonite. *Nature Materials*, 3(12):900–902, 2004.

[25] B. Pokroy, A. N. Fitch, P. L. Lee, J. P. Quintana, E. N. Caspi, and E. Zolotoyabko. Anisotropic lattice distortions in the mollusk-made aragonite: A widespread phenomenon. *Journal of Structural Biology*, 153(2):145–150, 2006.

[26] S. C. Fitzer, P. Chung, F. Maccherozzi, S. S. Dhesi, N. A. Kamenos, V. R. Phoenix, and M. Cusack. Biomineral shell formation under ocean acidification: A shift from order to chaos. *Scientific Reports*, 6:1–7, 2016.

[27] Y. Dauphin and A. Denis. Structure and composition of the aragonitic crossed lamellar layers in six species of Bivalvia and Gastropoda. *Comparative Biochemistry and Physiology - A Molecular and Integrative Physiology*, 126(3):367–377, 2000.

[28] N. Hallmann, M. Burchell, N. Brewster, A. Martindale, and B. R. Schöne. Holocene climate and seasonality of shell collection at the Dundas Islands Group, northern British Columbia, Canada-A bivalve sclerochronological approach. *Palaeogeography, Palaeoclimatology, Palaeoecology*, 373:163–172, 2013.

[29] T. A. McConnaughey and D. P. Gillikin. Carbon isotopes in mollusk shell carbonates. *Geo-Marine Letters*, 28(5-6):287–299, 2008.

[30] T.C. Hiebert. Saxidomus giganteus. In T. C. Hiebert, B. A. Butler, and A. L. Shanks, editors, *Oregon Estuarine Invertebrates: Rudys' Illustrated Guide to Common Species*. University of Oregon Libraries and Oregon Institute of Marine Biology, Charleston, OR, 3rd edition, 2015.

[31] J. H.E. Cartwright, A. G. Checa, and C. I. Sainz-Díaz. Nacre Is a Liquid-Crystal Thermometer of the Oceans. *ACS Nano*, 14(8):9277–9281, 2020.

[32] P. G. Butler, J. D. Scourse, C. A. Richardson, A. D. Wanamaker, C. L. Bryant, and J. D. Bennell. Continuous marine radiocarbon reservoir calibration and the ^{13}C Suess effect in the Irish Sea: Results from the first multi-centennial shell-based marine master chronology. *Earth and Planetary Science Letters*, 279(3-4):230–241, 2009.

[33] J. Scourse, C. Richardson, G. Forsythe, I. Harris, J. Heinemeier, N. Fraser, K. Briffa, and P. Jones. First cross-matched floating chronology from the marine fossil record: Data from growth lines of the long-lived bivalve mollusc Arctica islandica. *Holocene*, 16(7):967–974, 2006.

[34] M. Álvarez, I. Briz Godino, A. Balbo, and M. Madella. Shell middens as archives of past environments, human dispersal and specialized resource management. *Quaternary International*, 239(1-2):1–7, 2011.

[35] B. R. Schöne, S. D. Houk, A. D. Freyre Castro, J. Fiebig, W. Oschmann, I. Kröncke, W. Dreyer, and F. Gosselck. Daily growth rates in shells of Arctica islandica: Assessing sub-seasonal environmental controls on a long-lived bivalve mollusk. *Palaios*, 20(1):78–92, 2005.

[36] N. Hallmann, B. R. Schöne, G. V. Irvine, M. Burchell, E. D. Cokelet, and M. R. Hilton. an Improved Understanding of the Alaska Coastal Current: the Application of a Bivalve Growth-Temperature Model To Reconstruct Freshwater-Influenced Paleoenvironments. *Palaios*, 26(6):346–363, 2011.

[37] C. F. T. Andrus. Shell midden sclerochronology. *Quaternary Science Reviews*, 30(21-22):2892–2905, 2011.

[38] M. F. Etayo-Cadavid, C. F. T. Andrus, K. B. Jones, G. W. L. Hodgins, D. H. Sandweiss, S. Uceda-Castillo, and J. Quilter. Marine radiocarbon reservoir age variation in Donax obesulus shells from northern Peru: Late Holocene evidence for extended El Niño. *Geology*, 41(5):599–602, 2013.

[39] A. D. Wanamaker and D. P. Gillikin. Strontium, magnesium, and barium incorporation in aragonitic shells of juvenile Arctica islandica: Insights from temperature controlled experiments. *Chemical Geology*, (September 2017):0–1, 2018.

[40] G. A. Henkes, B. H. Passey, A. D. Wanamaker, E. L. Grossman, W. G. Ambrose, and M. L. Carroll. Carbonate clumped isotope compositions of modern marine mollusk and brachiopod shells. *Geochimica et Cosmochimica Acta*, 106:307–325, 2013.

[41] J. D. Scourse, A. D. Wanamaker, C. Weidman, J. Heinemeier, P. J. Reimer, P. G. Butler, R. Witbaard, and C. A. Richardson. The Marine Radiocarbon Bomb Pulse Across the Temperate North Atlantic: A Compilation of Δ14C Time Histories from Arctica Islandica Growth Increments. *Radiocarbon*, 54(2):165–186, 2012.

[42] M. Burchell, M. P. Stopp, A. Cannon, N. Hallmann, and B. R. Schöne. Determining seasonality of mussel collection from an early historic Inuit site, Labrador,

Canada: Comparing thin-sections with high-resolution stable oxygen isotope analysis. *Journal of Archaeological Science: Reports*, 21(2018):1215–1224, 2018.

[43] M. W. Betts, M. Burchell, and B. R. Schöne. An Economic History of the Maritime Woodland Period in Port Joli Harbour, Nova Scotia. *Journal of the North Atlantic*, 1001:18–41, 2017.

[44] Y. Chinique de Armas, U. M. Herrera Gonzalez, W. M. Buhay, J. M. Yero Masdeu, L. M. Viera Sanfiel, M. Burchell, C. Crann, E. R. Grau Gonzalez-Quevedo, and M. Roksandic. Chronology of the Archaeological Site of Playa Del Mango, Rio Cauto, Granma, Cuba. *Radiocarbon*, 62(5):1–16, 2020.

[45] Bernd R. Schöne. The curse of physiology - challenges and opportunities in the interpretation of geochemical data from mollusk shells. *Geo-Marine Letters*, 28(5-6):269–285, 2008.

[46] R. Berger, A. G. Horney, and W. F. Libby. Radiocarbon Dating of Bone and Shell from Their Organic Components. *Science*, 144(3621):999–1001, 1964.

[47] M. L. Keith and G. M. Anderson. Radiocarbon Dating: Fictitious Results with Mollusk Shells. *Science*, 141(3581):634–637, 1963.

[48] R. Berger, R. E. Taylor, and W. F. Libby. Radiocarbon content of marine shells from the California and Mexican West coast. *Science*, 153(3738):864–866, 1966.

[49] K. Douka, T. F. G. Higham, and R.E.M. Hedges. Radiocarbon dating of shell carbonates: old problems and new solutions. *Munibe*, 31:18–27, 2010.

[50] W. F. Libby. Radiocarbon Dating. *Science*, 133(3453):621–629, 1961.

[51] J. G. Carter, P. Harries, N. Malchus, A. Sartori, L. Anderson, R. Bieler, A. Bogan, E. Coan, J. Cope, S. Cragg, J. Garcia-March, J. Hylleberg, P. Kelley,

K. Kleemann, J. Kriz, C. McRoberts, P. Mikkelsen, Jr. J. Pojeta, P. W. Skelton, I. Temkin, T. Yancey, and A. Zieritz. Illustrated Glossary of the Bivalvia. In *Treatise Online, Number 48*, chapter 31. The University of Kansas Paleontological Institute, Lawrence, Kansas, 2012.

[52] A. D. Wanamaker, J. Heinemeier, J. D. Scourse, C. A. Richardson, P. G. Butler, J. Eiríksson, and K. L. Knudsen. Very long lived mollusks confirm 17th century AD tephra based radiocarbon reservoir ages for north Icelandic shelf waters. *Radiocarbon*, 50(3):399–412, 2008.

[53] R. Fernandes, S. Bergemann, S. Hartz, P. M. Grootes, F. Melzner, A. Rakowski, and M. Hüls. Mussels with Meat: Bivalve Tissue-Shell Radiocarbon Age Differences and Archaeological Implications. *Radiocarbon*, 54(3–4):953–965, 2012.

[54] S. Weiner. *Microarchaeology: Beyond the Visible Archaeological Record*. Cambridge University Press, New York, 2010.

[55] G. Magnani, P. Bartolomei, F. Cavulli, M. Esposito, E. C. Marino, M. Neri, A. Rizzo, S. Scaruffi, and M. Tosi. U-series and radiocarbon dates on mollusc shells from the uppermost layer of the archaeological site of KHB-1, Ra's al Khabbah, Oman. *Journal of Archaeological Science*, 34(5):749–755, 2007.

[56] C. A. Crann, S. Murseli, G. St-Jean, Z. Xiaolei, C. D. Ian, and W. E. Kieser. First status report on radiocarbon sample preparation techniques at the A. E. Lalonde AMS Laboratory (Ottawa, Canada). *Radiocarbon*, 59(3):16–20, 2017.

[57] S. Helama and B. C. Hood. Stone Age midden deposition assessed by bivalve sclerochronology and radiocarbon wiggle-matching of Arctica islandica shell increments. *Journal of Archaeological Science*, 38(2):452–460, 2011.

[58] A. Zazzo, O. Munoz, E. Badel, I. Béguier, F. Genchi, and L. G. Marcucci. A revised radiocarbon chronology of the aceramic shell midden of Ra's Al-Hamra 6 (Muscat, Sultanate Of Oman): Implication for occupational sequence, marine reservoir age, and human mobility. *Radiocarbon*, 58(2):383–395, 2016.

[59] B. Xu and K. M. Poduska. Linking crystal structure with temperature-sensitive vibrational modes in calcium carbonate minerals. *Physical Chemistry Chemical Physics*, 16(33):17634–17639, 2014.

[60] K. M. Poduska, L. Regev, E. Boaretto, L. Addadi, S. Weiner, L. Kronik, and S. Curtarolo. Decoupling local disorder and optical effects in infrared spectra: Differentiating between calcites with different origins. *Advanced Materials*, 23(4):550–554, 2011.

[61] L. Regev, K. M. Poduska, L. Addadi, S. Weiner, and E. Boaretto. Distinguishing between calcites formed by different mechanisms using infrared spectrometry: Archaeological applications. *Journal of Archaeological Science*, 37(12):3022–3029, 2010.

[62] D. Verma, K. Katti, and D. Katti. Photoacoustic FTIR spectroscopic study of undisturbed nacre from red abalone. *Spectrochimica Acta - Part A: Molecular and Biomolecular Spectroscopy*, 64(4):1051–1057, 2006.

[63] S. S. Mitra. Infrared and Raman Spectra Due to Lattice Vibrations. In Mitra S.S. Nudelman S., editor, *Optical Properties of Solids*, pages 333–451. Springer, Boston, MA, 1969.

[64] M. B. Toffolo. The significance of aragonite in the interpretation of the microscopic archaeological record. *Geoarchaeology*, 36(1):149–169, 2020.

[65] Y. Dauphin, J.-P. Cuif, H. Castillo-Michel, C. Chevallard, B. Farre, and A. Meibom. Unusual Micrometric Calcite–Aragonite Interface in the Abalone Shell Haliotis (Mollusca, Gastropoda). *Microscopy and Microanalysis*, 20(01):276–284, 2014.

[66] G. E. Webb, G. J. Price, L. D. Nothdurft, L. Deer, and L. Rintoul. Crytic meteoric diagenesis in freshwater bivalves: Implications for radiocarbon dating. *Geology*, 35(9):803–806, 2007.

[67] R. Enmar, M. Stein, M. Bar-Matthews, E. Sass, A. Katz, and B. Lazar. Diagenesis in live corals from the Gulf of Aqaba. I. The effect on paleo-oceanography tracers. *Geochimica et Cosmochimica Acta*, 64(18):3123–3132, 2000.

[68] W. B. White. Chapter 12: The carbonate minerals. In *The Infrared Spectra of Minerals*, pages 227–284. Mineralogical Society of Great Britain and Ireland, 1974.

[69] E. Beniash, J. Aizenberg, L. Addadi, and S. Weiner. Amorphous calcium carbonate transforms into calcite during sea urchin larval spicule growth. *Proceedings of the Royal Society B: Biological Sciences*, 264(1380):461–465, 1997.

[70] B. Xu, M. B. Toffolo, L. Regev, E. Boaretto, and K. M. Poduska. Structural differences in archaeologically relevant calcite. *Analytical Methods*, 7(21):9304–9309, 2015.

[71] V. Chu, L. Regev, S. Weiner, and E. Boaretto. Differentiating between anthropogenic calcite in plaster, ash and natural calcite using infrared spectroscopy: implications in archaeology. *Journal of Archaeological Science*, 35(4):905–911, 2008.

[72] M. B. Toffolo, L. Regev, E. Mintz, K. M. Poduska, R. Shahack-Gross, C. Berthold, C. E. Miller, and E. Boaretto. Accurate Radiocarbon Dating of Archaeological Ash Using Pyrogenic Aragonite. *Radiocarbon*, 59(1):231–249, 2017.

[73] M. Suzuki, K. Kubota, R. Nishimura, L. Negishi, K. Komatsu, H. Kagi, K. Rehav, S. Cohen, and S. Weiner. A unique methionine-rich protein–aragonite crystal complex: Structure and mechanical functions of the Pinctada fucata bivalve hinge ligament. *Acta Biomaterialia*, 100:1–9, 2019.

[74] M. Dusseault. Limits and Potential of FTIR Analysis in Archaeology. Bachelor's honours thesis, Memorial University of Newfoundland, 2019.

[75] M. B. Toffolo, G. Ricci, L. Caneve, and I. Kaplan-Ashiri. Luminescence reveals variations in local structural order of calcium carbonate polymorphs formed by different mechanisms. *Scientific Reports*, 9(1):1–15, 2019.

[76] R. Carlson, P. Szpak, and M. Richards. The Pender Canal Site and the Beginnings of the Northwest Coast Cultural System. *Canadian Journal of Archaeology*, 41(1):1–29, 2017.

[77] A. Martindale, G. T. Cook, I. Mckechnie, K. Edinborough, I. Hutchinson, M. Eldridge, K. Supernant, and K. M. Ames. Estimating marine reservoir effects in archaeological chronologies: Comparing Δr calculations in Prince Rupert harbour, British Columbia, Canada. *American Antiquity*, 83(4), 2018.

Chapter 2

Infrared Spectroscopy

This chapter will outline my use of infrared (IR) spectroscopy as a screening method to ensure samples are pristine prior to ^{14}C analysis. It also outlines my use of IR spectroscopy to study other variations in the marine shell $CaCO_3$ by comparing relative IR peak intensities. I outline the background and theory behind infrared spectroscopy and I describe my experimental methods. Lastly, I look at the data in two different ways: 1) to determine if the samples are contaminated and thus if the samples are suitable for ^{14}C analysis, and 2) to study changes in relative peak intensities, the causes of which are not entirely known. I will explore the following questions: 1) What does it mean for a sample to be pristine? 2) How can we detect diagenesis using IR spectroscopy? 3) What other types of variation in the marine shell $CaCO_3$ are detectable by IR spectroscopy?

2.1 Authorship Statement

All IR spectroscopy data was collected and analyzed by me at Memorial University of Newfoundland with some assistance from Dr. Kristin Poduska. I wrote a Python script that was used to construct the IR spectroscopy grinding curves, building off of

previous foundational work done by previous members of the Poduska research group: Dr. Ben Xu and Dr. Michael Grudich.

2.2 Background & Theory

Every material has a unique vibrational signature, and even atoms in solids are constantly in motion under thermal vibration. In the case of calcium carbonate ($CaCO_3$), the bending and stretching of the carbonate moiety, CO_3^{2-}, can be probed and the characteristic frequency of these vibrational modes measured by the frequencies of infrared radiation which are absorbed by, and cause vibrations in the material. These vibrational mode energies are affected by the local environment of the CO_3^{2-} moiety in the $CaCO_3$ lattice, resulting in different vibrational mode energies for different lattice arrangements of the $CaCO_3$. Identifying these differences in vibrational mode energies through the use of IR spectroscopy is useful in the study of mollusk shells because it makes it possible to distinguish between calcite and aragonite. This distinction allows for the detection of recrystallized calcite in our samples.

2.2.1 The Interferometer

IR spectrometers utilize a Michelson interferometer, a device that splits a light source (in this case an infrared beam) into two different beam paths, one that reflects back from a fixed mirror and one that reflects back from a scanning mirror that is free to move back and forth. Because of the difference in path length between the two beam paths, when the beams combine once again at the beam splitter, they will interfere either constructively or destructively depending on the path difference. The interference of the two infrared beams with one another results in a wider range of frequencies being produced, in this case those in the mid-infrared region, than that

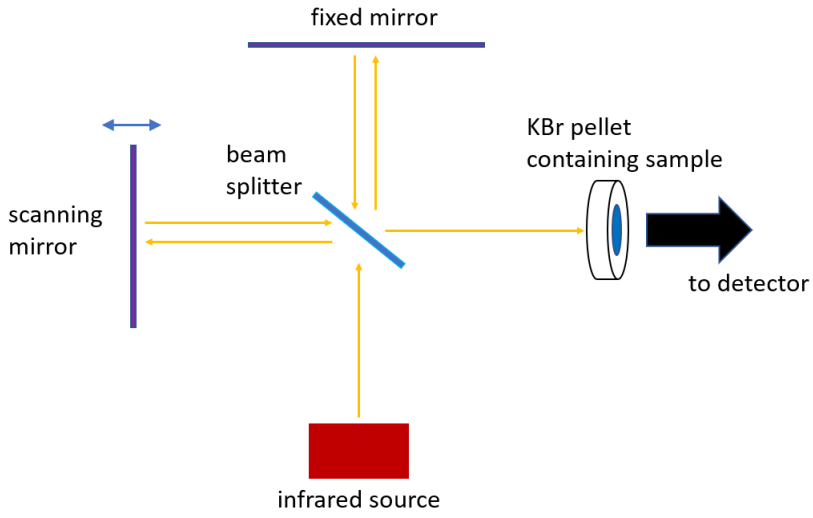

Figure 2.1: Schematic diagram of the interferometer used in the transmission IR measurements.

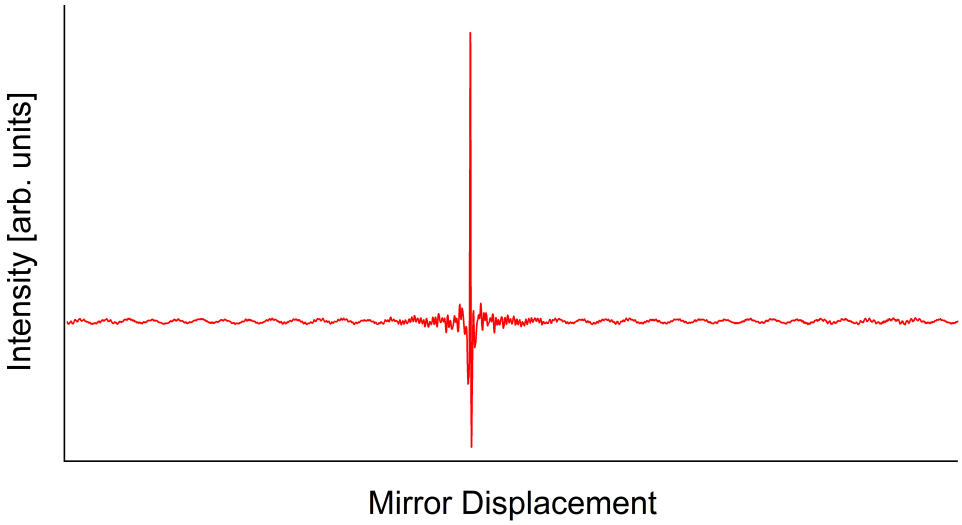

Figure 2.2: Interferogram containing all the relevant spectral information.

of a single infrared beam. The use of the interferometer allows the researcher to analyze the interaction of the sample with a range of different frequencies of infrared radiation rather than a single frequency. A schematic of the Michelson interferometer is shown in Figure 2.1. This beam then passes through the sample and heads toward the detector which records the signal as an interferogram.

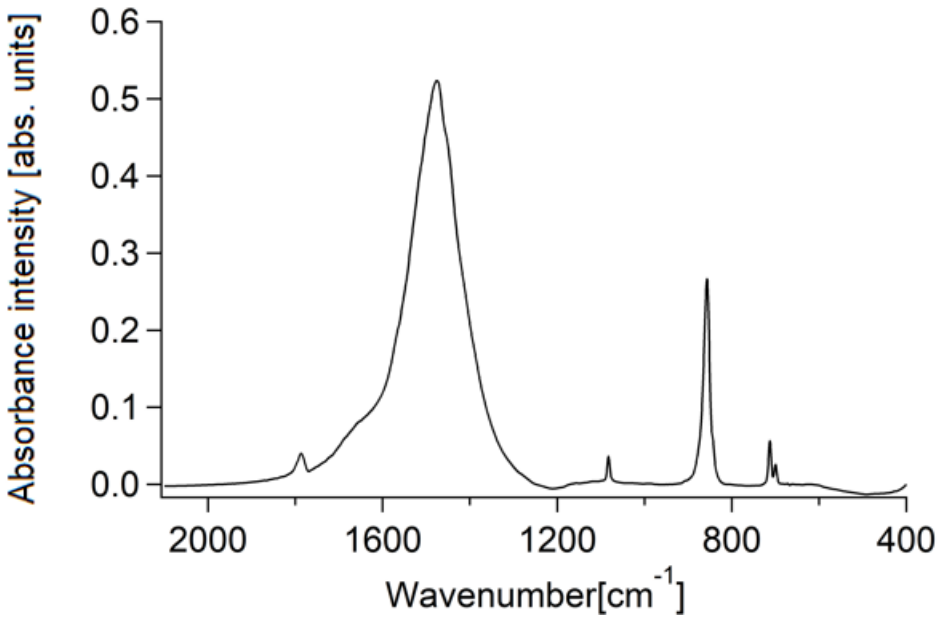

Figure 2.3: Transmission IR spectrum of aragonite obtained from applying a Fourier transform to the interferogram in Figure 2.2. Here the absorbance intensity is measured in absolute units.

The interferogram is the result of these interference patterns, and an example is shown in Figure 2.2. The interferogram records the intensity of the transmitted radiation as a function of the displacement of the moving mirror. The information on which frequencies of the infrared radiation were absorbed or transmitted by the material is contained within the interferogram, it only needs to be altered mathematically by means of a Fourier transform to convert the intensity as a function of mirror position (the interferogram) to the intensity of the transmitted IR beam as a function of frequency, which is shown in Figure 2.3.

2.2.2 Understanding Peak Positions and Intensities

The mass-spring model of a solid can be used as a starting point for understanding how changes in crystal structure affect IR spectra, even though this model lacks the consideration of long-range interactions between the atoms in the solid which are important in IR spectroscopy. Considering solids as a system of masses and springs, changing the separation between masses, and changing the masses themselves will affect the frequencies of the characteristic vibrational modes (the positions of the peaks in the spectra). It is possible to calculate the vibration frequency for a simple mass-spring system using the following equation

$$\omega = \sqrt{\frac{k}{\mu}}, \tag{2.1}$$

where ω is the frequency, k is the spring constant, and μ is the reduced mass which depends on the mass of both interacting atoms. By looking at this equation, it is obvious that changing the mass will affect the frequency. For a simple mass-spring system, the spring constant, k, also affects the frequency; k effectively represents the strength of the interactions between the masses. In IR spectroscopy, the strength of these interactions, as described by k in Equation 2.1, are analogous to the dipole moments of the interactions between atoms, since only those vibrational modes that have a change in dipole moment when they undergo stretching and bending due to the IR radiation will have peaks in the IR spectra

Changes in crystal structure and ionic substitutions can both affect the effective spring constant in Equation 2.1 by which the atoms in the solid will interact, which results in changes in the frequency of the vibrational modes. For the case of $CaCO_3$, the IR signatures of the different polymorphs are well known and can often be distinguished based on their vibrational mode frequencies [1]. The same goes for the ionic

substitutions of the cations into these lattices [1]. Note that with ionic substitutions and polymorph changes that while some peaks may shift, some may not, and new peaks may also appear. The effect that these changes in the material have on the IR spectra depends on the environment in which the CO_3 exists in the solid. The use of the simple mass-spring model ends there, as it cannot explain why or how changes in crystallinity (the periodic nature of the solid [2]), unit cell dimensions, or microstrain fluctuations in the lattice will affect the IR peak intensities or widths.

The factors mentioned above (ionic substitutions and changes in crystal structure and changes in crystallinity) may also affect the peak intensities because they change the environment in which the CO_3 vibrates, but there is currently no theoretical model that can effectively predict IR peak intensities. Additionally, the size of the particles in the sample powder being analyzed and scattering effects also play a role in IR peak widths and intensities [3–5]. Larger particle sizes will increase scattering, which in turn will cause a broadening of the peaks. Simultaneously, finer ground particles result in larger surface area and are thus able to absorb more radiation which will result in larger peak intensities [4, 5].

This does not mean that studying the peak intensities is useless. Looking at relative IR peak intensities can and does tell the researcher when something is different about two different samples, even if it is unable to distinguish exactly what that difference is.

It is then useful and necessary to consider the above factors together (IR peak positions, peak widths, and peak intensities) as it is not possible to untangle them all completely using IR spectroscopy alone. It is particularly useful to detect known factors first, such as the incorporation of Mg into the calcite lattice which results in a known peak shift, or the detection of a calcite-aragonite mixture [1].

Assignment of peaks in $CaCO_3$ spectra

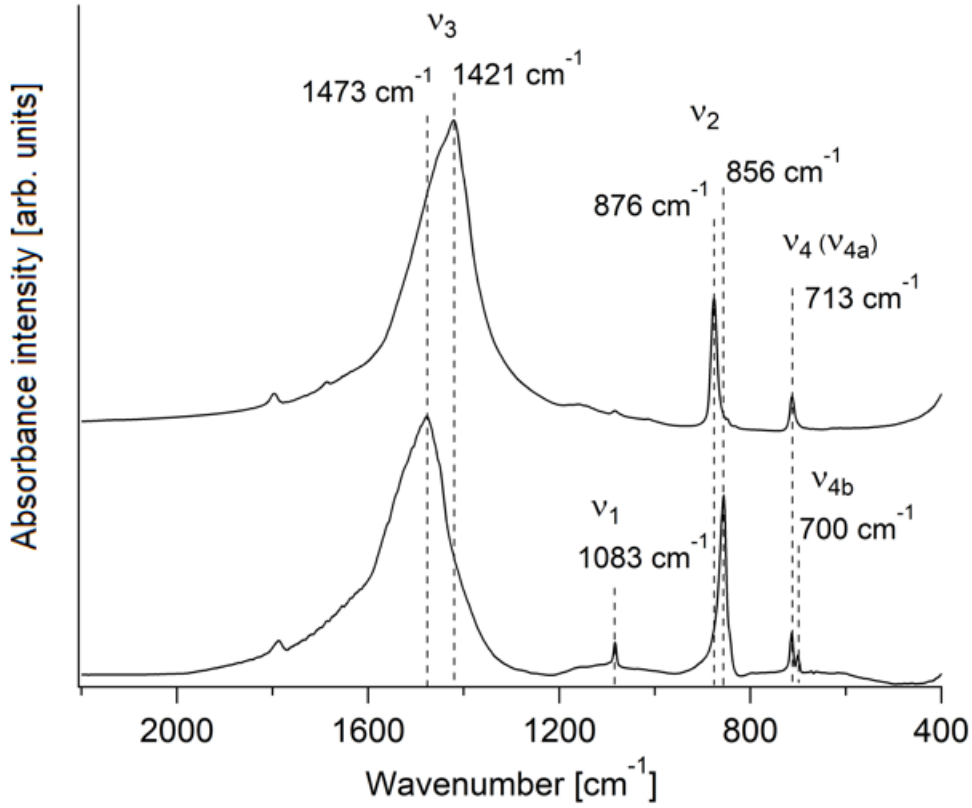

Figure 2.4: IR spectra for calcite (top) and aragonite (bottom) comparing peak locations between the two polymorphs. The absorbance intensity is measured in arbitrary units as the spectra have been scaled and shifted to be presented on the same plot.

The vibrational modes in $CaCO_3$ that appear as peaks in the IR spectra in the energy range of the mid-infrared are related to the motion within the carbonate moiety within the $CaCO_3$ lattice. By convention, the peaks in $CaCO_3$ are labelled using the Greek letter ν and have been attributed to specific vibrational modes in the solids by previous studies [1, 6]. Calcite and aragonite have very similar IR spectra; they both contain the same prominent peaks: ν_2, ν_3, and ν_4, with the ν_4 peak being a single peak in the calcite spectrum and two sub peaks - ν_{4a} and ν_{4b} - in the aragonite spectrum. The ν_2 peak is due to the out-of-plane bending of the CO_3 moiety, ν_3 asymmetric stretching, and ν_4 in-plane bending. The aragonite spectrum also contains a ν_1 peak

due to the symmetric stretching of the CO_3 moiety that is not present in the calcite spectrum. In Figure 2.4 the absorbance intensity is measured in arbitrary units as the spectra have been scaled and shifted to be presented on the same plot. The small peak around 1800 cm^{-1}C, is a combination mode $\nu_1+\nu_4$ that is present in both aragonite and calcite [1].

2.3 Experimental Details

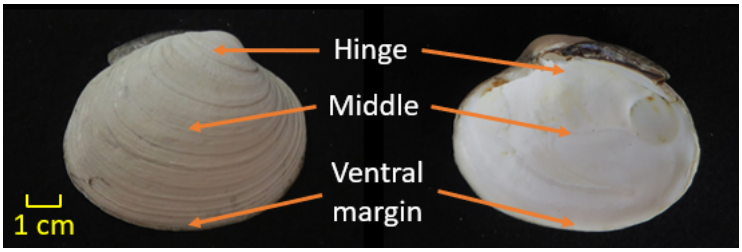

Figure 2.5: Sampling locations of the shell of *S. gigantea* for IR spectroscopy measurements.

I used a transmission detection geometry (transmission IR spectroscopy) for my IR measurements. For transmission IR spectroscopy, the compartment in which the sample is placed contains a slide where a sample pellet (i.e., the material being analyzed) can be inserted so that the IR beam passes directly through the sample. When the IR beam passes through the sample, specific frequencies will be absorbed, as discussed previously, and the recorded interferogram will only contain frequencies of IR radiation that were not absorbed by the sample. To see which frequencies are present or not present in the transmitted IR beam, a Fourier transform is performed so that it is possible to analyze the transmitted IR intensity as a function of wavenumber (which is directly proportional to energy and inversely proportional to wavelength), rather than a function of mirror displacement. The OPUS software completes the Fourier transform on the interferogram and the spectrum is shown directly in OPUS [7].

All samples of the shell of *S. gigantea* analyzed in this chapter are from Sechelt, British Columbia. I rinsed the shells with deionized water and scrubbed with a toothbrush to remove excess dirt. For transmission IR spectroscopy, samples of ∼1 mg were removed, using a small metal spatula, from both the inner and outer portions of the shell at the ventral margin, the hinge, and the middle of the shell. The sampling locations are shown in Figure 2.5. Saturation effects occur when a sample is optically opaque and practically effects the spectra by making the tops of the peaks appear jagged and noisy and affects the researchers ability to accurately determine peak positions, thus making it difficult to accurately interpret spectra. To reduce saturation effects and to prevent the pellet from being too opaque, after the shell samples were crushed into a fine powder they were mixed with an amount of potassium bromide (KBr) roughly 10 times greater than that of the shell powder. The KBr does not have any active modes in the infrared region of the EM spectrum and therefore does not show any peaks in the IR spectrum. The sample and KBr were grinded with a mortar and pestle into a fine powder to ensure that the $CaCO_3$ and KBr was homogenized and so that the $CaCO_3$ would be well dispersed within the final pellet. I then pressed the powder into a small pellet that was placed inside the sample holder. I will refer to this pellet containing both KBr and the sample powder as a KBr pellet.

The spectra were collected using a Bruker-Alpha II spectrometer with 32 scans and a resolution of 4 cm^{-1} in the mid IR range: from 4000 to 400 cm^{-1}. This combination of settings is a reasonable balance for obtaining a high resolution spectrum with a reasonable sample collection time. The spectra shown in the upcoming section do not include the higher wavenumber region, as no peak characteristic of $CaCO_3$ samples are present in that region.

I determined the peak locations by picking the highest point of the peak and measuring the wavenumber manually, with the a precision of about ± 2 cm^{-1}. This

precision is based solely on the ability to pick the position of the peak within the OPUS software.

2.4 Results

In this section, I present the results of my IR spectroscopy analysis in screening for diagenesis by studying individual IR spectra. I also present my analysis of relative peak intensities using the grinding curve technique, which I use to study intrashell differences in the $CaCO_3$ as well as differences between shells that are not immediately apparent when looking at individual spectra.

2.4.1 Screening for Diagenesis: Looking for Calcite

Table 2.1: Comparison of peak locations in aragonite and calcite IR spectra from relevant literature. All peak locations are reported in cm^{-1}.

		ν_1	ν_2	ν_3	ν_4	
					a	b
calcite [8]		N/A	875	1436	N/A	712
calcite [1]		N/A	872	1420	N/A	710
aragonite [8]		1084	857	1476	700	712
aragonite [9]		1083	854	1488, 1440	700	713
hinge	inner	1083	858,876	1473	700	713
	outer	1083	860	1473	700	713
middle	inner	1083	856	1473	700	713
	outer	1083	856	1473	700	713
ventral margin	inner	1083	858	1473	700	713
	outer	1083	856	1473	700	713
note: uncertainty on the wavenumbers is ± 2 cm^{-1}.						

I used IR spectroscopy to ensure that the shells were pristine aragonite - free from contaminating calcite - as pristine samples are crucial for accurate ^{14}C dating. To thoroughly evaluate whether or not the samples were pristine, I chose to take samples

from several different locations on both the inner and outer portions of the shells. These sampling locations are shown in Figure 2.5.

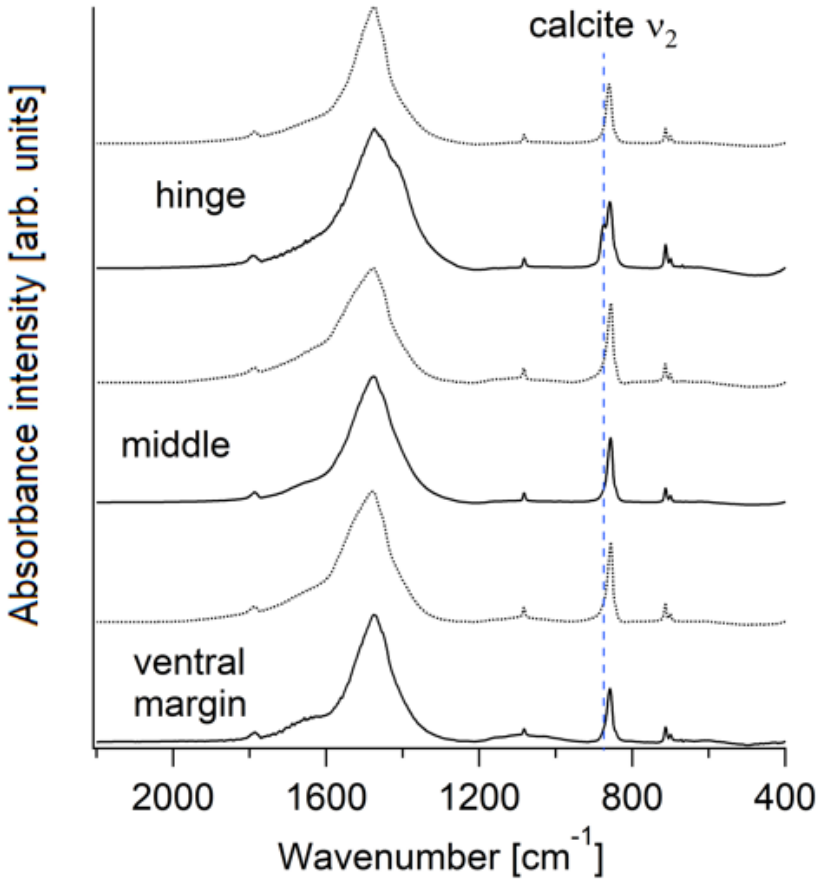

Figure 2.6: IR spectra from the shell of *S. gigantea* from Sechelt. Solid lines indicate the inner shell and dotted lines indicate the outer shell.

Figure 2.6 shows the individual spectra from different locations on both the inner and outer shell of *S. gigantea* samples from Sechelt, British Columbia and the locations of specific peaks from these spectra are recorded in Table 2.1 alongside values from the literature. The expected location of the calcite ν_2 peak is marked on the Figure. There is a prominent calcite ν_2 peak on the inner portion of the shell at the hinge which is more clearly shown in Figure 2.7 in the next subsection. Since the shell of *S. gigantea* is known to be only aragonite, the presence of calcite would suggest

diagenesis, i.e. the dissolution and reprecipitation of aragonite as calcite, and these shells would not be considered suitable for ^{14}C dating.

Note that there is some variability among values from the literature in Table 2.1 that is greater than the uncertainty I have assigned to my measurements (2 cm^{-1}). The uncertainty attached to my measurement value is only based on the accuracy of picking the top of the IR peak. The variation among the values in Table 2.1 is not unusual, as aragonites of different origins (geogenic, pyrogenic, and biogenic), as well as biogenic aragonites from different species and with different microstructures have been recorded to have slightly different IR peak positions, even when they are pristine aragonite [10].

Given that calcite is considered a tell-tale sign of diagenesis, this would rule out this sample for ^{14}C analysis. In my ^{14}C analysis (Chapter 3), any samples that appeared to be contaminated by calcite were not used for ^{14}C analysis. It takes no more than a glance to see the calcite ν_2 peak in an aragonite spectrum, but the presence of a calcite ν_2 peak in an aragonite spectrum is not the only indicator of diagenesis. In the next section I analyze the spectra more closely to look for other signs of diagenesis.

2.4.2 Other Spectral Clues for Possible Contamination or Diagenesis

After determining that at least one of the samples - one taken from the hinge on the inner side of the shell - displays a calcite ν_2 peak, I examined the spectra a little more closely to see if there were any other clues that could provide evidence of variation in the aragonite that could be due to diagenesis. As mentioned previously, aragonite can dissolve and recrystallize as calcite or aragonite, although aragonite recrystallization has been detected in only a couple circumstances, it is quite rare [8,11–13]. There may also be natural variations in the crystallinity and crystal structure of the aragonite in

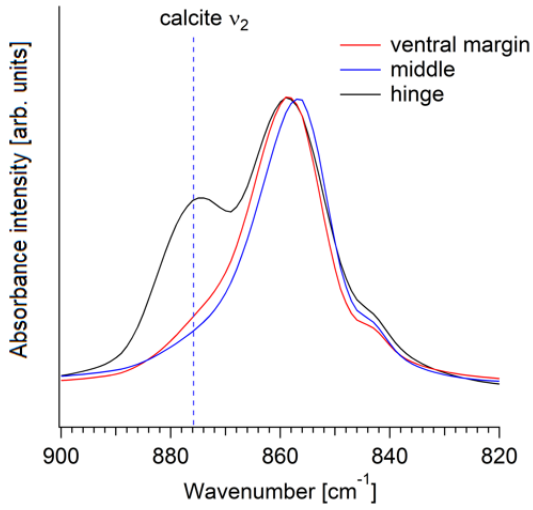

Figure 2.7: The ν_2 IR peak from the inner portion of the shell of *S. gigantea* from Sechelt, British Columbia.

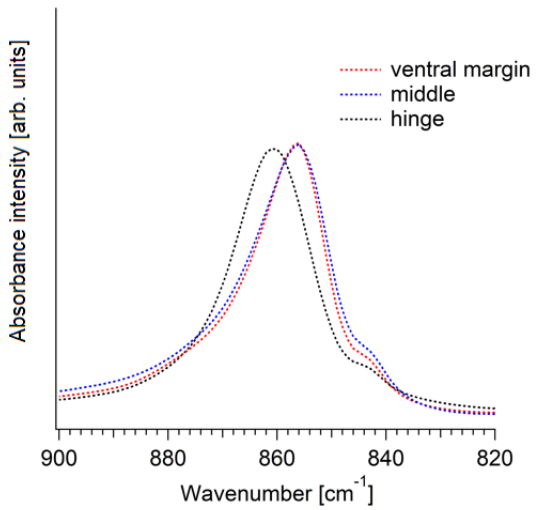

Figure 2.8: The ν_2 IR peak from the outer portion of the shell of *S. gigantea* from Sechelt, British Columbia.

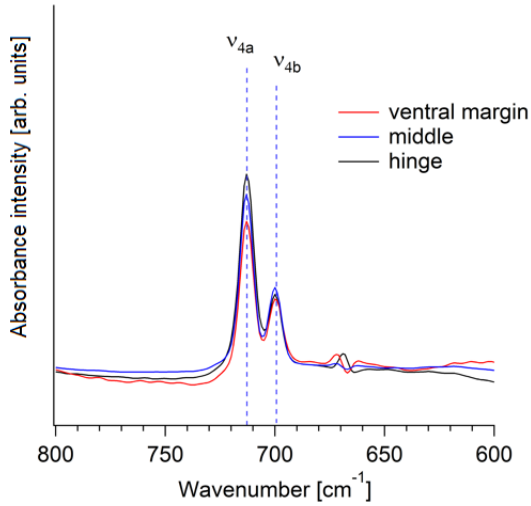

Figure 2.9: The ν_{4a} and ν_{4b} IR peaks from inner portion of the shell of *S. gigantea* from Sechelt, British Columbia.

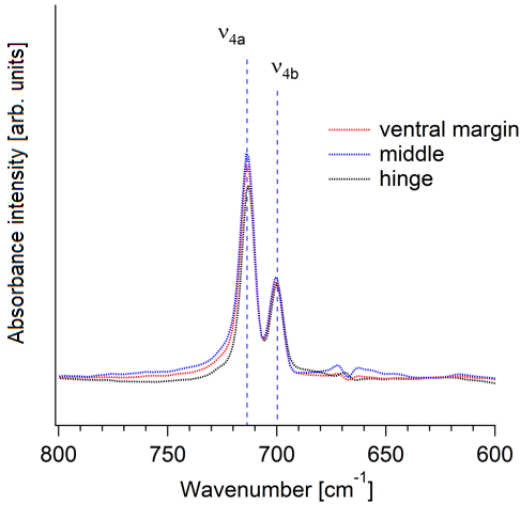

Figure 2.10: The ν_{4a} and ν_{4b} IR peaks from the outer portion of the shell of *S. gigantea* from Sechelt, British Columbia.

different portions of the shell. By studying the spectra from portions of the shell that were still aragonite, I looked for clues that may indicate diagenesis and to investigate how different parts of the shell may show different signatures in the infrared.

The individual IR spectra indicate that the samples are indeed primarily aragonite

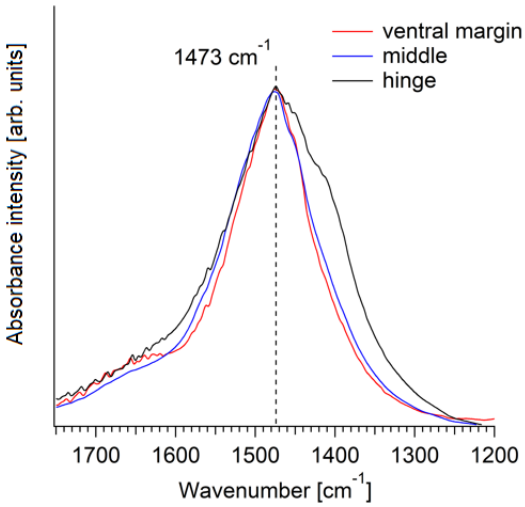

Figure 2.11: The ν_3 inner peaks from the IR spectra of the samples from Sechelt, British Columbia.

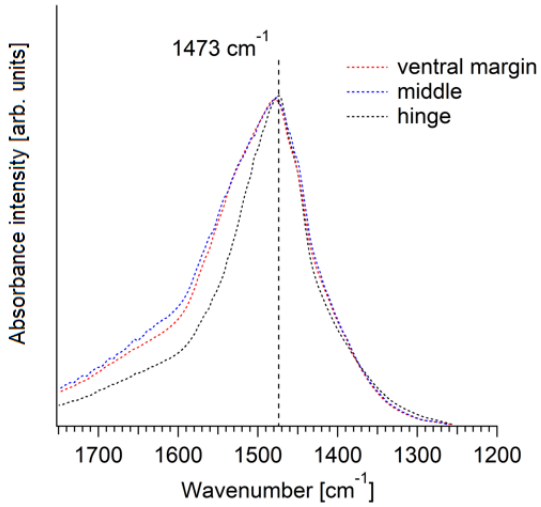

Figure 2.12: The ν_3 outer peaks from the IR spectra of the samples from Sechelt, British Columbia.

as the peaks present and their wavenumbers match with those expected for aragonite samples (see comparison between peak positions in Table 2.1). I note that the ν_2 and ν_3 peak positions in my data do not match the previous reported values exactly, but slight variations in the position of these peaks are not unexpected, as much of the literature records variation of a few wavenumbers in these peak locations (see Table 2.1).

Both aragonite and calcite can accommodate ionic substitutions into their lattices. In biomineralization studies Sr and Mg are often a focus because of their ability to inform seawater conditions in which the $CaCO_3$ biomineralized, but they do not necessarily indicate diagenesis [14, 15]. In calcite, the ν_4 band will shift to higher wavenumbers with increasing Mg content [8, 16], but in aragonite there is evidence of the ν_2 wavenumber shifting as a function of Sr and Mg content [15]. In my samples there are no significant peak shifts to indicate any ionic substitutions.

Apart from the spectrum obtained from the inner hinge portion of the shell, which

shows a distinct calcite ν_2 peak that appears as a shoulder on the aragonite peak, the IR spectra appear to be pristine aragonite. There are slight peak shifts, but they are no greater than the expected variation seen within the previous literature (Table 2.1). I also note that there are no detectable shifts in the ν_4 peak in my samples, which provides further reassurance that there are no ionic substitutions in the aragonite lattice.

Looking again at the ν_2 peak in Figure 2.8, note that there is a shoulder on the lower wavenumber side, around 844 cm^{-1}. This ν_2 shoulder has been documented in other experimental studies on aragonite, and is likely due to the ^{13}C absorption specifically [1, 15, 17]. The position of this shoulder remains constant in my samples, even in the sample that displays the presence of calcite (Figure 2.7). Dauphin et al. [15] monitored the position of this peak shoulder in aragonites with changing Mg and Sr concentrations and determined that it remained unchanged. This peak is therefore an expected feature of the aragonite IR spectrum and does not provide any further information on diagenesis or contamination.

The ν_3 peak also shows some differences in shape at different sampling locations, while still maintaining the same peak location (see Figures 2.11 and 2.12). The ν_3 peak is more difficult to understand. The ν_3 peak is made up of at least two sub-peaks that are related to the isotopic composition of the carbon (^{12}C vs. ^{13}C) in the $CaCO_3$ [17]. The isotopic composition of ^{12}C vs. ^{13}C in my samples is likely not changing significantly as all samples come from natural estuarine environments which are not intentionally enriched in either of these isotopes. However, differences in scattering among particles dispersed within the KBr pellets could affect the intensities of these smaller peaks and change the shape of the overall apparent peak.

The best way to analyze changes in the ν_3 peak is to look at it in conjunction with the other peaks. The spectrum that shows the most marked difference in the

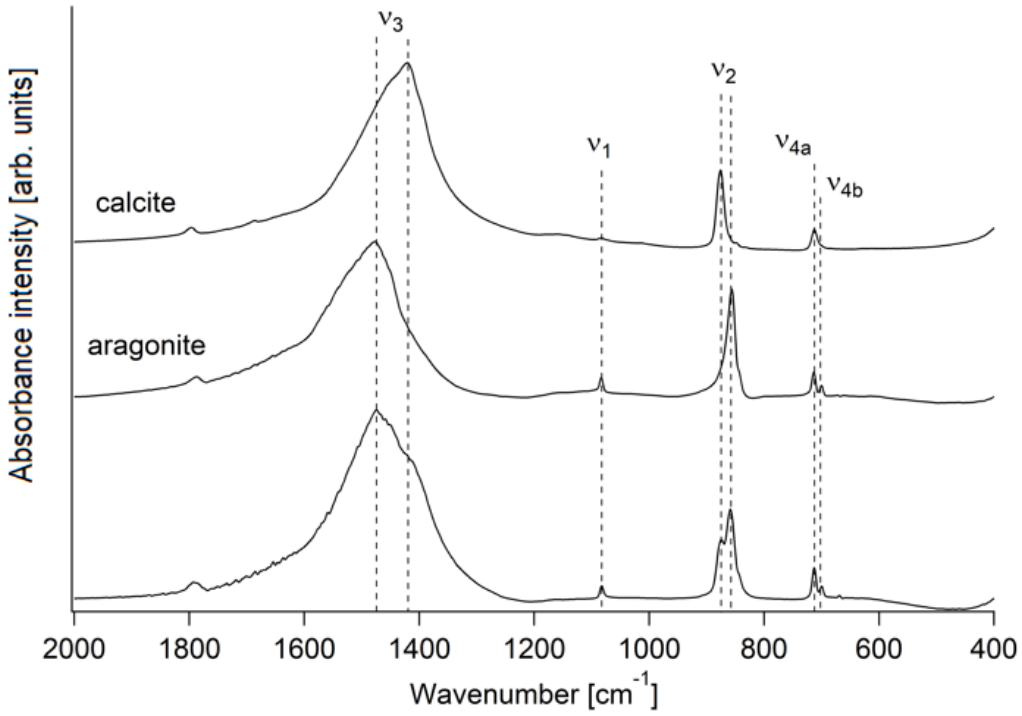

Figure 2.13: Comparison of calcite and aragonite IR spectra with the spectra from the inner hinge portion of the *S. gigantea* shell (bottom).

shape of the ν_3 peak is also the one that shows the prominent calcite ν_2 shoulder - the inner hinge spectrum. In the literature, the ν_3 peak has a different expected location for calcite than it does for aragonite and the IR spectra with a ν_2 calcite signature also shows a shoulder on the ν_3 toward lower wavenumber which seems to correspond with that of calcite. This comparison is shown in Figure 2.13. The presence of calcite seems to be the most likely explanation for the differences seen in the ν_3 peaks of that specific spectrum. I highlight once again that although I may not be able to pinpoint the exact cause for the changes in the ν_3 peak, the calcite ν_2 peak alone is enough for me to rule out the use of this sample for ^{14}C analysis.

For the other spectra, I do not see shifts in the other peaks that I could conclusively attribute to significant compositional changes. These differences stem from changes in the aragonite other than ionic substitutions, although the exact cause is unknown.

This is discussed more in the next section.

2.5 Grinding Curves

In the previous section, I analyzed each spectrum individually, considering peak positions and peak shapes, with the goal of looking for evidence of a phase change from aragonite to calcite and the presence of ionic substitutions in the aragonite lattice. In this section, I analyze spectra that did not show any evidence of a polymorph change or compositional changes by looking at changes in relative peak heights as I grind the sample powder more times.

This type of analysis cannot be done by looking at only one spectrum; rather, it requires multiple spectra obtained from the same sample. However, I emphasize that the analysis completed in the previous section - looking for signatures of calcite or ionic substitutions - should be done before looking at peak intensities since the analysis of these intensities is complicated by these factors.

Only spectra that did not show any calcite signatures or significant peak shifts were used to construct the grinding curves in the next section.

2.5.1 Details of the Grinding Curve Technique

Grinding curves are a systematic way of studying relative IR peak intensity changes and tracking their changes as a function of how well the sample powder is dispersed within the KBr pellet. The dispersion of the sample powder within the KBr pellet, and thus the relative IR peak intensities are affected by the grinding intensity of the sample powder, which affects both the size and distribution of the particles within the KBr pellet. As the sample and KBr particles are grinded more times, they become smaller and the powder becomes more homogenized, resulting in the sample being

more evenly dispersed throughout the KBr pellet, which reduces scattering and results in sharper IR peaks [5]. However, the rate at which certain IR peaks sharpen is not the same.

I mixed the aragonite samples with KBr and ground it until the powder was homogenized to ensure that the aragonite would be well dispersed within the KBr pellet. After obtaining a spectrum from that pellet, I ground up the pellet again with the mortar pestle and pressed it into another pellet, obtained another spectrum, and so on. This was repeated until the spectra became saturated and the tops of the IR peaks were no longer sharp. Grinding the sample into a more fine powder will increase the surface area, and eventually the surface area will become large enough to result in the sample being optically opaque and the spectra being saturated. This procedure of repetitive grinding could be continued even further by removing a small amount of the powder and adding more KBr to reduce saturation, and thus obtain more data points for the grinding curve.

In a study by Regev et al. [18], calcites formed by geogenic and pyrogenic processes had distinct IR grinding curves. The IR grinding curves from different calcites were offset with respect to one another and displayed different slopes due to their differing degrees of crystalline order [18]. The grinding curve method can serve as a qualitative method for studying changes in the structural order of $CaCO_3$ [18]. While the grinding curve method has been shown to be a useful technique for understanding structural changes in $CaCO_3$, specifically calcite and aragonite, I also highlight that the grinding curve analysis method is not standard, but has gained some attention in the biomineralization and archaeology communities [5, 10, 18–20].

Absolute peak intensities are not well suited to provide information about the sample because they depend on the amount of sample and the size of the sample particles distributed within the KBr pellet, which are difficult experimental parameters to

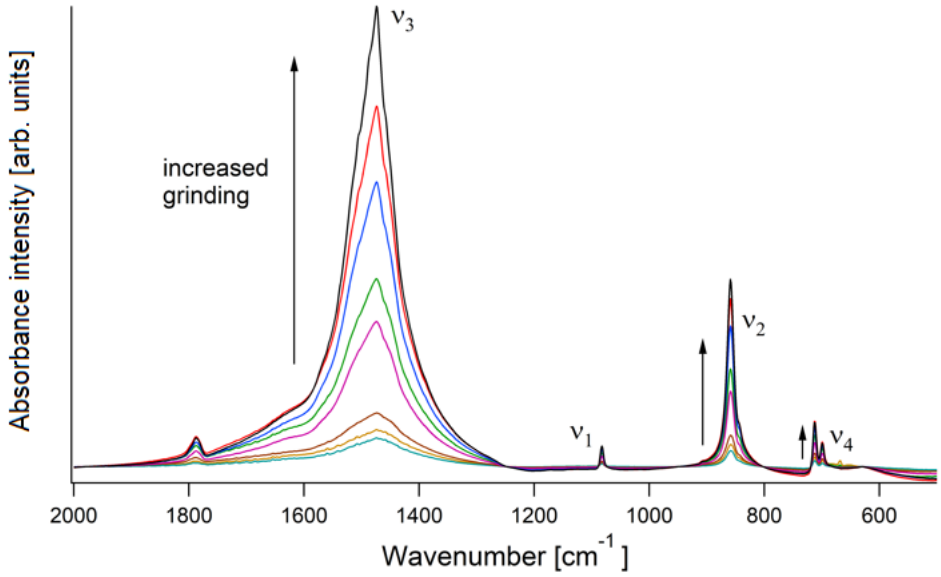

Figure 2.14: Aragonite IR spectra with peaks shown as increasing in intensity as the sample is repeatedly grinded.

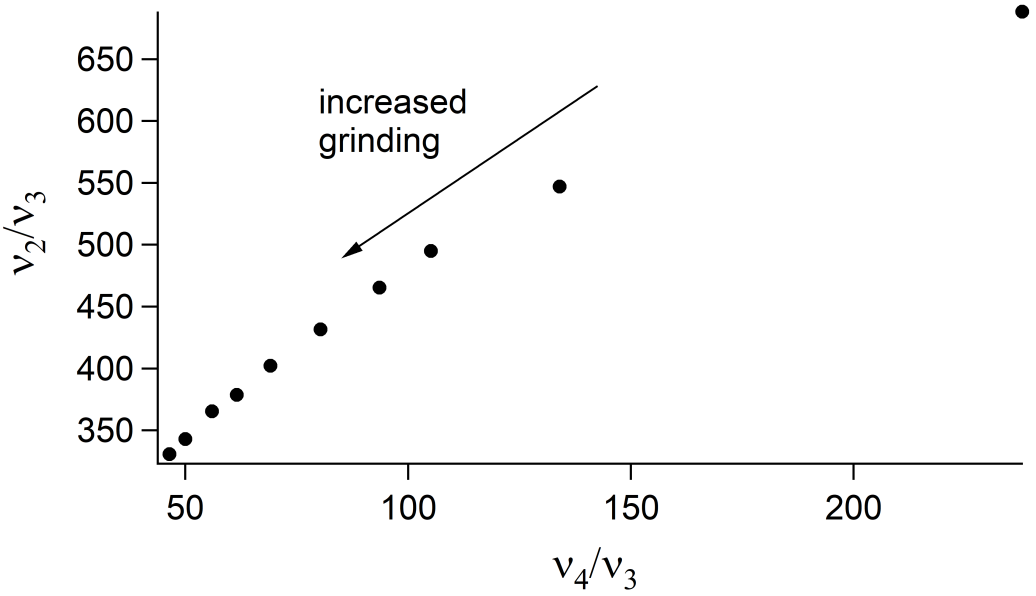

Figure 2.15: Example of an IR grinding curve constructed by normalizing the intensities of the ν_2 and ν_4 peaks to the ν_3 peak and plotting the normalized intensities against each other. The values of the peak ratios ν_2/ν_3 and ν_4/ν_3 have been multiplied by 1000.

replicate for each measurement. However, relative peak intensities can be used when comparing samples with different degrees of grinding. When I complete the process of

repeatedly grinding the sample and pressing it into a pellet more times, that creates a larger amount of smaller particles that are more evenly dispersed throughout the pellet, which can absorb the IR radiation better and lessens the effects of scattering, resulting in a sharpening of the IR peaks [5]. Figure 2.14 shows how the spectra change when I grind and repress the KBr pellet more times.

Grinding curves are constructed by repeatedly grinding and repressing a KBr pellet containing a sample and plotting the intensity of the ν_2 peak normalized to the ν_3 peak against the ν_{4a} peak (for the remainder of the chapter simply referred to as the ν_4 peak) normalized to the ν_3 peak. Each data point in a grinding curve, like the one shown in Figure 2.15, represents data from a single IR spectrum. This method decouples the effects of particle size and scattering in the KBr pellet from other factors that influence IR peak intensities such as crystallinity and microstrain fluctuations [5, 21]. The grinding of the pellet has the largest effect on the peak intensities. By analyzing the changes in these peak intensities as a function of the grinding of the pellets, patterns emerge that are due to other properties intrinsic to the samples rather than optical effects [5]. As described by Poduska et al. [5], the shape of the grinding curves, i.e. the overall trend that occurs when the pellets are grinded repeatedly, is due mainly to optical effects, but the offset of these curves with respect to one another can be influenced by structural factors in the samples like crystallinity and microstrain fluctuations.

The choice of plotting ν_2/ν_3 vs. ν_4/ν_3 is somewhat arbitrary, but is based on previous theoretical and experimental work that has shown that the ν_2 and ν_4 peak widths and heights depend on unit cell distortions and grinding [3,18]. Plotting their intensities normalized to ν_3 can decouple the effects of grinding, which affects particle size and distribution of the particles in the KBr pellet, from other factors intrinsic to the material being analyzed that affect the IR peak intensities [5]. Work done by

Figure 2.16: Sampling locations for IR grinding curve analysis on the shell of *S. gigantea*

Xu et al. [21, 22] has corroborated this with X-ray diffraction data by measuring the lattice constants of the calcite crystal structure and correlating such measurements with that of ionic substitutions (particularly Mg for Ca), microstrain fluctuations, and crystal domain size. Each of these factors affects the offset of the IR grinding curves.

2.5.2 Results

I studied the effects of repeatedly grinding the KBr pellets on the IR spectra for three additional shell samples from Sechelt. These samples were taken from the middle portion of the shell - from both the inner and outer sides (shown in Figure 2.16). I first analyzed the samples following the approaches outlined above: first checking for calcite and any other peaks not characteristic of aragonite, and analyzing peak positions to ensure that there were no signs of significant shifts that could indicate ionic substitutions. Ionic substitutions into the lattice may also affect the relative peak intensities and thus the grinding curves, so it is important to rule that out before interpreting the grinding curves [10].

Before constructing the grinding curves, I display the spectra from the inner and outer portion of the shell as the grinding intensity is increased. The spectra from the inner and outer portion of one of the shells are shown in Figure 2.17 and 2.18 respectively. As I repeatedly grind the samples more times, the peaks sharpen.

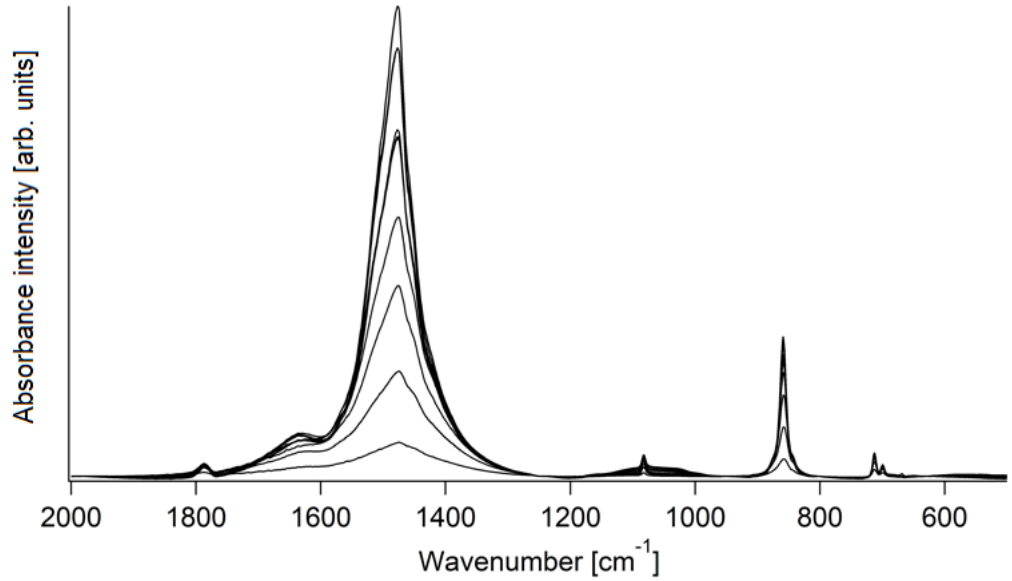

Figure 2.17: IR spectra taken with increased grinding intensities as evidenced by the sharpening of peaks. Sample taken from the inner shell of *S. gigantea* from Sechelt.

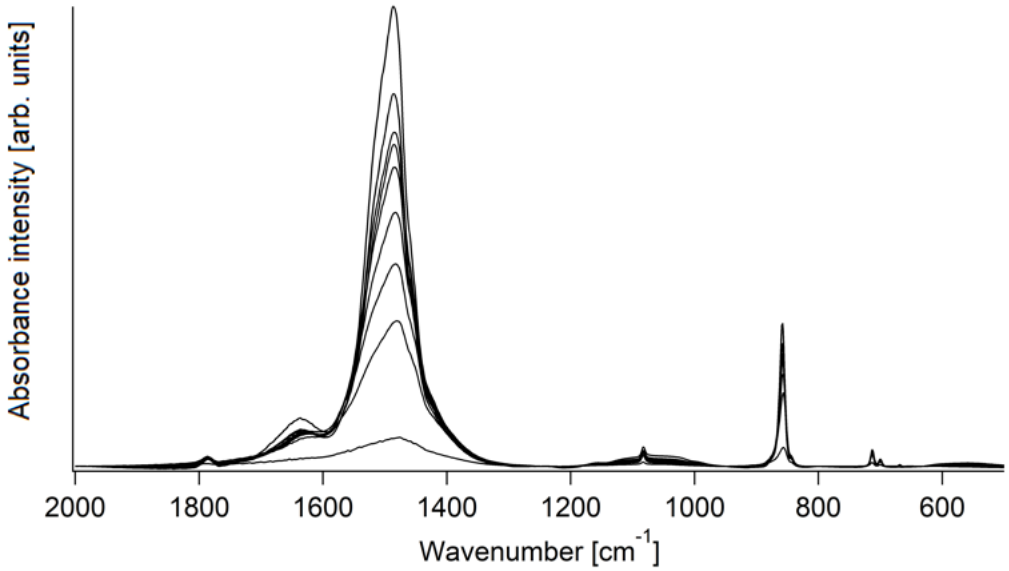

Figure 2.18: IR spectra taken with increased grinding intensities as evidenced by the sharpening of peaks. Sample taken from the outer shell of *S. gigantea* from Sechelt.

Because grinding affects the peak intensities, it can make some features come into focus that may not have been visible otherwise. For example, Figure 2.19 shows the

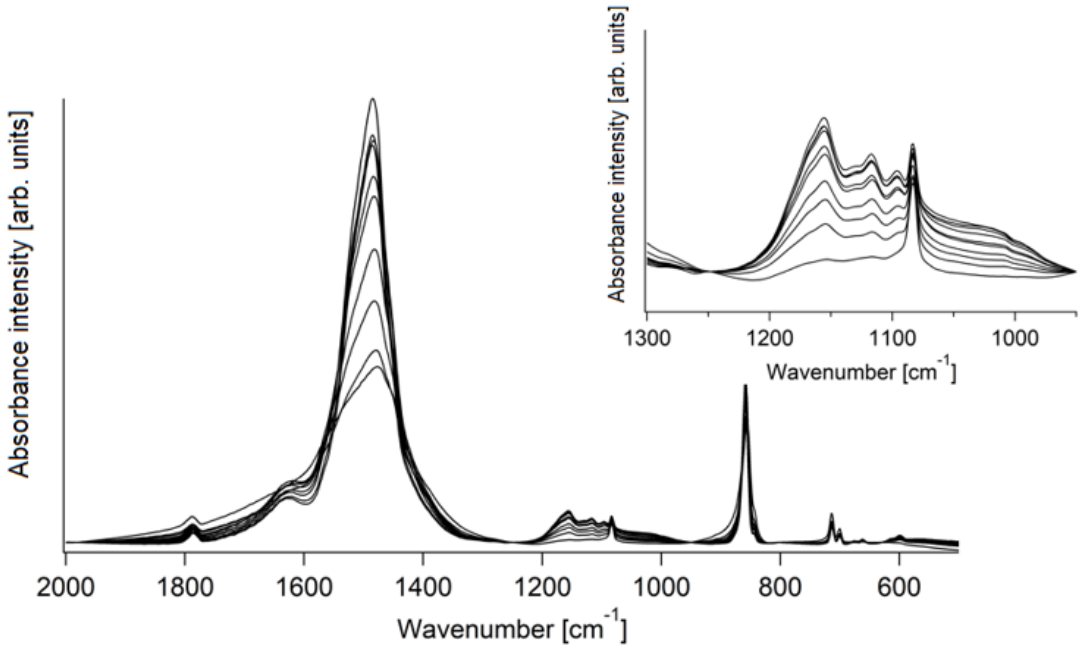

Figure 2.19: Spectra taken from the outer shell of a *S. gigantea* sample from Sechelt. The inset figure shows the changes surrounding the ν_1 peak with increased grinding.

spectra taken from the outer shell of one of the samples. Note the changes in the region around the ν_1 peak as I repeatedly grind the sample more times. The three peaks that come into focus with intense grinding are located at 1155 cm^{-1}, 1116 cm^{-1}, and 1096 cm^{-1}. These peaks are most likely due to the presence of β-chitin, which is the main component of the proteinaceous matrix that encompasses the aragonite crystals throughout the shell. There is β-chitin in small amounts in all samples as it makes up $\sim$1% of the shell material, so this is not a surprise, and these peaks are not attributed to any form of contamination or diagenesis. The infrared signatures of β-chitin only fall in the region around the ν_1 peak and do not appear to cause any unexpected changes in the the other IR peaks that are used to construct the grinding curves [23]. Given that I did not see evidence of any other features that are not unique to aragonite anywhere else in this spectrum, I proceeded to constructing the grinding curves.

I constructed six grinding curves: one from the inner portion and one from the outer portion of each of the three shells. The grinding curves are shown in Figure 2.20. There is a consistent shift in these curves between the inner and outer shell. The inner portion of the shell is nacre and the outer portion is crossed lamellar. The nacre and crossed lamellar microstructures have different crystal sizes; the nacre platelets are about 10 μm in size and the lamellae in the crossed lamellar structure are about 1 μm in size. However, it is not completely clear if this arrangement of the platelets and lamellae, which is on the order of μm is what is causing the shift in the grinding curves.

Suzuki et al. [10] reported distinct grinding curves for crossed lamellar and nacreous aragonite, and my grinding curves are equally distinctive. Suzuki et al. [10] also articulate that the shift in these grinding curves may not simply be due to the microstructures of the aragonite on the order of μm, but may be due to changes in crystallinity within those microstructures. However, by only looking at the grinding curves I cannot attribute these shifts directly to crystallinity changes as this would need to be verified by directly studying the crystallinity through x-ray diffraction for example [21]. Nonetheless, the grinding curves alone do show that there are differences in both the nacre and crossed lamellar aragonites throughout the shell that are not due to ionic substitutions or the presence of calcite.

In my undergraduate honours thesis in archaeology [24], the variation between the inner and outer portion of shells were studied for the marine bivalve mollusks *Mya arenaria* from Nova Scotia and *Saxidomus gigantea* from British Columbia, as well as samples of the gastropod (snail) *Pomacea paludosa* from Cuba. All of these grinding curves displayed a similar shift between the curves from the inner and the outer portion of the shell. This additional data is presented in Appendix A.

Now I consider only the three grinding curves from the inner portions of each of

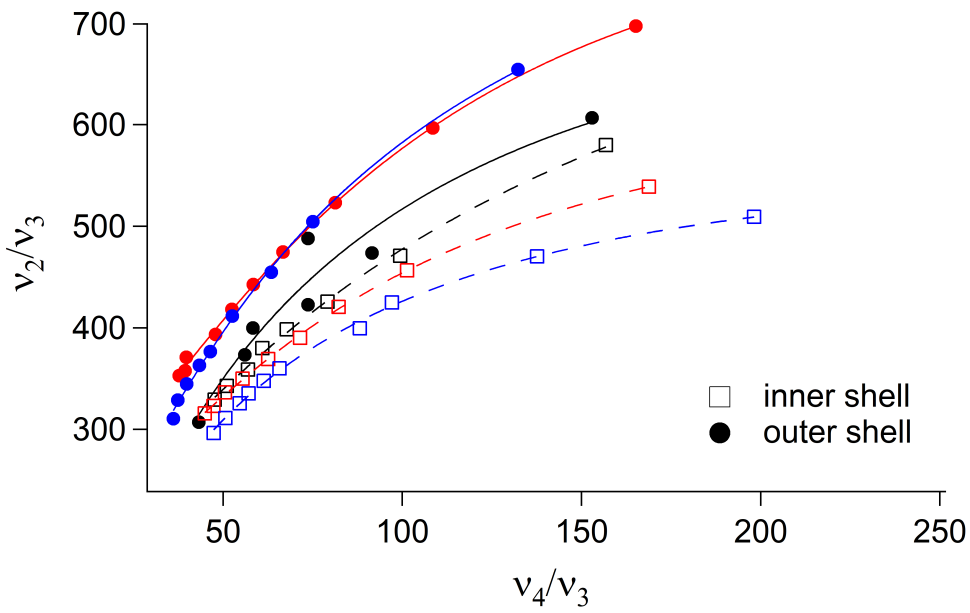

Figure 2.20: *S. gigantea* grinding curves from Sechelt B.C. Each colour represents one bivalve shell sample, the dotted lines with open squares indicate samples from the inner shell and the solid lines with circles indicate outer shell. The peak intensity ratios (ν_2/ν_3 and ν_4/ν_3) have been multiplied by 1000.

the shells: the dotted curves in Figure 2.20. Note that there is variation among these grinding curves. The same can be said for the three grinding curves from the outer portions of each of the shells: the solid curves in Figure 2.20. The shifts between these grinding curves indicate a consistent and reproducible difference between the crossed lamellar and nacre microstructures that are likely not linked to the organization of the crystals on the order of μm, but I cannot determine exactly what causes this difference by only considering the grinding curves.

In this thesis work, I did not have the means to determine whether or not these variations are natural or if they are a product of diagenesis. It is entirely possible that the variations within the same aragonite microstructure are natural variations that are a product of the biomineralization process, whereby the mollusk shell carbonate is biomineralized with built-in structural differences. This is evidenced by the variability in grinding curves between different biogenic microstructures, all of which

were biomineralized by marine organisms, recorded by Suzuki et al. [10]. It is also possible that these variations are linked to the form of diagenesis that results in the recrystallization of aragonite as aragonite, and that the recrystallized aragonite may have a different degree of crystallinity. Because this kind of diagenesis is very rare, more work would need to be done to confirm this. Regardless, my results confirm that there are indeed differences in the aragonite between the inner and outer shell of a single mollusk shell. My results also demonstrate that there are variations in the grinding curves of the same aragonite microstructures between individual shell samples.

2.6 Summary

Infrared spectroscopy was used to screen for diagenesis and to study relative intensity changes in the IR peaks of samples of *S. gigantea* from Sechelt, British Columbia. I first analyzed my IR spectra focusing on the detection of the conversion of aragonite to calcite, which is the most common form of diagenesis in archaeological marine bivalves. Calcite was present only at the hinge portion of one of my shell samples. I then studied the peak shifts in my IR spectra to determine if there were any signatures of ionic substitutions in the aragonite lattice, which may also be evidence of diagenesis.

After I confirmed that my samples did not show any evidence of contamination or diagenesis, I used the relative peak intensities of three characteristic aragonite peaks to construct grinding curves - a method of systematically studying shifts in relative peak intensities. There is a consistent shift in the grinding curves obtained using powder from the inner nacreous portion of the shell and from the outer crossed lamellar portion of the shell. The grinding curves also show that there are variations in the relative peak intensities within both the crossed lamellar and nacreous portions

of the shell. However, the grinding curves alone cannot explain precisely what it is about the aragonites that causes these changes in relative peak intensities.

While using IR spectroscopy to detect calcite and ionic substitutions within the calcium carbonate lattice are quite standard screening practices, the grinding curve technique is not typically used as a screening practice prior to ^{14}C analysis because it is not clear what the relationship is between variations in the grinding curve and diagenesis. At this point, it is unclear if the grinding curve variations within the crossed lamellar and nacreous portions of the shell are natural variations or if they signify some form of diagenetic alteration. Nonetheless, there is clearly variation in the grinding curves within the shell that cannot be fully explained yet.

The experiments conducted in this chapter illustrate the strength of IR spectroscopy to detect diagenesis by searching for calcite and other spectral features, but also demonstrate its ability to study variations that are not apparent when looking at a single spectrum.

Bibliography

[1] W. B. White. The carbonate minerals. In V. C. Farmer, editor, *The Infrared Spectra of Minerals*, chapter 10. Mineralogical Society of Great Britain and Ireland, 1974.

[2] International Union of Pure and Applied Chemistry. IUPAC Compendium of Chemical Terminology – The Gold Book, 2009.

[3] R. Gueta, A. Natan, L. Addadi, S. Weiner, K. Refson, and L. Kronik. Local atomic order and infrared spectra of biogenic calcite. *Angewandte Chemie - International Edition*, 46(1-2):291–294, 2007.

[4] B. Xu, M. B. Toffolo, L. Regev, E. Boaretto, and K. M. Poduska. Structural differences in archaeologically relevant calcite. *Analytical Methods*, 7(21):9304–9309, 2015.

[5] K. M. Poduska, L. Regev, E. Boaretto, L. Addadi, S. Weiner, L. Kronik, and S. Curtarolo. Decoupling local disorder and optical effects in infrared spectra: Differentiating between calcites with different origins. *Advanced Materials*, 23(4):550–554, 2011.

[6] S. S. Mitra. Infrared and Raman Spectra Due to Lattice Vibrations. In Mitra S.S. Nudelman S., editor, *Optical Properties of Solids*, pages 333–451. Springer, Boston, MA, 1969.

[7] Bruker. *OPUS Spectroscopy Software Version 7 Quick Reference Guide*.

[8] S. Weiner. *Microarchaeology: Beyond the Visible Archaeological Record*. Cambridge University Press, New York, 2010.

[9] F. A. Andersen and L. Brecevic. Infrared Spectra of Amorphous and Crystalline Calcium Carbonate. *Acta Chemica Scandinavica*, 45:1018–1024, 1991.

[10] M. Suzuki, Y. Dauphin, L. Addadi, and S. Weiner. Atomic order of aragonite crystals formed by mollusks. *CrystEngComm*, 13:6780–6786, 2011.

[11] K. Douka, T. F. G. Higham, and R. E. M. Hedges. Radiocarbon dating of shell carbonates: old problems and new solutions. *Munibe*, 31:18 – 27, 2010.

[12] R. Enmar, M. Stein, M. Bar-Matthews, E. Sass, A. Katz, and B. Lazar. Diagenesis in live corals from the Gulf of Aqaba. I. The effect on paleo-oceanography tracers. *Geochimica et Cosmochimica Acta*, 64(18):3123–3132, 2000.

[13] G. E. Webb, G. J. Price, L. D. Nothdurft, L. Deer, and L. Rintoul. Crytic meteoric diagenesis in freshwater bivalves: Implications for radiocarbon dating. *Geology*, 35(9):803–806, 2007.

[14] N. Guzmán, Y. Dauphin, J. P. Cuif, A. Denis, and L. Ortlieb. Diagenetic changes in Concholepas concholepas shells (Gastropoda, Muricidae) in the hyper-arid conditions of Northern Chile - implications for palaeoenvironmental reconstructions. *Biogeosciences*, 6(2):197–207, 2009.

[15] Y. Dauphin. Infrared Spectra and Elemental Composition in Recent Carbonate Skeletons: Relationships between the ν_2 Band Wavenumber and Sr and Mg Concentrations. 53(2):184–190, 1999.

[16] R. Z. Wang, L. Addadi, and S. Weiner. Design strategies of sea urchin teeth : Structure, composition and micromechanical relations to function. *Philosophical Transactions of the Royal Society B: Biological Sciences*, 352(1352):469–480, 1997.

[17] B. Xu, A. Hirsch, L. Kronik, and K. M. Poduska. Vibrational properties of isotopically enriched materials: the case of calcite. *RSC Advances*, 8:33985–33992, 2018.

[18] L. Regev, K. M. Poduska, L. Addadi, S. Weiner, and E. Boaretto. Distinguishing between calcites formed by different mechanisms using infrared spectrometry: Archaeological applications. *Journal of Archaeological Science*, 37(12):3022–3029, 2010.

[19] K. M. Poduska, L. Regev, F. Berna, E. Mintz, I. Milevski, H. Khalaily, S. Weiner, and E. Boaretto. Plaster Characterization At the PPNB Site of Yiftahel (Israel)

Including the Use of ^{14}C: Implications for Plaster Production, Preservation, and Dating. *Radiocarbon*, 54(3):887–896, 2012.

[20] B. Xu, M. B. Toffolo, E. Boaretto, and K. M. Poduska. Assessing Local and Long-Range Structural Disorder in Aggregate-Free Lime Binders. *Industrial and Engineering Chemistry Research*, 55(30):8334–8340, 2016.

[21] B. Xu, M. B. Toffolo, L. Regev, E. Boaretto, and K. M. Poduska. Structural differences in archaeologically relevant calcite. *Analytical Methods*, 7:9304–9309, 2015.

[22] B. Xu. *Assessing different types of disorder in carbonate minerals with vibrational spectroscopy*. PhD thesis, Memorial University of Newfoundland, 2015.

[23] S. Weiner. Kimmel Center for Archaeological Science Infrared Spectra Library, 2021. data retrieved from `https://www.weizmann.ac.il/kimmel-arch/infrared-spectra-library`.

[24] M. Dusseault. Limits and Potential of FTIR Analysis in Archaeology. Bachelor's honours thesis, Memorial University of Newfoundland, 2019.

Chapter 3

Radiocarbon

In this chapter, I use accelerator mass spectrometer (AMS) ^{14}C analysis to study the ^{14}C signal in the mollusk shell samples at three different locations within the shell. While infrared spectroscopy (IR) provides a way to screen for diagenesis, AMS ^{14}C analysis measures the actual amount of ^{14}C within the $CaCO_3$, which can then be calibrated to calculate age. Here I will provide details on the theory and background of ^{14}C dating and our sampling strategies. Then I present both the uncalibrated and calibrated data. I look at both the uncalibrated fraction of modern carbon (F14C) measurements and the calibrated age ranges to explore what it means for intrashell measurements to be different and how perceptions of intrashell variation depend on calibration.

3.1 Authorship Statement

This chapter contains ^{14}C data that was obtained in July 2018 at the Lalonde AMS Laboratory at the University of Ottawa. Dr. Meghan Burchell, Anna Sparrow, and I were present for the entirety of the sample preparation process and assisted in the preparation following instructions and guidance from the laboratory staff. The

AMS measurements were completed by the laboratory staff, and the F14C data was emailed to us with all corrections applied (normalized to the appropriate standards and corrected for fractionation), except for calibration and the local marine reservoir correction (ΔR) which was completed by me. I completed all data analysis by investigating ΔR corrections and calibration curves. All interpretations and written work were completed by me with comments and feedback from Dr. Kristin Poduska and Dr. Meghan Burchell.

3.2 ^{14}C Dating: Theory and Background

The isotope ^{14}C is created in the atmosphere when cosmic rays collide with air particles to produce neutrons, which then collide with the ^{14}N nucleus. When ^{14}N, which is abundantly present in the earth's atmosphere, reacts with the neutrons, the result is a release of a proton and the formation of the radioactive isotope carbon-14 [1]. The isotope ^{14}C is an unstable radioactive isotope of carbon and it will eventually decay back to ^{14}N. This transition has a half-life of 5700$\pm$30 years [2]. Because cosmic rays have been bombarding the atmosphere on a time scale much longer than that of the lifetime of ^{14}C, the earth is in a steady state of formation and disintegration of ^{14}C apart from slight deviations that are accounted for by calibration [1].

All living things are constantly exchanging carbon with their surroundings, which keeps the ^{14}C signal of their organic tissues in equilibrium with that of their environment while they are living. Once an organism dies this exchange stops and the ^{14}C decays according to the half-life mentioned above. For marine mollusks, which incorporate carbon from their marine environment into their shells, this exchange stops once the shell mineral is deposited. The steady state approximation allows for the measurement of the time since death (the time since cessation of growth in the

case of mollusk shells) by comparing the ^{14}C content of a dead sample with that of the current amount of ^{14}C in the environment. The age of the sample can then be calculated using the half-life of ^{14}C. Therefore, a simple age calculation can be done using

$$A_s = A_0 e^{-t/T_{1/2}}, \tag{3.1}$$

where A_s is the sample activity, A_0 is the present activity in the environment, and $T_{1/2}$ is the half-life. This equation can be arranged to solve for t, the time since death.

3.2.1 Calibration Curves

Because the amount of ^{14}C in the atmosphere has not remained exactly constant over time, calibration curves are necessary to determine the correct age of a sample. Fraction of modern carbon (F14C) values are used in the calibration process. The F14C is calculated by comparing the ratio of the amount of ^{14}C to the amount of ^{12}C in the sample to that of a standard, following

$$F14C = \frac{(^{14}\mathrm{C}/^{12}\mathrm{C})_{sample}}{(^{14}\mathrm{C}/^{12}\mathrm{C})_{standard}}. \tag{3.2}$$

AMS ^{14}C measurements are first reported as F14C values and these values are then converted into dates by means of calibration with the appropriate calibration curve, not by using equation 3.1.

The first calibration curve constructed by Arnold and Libby in their 1949 publication [3], based on their work of ^{14}C dating samples with known age, is the basis on which other calibration curves were constructed. For example, in the 1960's, studies using tree ring sequences from Bristlecone Pine further demonstrated that there was not exactly a direct relationship between the time since tree death and the ^{14}C

determination because of the fluctuations of ^{14}C levels in the environment from year to year [4]. These fluctuations necessitate an appropriate correction. Using the same principles as Arnold and Libby, researchers constructed the first high-precision curves for terrestrial samples. The first high precision calibration curves were published by Stuiver and Pearson in 1986 and mapped dates back to about 2500 BC [5, 6].

Since their introduction in the 1980's, more data have been added to these high resolution curves, extending them farther back in time to about 50,000 years ago; the limit of ^{14}C dating. There now exist calibration curves for both the northern and southern hemispheres (IntCal and SHCal curves respectively), constructed using an expanse of corals, fossils, sediments, and dendrochronologies. Curves are kept up to date with new publications every few years, with the most recent curves available for use in calibration being the IntCal and SHCal 2009, 2013, and 2020 curves, accessible through the OxCal calibration program [7–12].

3.2.2 Considerations Specific to Marine Dates

When analyzing our samples, and any other samples with a marine signature, it is important to take into consideration the global marine carbon reservoir. Most, if not all, of the ^{14}C in our marine shell samples is derived from dissolved inorganic carbon (DIC) in seawater. The ocean exchanges CO_2 with the atmosphere, resulting in the formation of CO_3^{2-}, HCO_3^{1-}, and H_2CO_3 as well as some remaining $CO_{2(aq)}$ in the seawater [13, 14]. When carbon gets locked in the ocean in these forms, it prevents it from remaining evenly mixed with the global atmospheric reservoir [1]. On average, this results in the carbon in the ocean being "older" than the carbon in the atmosphere because the carbon gets trapped in the form of DIC and, depending on ocean mixing patterns, may remain out of equilibrium with atmospheric carbon for long periods of time allowing the marine ^{14}C to decay without being replenished.

Marine calibration curves

The 1986 publication by Stuiver and Pearson presented calibration curves for marine samples in addition to those for terrestrials samples [15]. These curves mapped the ^{14}C ages of marine samples back 9000 years [15]. They also mapped out differences in the global reservoir age (R) of the deep ocean over the last 6000 years, which reflects the offset in ^{14}C age between the ocean and the atmosphere.

Using a marine calibration curve for marine samples accounts for the variability in the global marine reservoir age over time. As with the atmospheric curves, these curves are updated every few years, with the most recent curves being released in 2009, 2013, and 2020 [7–11].

Local marine reservoir corrections

Stuiver and Pearson's analysis of marine ^{14}C dates included two calibration curves, one for deep ocean waters, and one for the mixed surface waters [15]. There are no longer separate curves for deep ocean waters and surface waters, but this additional offset can be accounted for by applying a local marine reservoir correction (ΔR).

For samples that have a partially or fully marine signature, an additional local marine reservoir correction is necessary. Local variability in the mixing of deep ^{14}C depleted seawater with surface waters, often called upwelling patterns, results in the deviation of local marine ^{14}C signatures from that of the global marine reservoir. The local marine reservoir correction ΔR takes into account these local marine conditions and is applied prior to calibrating the F14C measurement to the appropriate marine calibration curve. More details on the effects of ΔR on calibration are discussed in Appendix B.

There are several databases available that compile many ΔR values: the 14CHRONO online database through Queen's University Belfast University (http://calib.org/marine/)

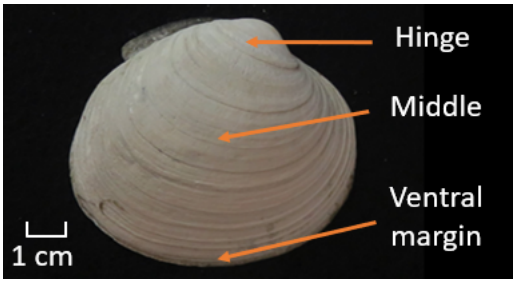

Figure 3.1: Sampling locations for ^{14}C on the shell of *S. gigantea*.

[12], and data from a 2006 publication by the Geological Survery of Canada (GEOSCAN) available through geoscan.nrcan.gc.ca [16].

3.3 Experimental details

Dr. Meghan Burchell, Anna Sparrow, and I used mollusk shells from Deep Bay (DiSe-7) and Comox (DkSf-20), two archaeological shell midden sites located on Vancouver Island, British Columbia, for the ^{14}C analysis. Samples in which we detected calcite were not used for ^{14}C analysis as this indicates the likely presence of non-original carbon and would diminish confidence in the ^{14}C measurements.

We cleaned the shells with water, and any surface contaminants that could easily be detected by eye were removed with a handheld Dremel tool. The inner remineralized layer of the shell was removed by the Dremel tool. The outermost proteinaceous layer of the shell, the periostracum, does not preserve well, but any suspected remnants of this layer were also removed with the Dremel tool so that only the crossed lamellar layer reamined.

We investigated intrashell variation using three shells: two from Deep Bay (DiSe-7) and one from Comox (DkSf-20). Sampling locations on the shells of *S. gigantea* are shown in Figure 3.1. Samples roughly 1cm by 1cm were cut from the ventral margin, the hinge, and the center portion of the shell. For all other shell samples,

only a sample was cut from the ventral margin. To get an acceptable amount of carbon for the AMS measurement, samples of $CaCO_3$ between 1-3 mg are required, which corresponds to about 0.4 mg of carbon. In this chapter, I display measurements from the three shells selected to analyze intrashell variation. Additional dates were obtained from other shells, with one measurement per shell, and these are displayed in Appendix B as they do not contribute to the discussion on intrashell variability.

The following steps, outlined in detail in [17], were done with direction from the Lalonde laboratory staff. Each of the samples were etched in HCl acid to remove the outer 20% of shell material, which would likely contain any contaminated carbonate or surface contaminants. The shell carbonate samples were crushed using a mortar and pestle and reacted with H_3PO_4 (phosphoric acid) via

$$2H_3PO_4 + 3CaCO_3 \longrightarrow 3CO_2 + Ca_3(PO_4)_2 + 3H_2O. \tag{3.3}$$

After allowing the reaction to occur over night, the CO_2 is collected and purified by means of a glass vacuum extraction line in order to obtain the pure CO_2. The purified CO_2 was sealed in a breakseal and we proceeded to the graphitization step.

Finally, the CO_2 collected in the breakseal was graphitized by the addition of hydrogen gas in a semi-automated graphitization line following

$$2H_2 + CO_2 \longrightarrow 2H_2O + C, \tag{3.4}$$

in the presence of iron and hydrogen. The water vapour is pumped away, leaving only the carbon. This process allows for the collection of elemental carbon from the $CaCO_3$ in the form of graphite, which is then analyzed by the AMS system [17]). Through this sample preparation process and particularly through the reaction with H_3PO_4, most if not all proteinaceous components of the shell are removed. Therefore

the elemental carbon that is collected is primarily from the mineral portion of the shell. I also note that the procedure used to prepare the samples is specific to the Lalonde laboratory and that different labs may have their own unique set of protocols for the treatment of shell carbonate [18, 19].

The laboratory technicians ran the graphite (carbon) samples in the AMS system and applied the appropriate corrections which I discuss in the next subsection. Details on the mass spectrometer are mentioned in Appendix B.

3.3.1 Corrections and Calibration

In this subsection I outline the corrections that were made to the AMS measurements to obtain the F14C measurements as well as details on the local marine reservoir correction and calibration used for our shell samples.

Standards and measurement corrections

Fractionation is the process whereby the ratios of the isotopes of carbon - $^{13}C/^{12}C$ and $^{14}C/^{12}C$ - are altered from their natural ratios as they are incorporated into living organisms. The process of fractionation ultimately alters the abundance of ^{14}C in an organism. A similar process of fractionation also occurs due to the AMS measurement preparations and procedure. The type of fractionation due to the AMS measurements themselves is called machine fractionation.

Both types of fractionation can be accounted for comparing the $\delta^{13}C$ ($^{13}C/^{12}C$) values between the sample and a standard. Pee Dee Belemnite is the standard used to correct for fractionation. Details on this calculation are covered in Appendix B.

As mentioned in Section 3.2, to calculate F14C the activity of the sample must be compared to that of a standard. Oxalic acid is used as the international standard against which all ^{14}C measurements are made. The oxalic acid standard is used in

the calculation of F14C as follows

$$F^{14}C = \frac{(^{14}\mathrm{C}/^{12}\mathrm{C})_{sample}}{(^{14}\mathrm{C}/^{12}\mathrm{C})_{oxalicacid}}. \tag{3.5}$$

In this calculation, both measurements on the sample and the oxalic acid standard have been corrected for fractionation. This calculation is also done at the Lalonde AMS laboratory and the F14C measurements in this chapter have been corrected according to the appropriate standards and the errors due to fractionation are minimal.

Calibration and local marine reservoir corrections

I calibrated all dates in the free ^{14}C calibration program, Oxcal, using the 2013 calibration curves [20]. I also note that this analysis was done prior to the release of the 2020 calibration curves and that the updated curve has no effect on the F14C values.

The Lalonde AMS lab uses ΔR values from the 14CHRONO database [12] unless supplied a specific value by the researchers submitting the samples. Upon receiving the F14C data from the lab, I used a ΔR of 226$\pm$70 for the calibration of my samples. This value was calculated in 2017 by Carlson et al. [21] using archaeological bone with a predominantly marine signature from Pender Island, British Columbia. This site is located on the southernmost edge of Vancouver Island, about 160 km from Deep Bay and Comox.

While this ΔR value is not from the same exact geographic region as our shell samples, it is from roughly the same time frame as our samples. The only ΔR values calculated for Deep Bay and Comox specifically are modern; they were calculated using live-collected mollusks in 2006 [16]. The effect of the choice of ΔR typically just results in a shift in calibrated age ranges. This is discussed more in Appendix B.

3.4 Results

The shells were sampled at three different locations along the axis of growth to study the intrashell variation in ^{14}C content. Sampling locations presented here show the ^{14}C content in the crossed lamellar layer of aragonite. This layer contains primarily DIC and was deposited at the time of biomineralization and likely does not contain any signatures of metabolic carbon.

The data presented in Table 3.1 displays each sample having a sample name which was assigned to them by the Burchell Lab group, and each having a lab ID which was assigned to them by the Lalonde AMS laboratory. I will refer to the samples by their sample name.

3.4.1 Uncalibrated Measurements

Table 3.1: Fraction of modern carbon (F14C) measurements for three *Saxidomus gigantea* bivalve mollusks from Deep Bay and Comox, British Columbia

shell ID	sample name	sampling location	F14C
DiSe7_1	DiSe7_1M	margin	0.817(2)
	DiSe7_1C	center	0.812(2)
	DiSe7_1H	hinge	0.808(2)
DiSe7_2	DiSe7_2M	margin	0.851(2)
	DiSe7_2C	center	0.852(2)
	DiSe7_2H	hinge	0.849(2)
DkSf20	DkSf20_M	margin	0.760(2)
	DkSf20_C	center	0.759(2)
	DkSf20_H	hinge	0.759(2)

Only the F14C values are reported in Table 3.1. This is the raw data obtained from the AMS measurement prior to calibration. Comparing the intrashell measurements, only one of the three shell samples, DiSe7_1 (DiSe7_1M, DiSe7_1C, and DiSe7_1H) shows different F14C values within their uncertainties. For the other two shells, the

F14C values overlap and are not considered significantly different.

The F14C values are not usually of interest to archaeologists because they are not an age measurement, but rather reflect the raw amount of ^{14}C in the shell carbonate. However, this measurement is valuable for to look at because rather than being concerned with the age range associated with each portion of the shell, I am more concerned with looking at the variation in the amount of ^{14}C throughout the shell. It is clear from looking at Table 3.1 that the intrashell measurements are only significantly different for one of the three shell samples - DiSe7_1.

The DiSe7_1 samples show greater F14C at the margin of the shell and, according to the three measurements shown here, consistently decrease in F14C as the sampling location approaches the hinge region. To analyze this variation, it is necessary to consider the basic growth patterns of these shells: they grow outwardly from the hinge to the ventral margin. Considering that the carbonate at the ventral margin was biomineralized after the carbonate at the hinge, and is thus younger than the carbonate at the hinge, I would generally expect a slightly larger F14C in the ventral margin portion of the shell, similar to the pattern displayed in the DiSe7_1 shell.

Considering what I know about growth patterns and more specifically that the carbonate at the ventral margin was deposited after the carbonate at the hinge, I would actually expect to see a pattern similar to the one seen in the data from the DiSe7-1 shell, where the F14C measurement on the carbonate at the ventral margin is larger than that at the hinge, which translates into the hinge region containing older carbon than the margin. The nuances of this point are discussed in more detail in Section 3.4.3.

Analyzing the raw F14C measurements is helpful for identifying variability in the content of ^{14}C throughout the shell, however it does not provide a full picture of intrashell variability. To analyze the intrashell ^{14}C variability in more depth, I must

also consider the calibrated dates.

3.4.2 Calibrated Dates

In a sense, looking at raw F14C measurements is beneficial because it allows the researcher to ask questions directly about the amount of ^{14}C in the sample and whether it differs significantly throughout the shell. However, calibration is necessary to account for fluctuations in the global carbon reservoir and obtain age ranges, and both F14C measurements and calibration must be used together to make environmental or oceanographic interpretations.

In this subsection I calibrate the ^{14}C dates to both the marine and atmospheric calibration curves. To be absolutely clear, this is a purely illustrative exercise to show the importance of the correct choice of calibration curve. The marine mollusk shell studied here may contain a small atmospheric signature, being that the mollusks live in an intertidal zone. For that reason, the correct choice of calibration curve may be some combination of marine and atmospheric curves. Determining what proportion of a sample's ^{14}C signal may be marine and what proportion may be atmospheric is a standard procedure that involves comparing the carbon-13 isotope of the sample to that of two other samples: one known to be fully marine and one known to be fully terrestrial. Dr. Meghan Burchell, Anna Sparrow, and I were unable to complete this calculation because we did not have the suitable fully marine and fully terrestrial samples.

In Table 3.2 the F14C measurements are reported with their uncertainties, and dates are calibrated to both the Marine13 curve and the atmospheric IntCal13 curve. The dates are reported in calibrated years before 1950, also referred to as years before present (cal BP), as per ^{14}C dating conventions [1]. I emphasize strongly that no interpretation should be made on the dates obtained using the atmospheric curve.

Table 3.2: Marine and atmospheric calibrated ages for the intrashell 14C measurements of *Saxidomus gigantea* bivalve mollusks from Deep Bay and Comox, British Columbia. A ΔR of 226$\pm$70 is used for the Marine13 calibration.

sample name	F14C	Marine13 (cal BP)	IntCal13 (cal BP)
DiSe7_1M	0.817(2)	1130-770 (95.4%)	1567-1476 (65.9%), 1465-1415 (29.5%)
DiSe7_1C	0.812(2)	1175-824 (95.4%)	1686-1677 (2.0%), 1620-1531 (93.4%)
DiSe7_1H	0.808(2)	1221-899 (95.4%)	1698-1645 (35.3%), 1639-1560 (60.1%)
DiSe7_2M	0.851(2)	769-515 (95.4%)	1288-1228 (64.7%), 1210-1182 (30.7%)
DiSe7_2C	0.852(2)	758-609 (95.4%)	1285-1220 (60.7%), 1215-1181 (34.7%)
DiSe7_2H	0.849(2)	784-519 (95.4%)	1293-1235 (74.6%), 1207-1185 (20.8%)
DkSf20_M	0.760(2)	1711-1346 (95.4%)	2309-2219 (57.4%), 2213-2149 (38.0%)
DkSf20_C	0.759(2)	1735-1360 (95.4%)	2315-2152 (95.4%)
DkSf20_H	0.759(2)	1742-1365 (95.4%)	2320-2290 (14.3%), 2276-2153 (81.1%)

When calibrated to the marine curve, the ΔR of 226$\pm$72 is applied as the local marine reservoir correction [21]. The error on the ΔR value is only reflective of the error on the value that was calculated by Carlson et al. [21] using marine and terrestrial bone pairs from Pender Island, British Columbia. There are likely additional errors pertaining to the fact that the samples used to calculate this ΔR value may have been subject to slightly different oceanographic conditions than those that were analyzed in this work from other areas in the Salish Sea. Quantifying the errors associated with ΔR in this case is beyond the scope of this thesis, but would be a valuable exercise to conduct in a future study, perhaps by following a similar approach to Martindale et al. [22] that compares all of the available ΔR measurements from the surrounding region where the samples were collected. This is discussed in more detail in Appendix B. The application of the ΔR correction to the marine calibration is completed automatically in the OxCal program and uses a Markov chain Monte Carlo algorithm to complete the subtraction. Details on the mathematics behind this calculation can be found in the OxCal manual [23].

I present both choices of calibration to illustrate the two extreme possibilities

for what the calibrated age ranges of our samples could be. The majority of these samples happen to have F14C values that fall on a particularly flat, wiggly portion of the IntCal13 curve, which is why the calibrated ranges in the last column have multiple modes (see Figure 3.2). Generally, the use of a terrestrial curve over a marine curve will result in a shift in the dates to older values, because of the global marine reservoir, but as shown in Table 3.2 it can also result in multiple ranges of probability. In other words, the probability range becomes bimodal or multimodal. Ultimately, this may expand the uncertainty in the possible age of the sample.

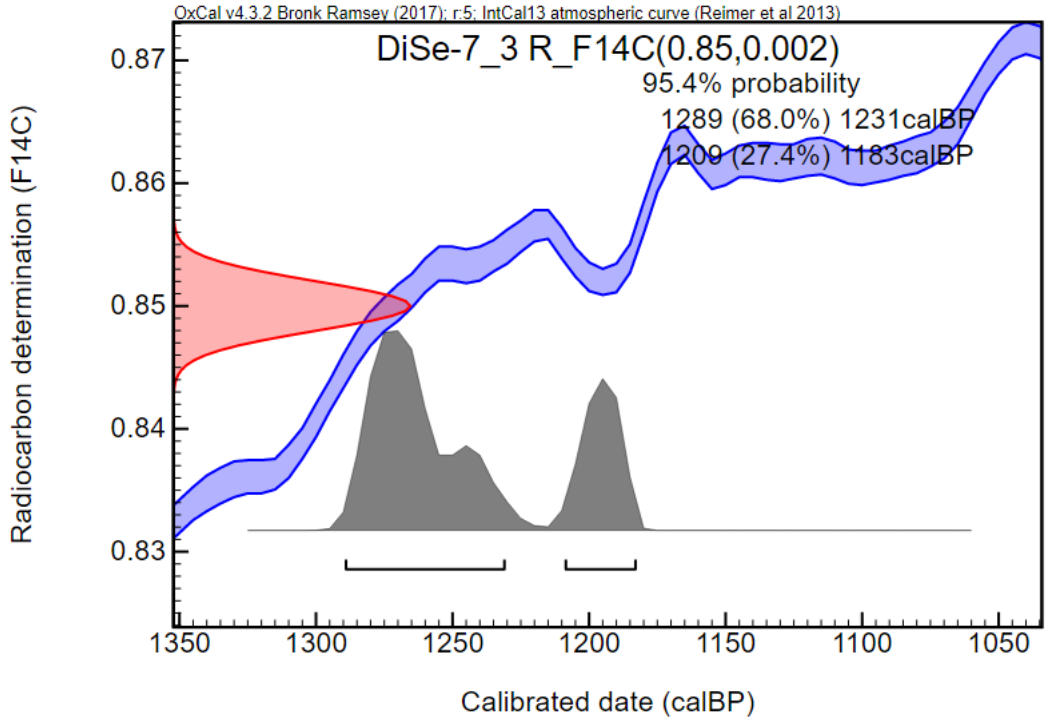

Figure 3.2: Calibration of a ^{14}C measurement from a shell sample from DiSe-7 to the IntCal13 curve.

Looking only at the age ranges as opposed to looking at the F14C values to understand intrashell ^{14}C variability can also be slightly misleading. Note that the F14C measurements for samples DiSe7_1M, DiSe7_1C, DiSe7_1H do not overlap within their uncertainties, but when these F14C measurements are calibrated, their

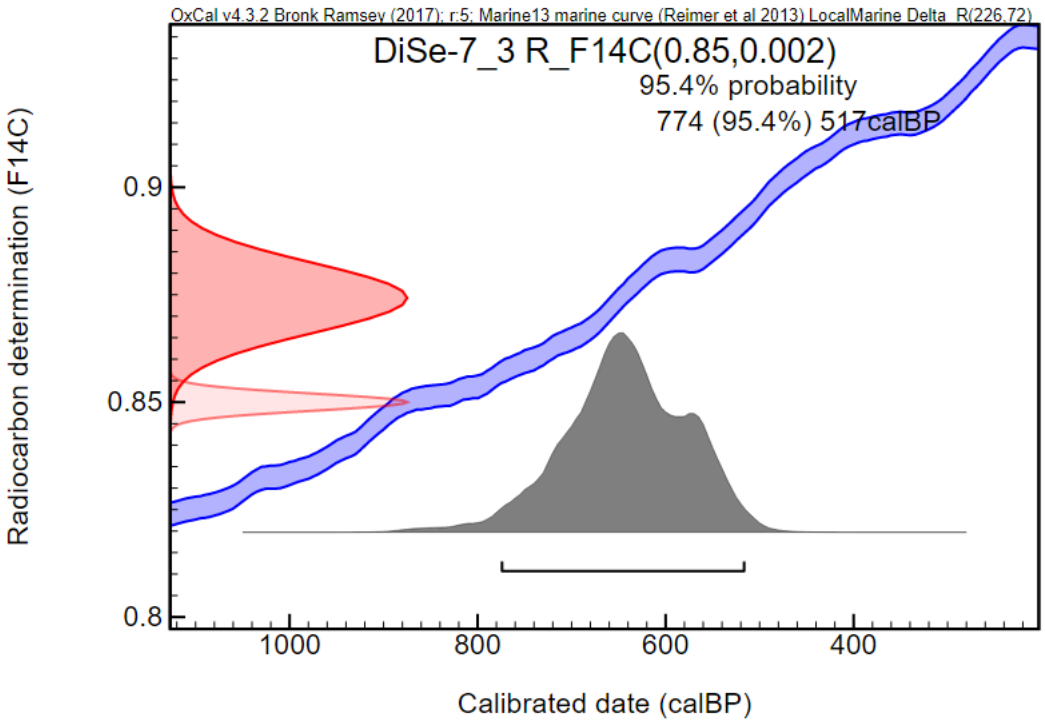

Figure 3.3: Calibration of a ^{14}C measurement from a shell sample from DiSe-7 to the Marine13 curve. With the ΔR of 226$\pm$72, as reported by Lalonde. Note that the lightly shaded gaussian on the y-axis represents the F14C measurement after the ΔR has been applied.

calibrated ranges do overlap. However, simply noting that the ranges overlap is also a simplification.

When looking at the calibrated age ranges written out in a table, the complexity of these probability distributions is not clear. I calibrated these dates to the 95.4% probability range, meaning that the real age of the sample has a 95.4% chance of falling within the calibrated ranges presented. Calibrating to this probability range is commonly referred to as calibrating to 2σ, even though the final probability distribution is not Gaussian. Figures 3.2 and 3.3 show what the probability distributions look like for both the atmospheric and marine calibrations, respectively. All three of the intrashell measurements for the DiSe7_1 samples are shown calibrated to the marine curve in Figure 3.5 and to the atmospheric curve Figure 3.4. Note that the

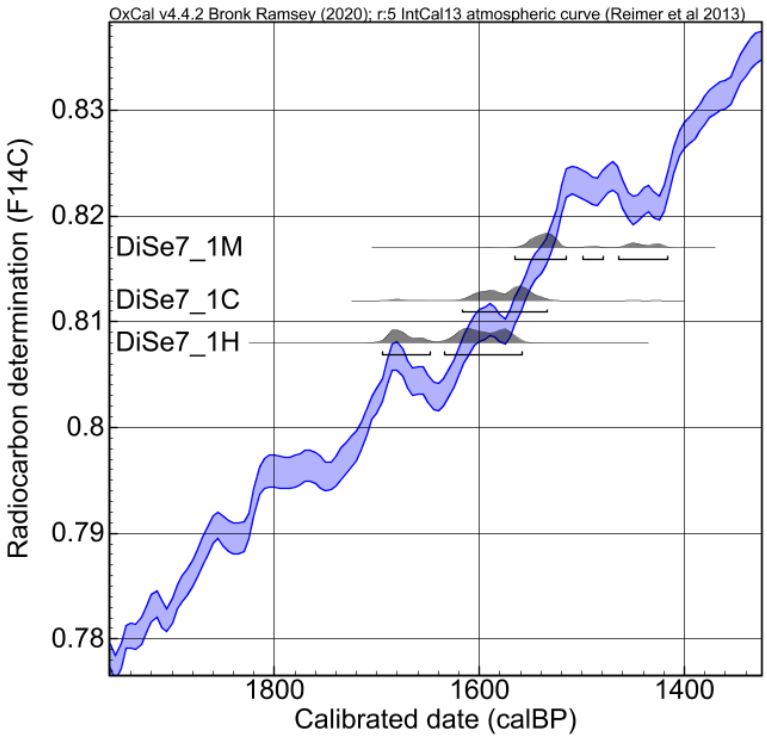

Figure 3.4: Intrashell ^{14}C dates from DiSe7-1 calibrated to the IntCal13 atmospheric curve.

F14C is modeled as a Gaussian distribution, but because the calibration is a non-linear transformation, after computing the calibrated age range the distribution is no longer Gaussian. Within the 2σ calibrated range, there are regions where the real age of the sample has a higher probability of falling and regions where the real age has a lower probability of falling. This is a product of the method of calibrating dates that is built into OxCal. The mathematical details behind OxCal calibration, which uses Bayesian analysis and Markov chain Monte Carlo analysis to determine these probabilities, is outlined in the OxCal manual [23].

Considering both F14C and calibrated age ranges illustrates how different the picture of intrashell variability is from looking at a raw F14C measurement compared to calibrated age ranges. The picture of variability goes from three intrashell F14C measurements, which are simply three numbers with a $\pm$ attached to them, to the

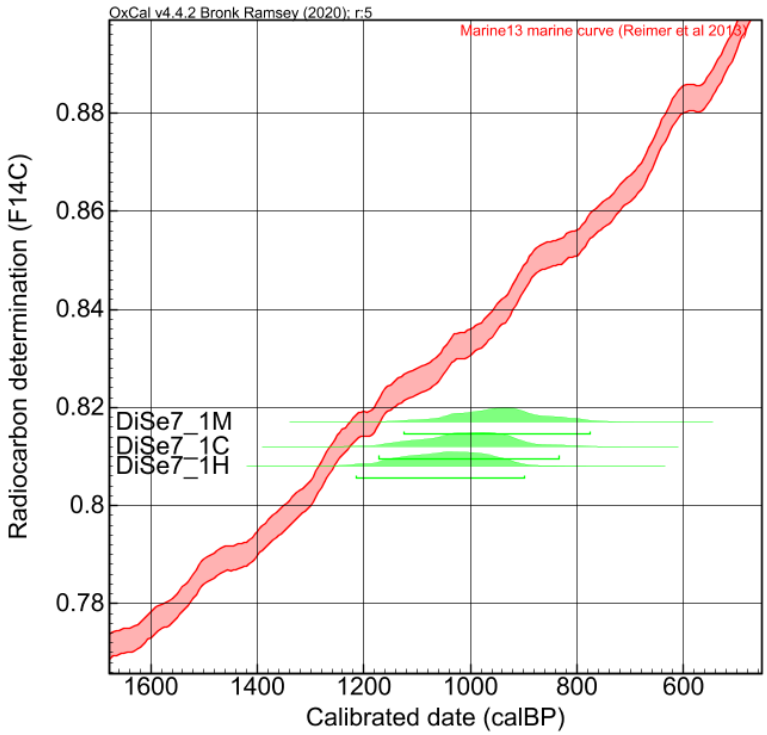

Figure 3.5: Intrashell ^{14}C dates from DiSe7-1 calibrated to the Marine13 marine curve.

calibrated ranges which are non-Gaussian probability distributions that represent the possible ages of the three different shell samples.

The reason that calibration results in a more complex probability distribution for the calibrated age ranges is the variability in the global carbon reservoir and environmental conditions. That variability, on a global scale, is captured in the calibration curves. In this thesis work, I do not intend to make any interpretations on environmental conditions, upwelling conditions, or the archaeological significance of these dates, but in the next section I illustrate why looking at the complex calibrated age ranges is important for understanding intrashell variability.

3.4.3 What Does it Mean for ^{14}C Measurements to be "Different"?

The question that would be useful to answer is whether or not the variation or lack thereof in the F14C measurements is expected based on the ontogenetic growth of the mollusk and fluctuations in the marine carbon reservoir throughout that period of growth. In this subsection, I explore how the F14C and the calibrated age ranges can be used together to obtain a more complete and accurate understanding of intrashell ^{14}C variation.

The calibration curves take into account variations in the global carbon reservoir, which can allow for there to have been multiple moments in time when the F14C signal in the environment was the same. To work around this, the key is to not have to rely on the ^{14}C measurements of my samples to determine their age. If I knew, either by having a known collection year or another secure ^{14}C measurement on a different sample, what the age of my sample was, and I also knew my shell to have a 100% marine signature, I could do a simple reverse calibration to determine the expected range of F14C within the shell. For example, if I knew my shell sample was 600 years old, I could do a reverse calibration using 600 years BP as the age, and work backwards to get a corresponding range of expected F14C values for my sample. If I know what the ΔR for the region is, then I can apply that to my expected F14C value and compare that computed expected F14C value for my sample, with the value that I measured experimentally.

Within that analysis method I could further account for intrashell variation by consulting sclerochronologists to determine the ontogenetic age of the mollusk, and work backwards to determine the difference in age between the three sampling locations at the hinge, middle, and ventral margin to get three corresponding expected

F14C measurements. This type of analysis would give a concrete way to analyze how much my measured F14C values deviate from the expected values. Unfortunately, I cannot do this analysis exactly because I do not know the exact age of my samples. However, I will use reasonable assumptions about my samples to demonstrate how this type of analysis would work.

While I do not know the exact ontogenetic age of my samples, I do know that *S. gigantea* has a lifespan of about 20-25 years [24] and so I assume my samples are no older than this. I also know that the $CaCO_3$ deposited at the ventral margin - the region of most recent growth - was deposited after the $CaCO_3$ at the hinge. Considering only the growth of these bivalves, I would expect to see a higher F14C value at the ventral margin and more depleted F14C value at the hinge. I would also assume that the longer the lifespan of an individual mollusk, the more pronounced the differences in F14C measurements throughout the shell.

However, because of the amount of sample needed for a ^{14}C measurement, it is not possible to sample within a single growth line, i.e. a single year of growth. There is likely no more than roughly 5 years of growth that is averaged over in each of the intrashell measurements. The amount of material which is analyzed is effectively time averaged, which likely also affects how pronounced the differences in the ^{14}C measurements will be [25]. For my illustrative example, I will ignore the effects of time averaging.

Based on the reasonable assumptions made above, I chose three calendar dates, each separated by about 10 years, that would theoretically correspond to three intrashell dates sampled in the same way that Dr. Burchell, Anna Sparrow, and I sampled ours for this study.

These three intrashell samples do not have the same age as each other, but when we project them up onto the calibration curves and then over onto the y axis, we see

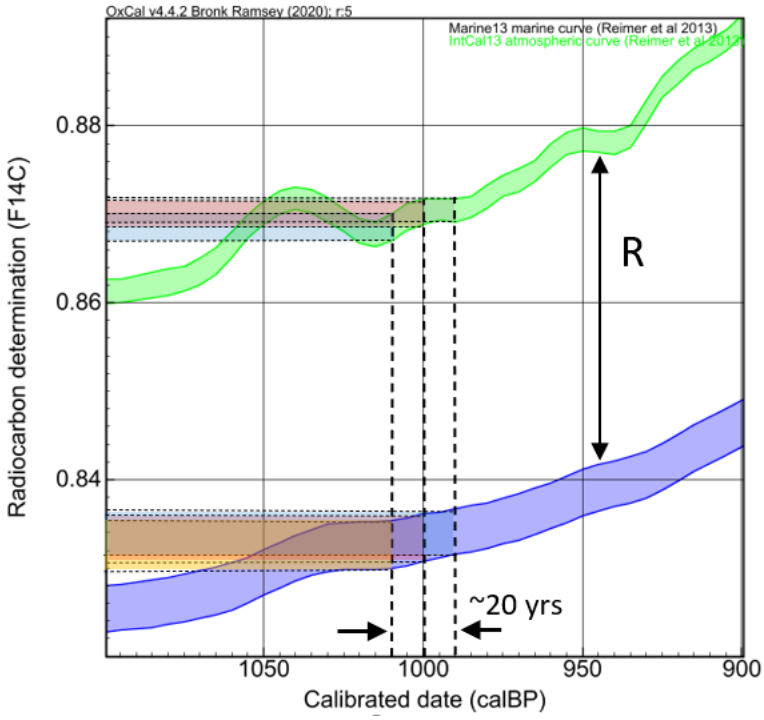

Figure 3.6: Illustration of how an age difference does not necessarily correspond to differences in F14C measurements

that the F14C ranges overlap (see Figure 3.6). The measurements used to construct the calibration curves themselves also have measurement errors attached to them, which is why the curve is a thick line. To get an estimate of what the expected F14C values would be, I use a variation of intercept method. This entails mapping the dates on the x-axis in Figure 3.6 up to the calibration curve and marking the two points of intersection with the curve, at the bottom edge and the top edge, and then projecting these intersection points over to the y-axis to determine the corresponding F14C value. The intercept method is not generally recognized as a good method for calibrating F14C measurement [26], but here I only use it as a method of qualitative analysis in working backwards from a known age.

A function is available in Oxcal, called R_simulate, which finds the appropriate equivalent F14C measurement for a calendar age input, similar to what I described

above, and then calibrates that modeled F14C measurement to obtain probability ranges for the calibrated date.

The illustration presented above of my approach to understanding what it means for intrashell measurements to be "different" highlights that, given our samples are roughly 20 years old, I would not actually expect there to be much of a spread in the F14C measurements. The spread in the F14C values is dictated by the age of the sample, as this will shift the portion of the calibration curve, whether bumpy or smooth, that the age values intersect with. I reiterate that this is why independent time measurements, which effectively anchor which portion of the curve is used, would be necessary to complete the reverse calibration analysis process accurately.

Looking at my data through this lens, it seems as though the measurements on the DiSe-7 sample are somewhat problematic, because even for a shell that is about 20 years old, I would not expect to see much variation in the F14C values. Given that the previous chapter centered around using infrared spectroscopy to identify which samples were suitable for ^{14}C dating and identifying any traces of aragonite that were not pristine, your first thought might be that these aragonitic samples were not pristine and have some kind of diagenetic signature. I am unable to completely rule this out because diagenesis can affect samples in unpredictable ways, and due to the limitations on experiments because of the pandemic, I was not able to conduct an in depth investigation of possible diagenetic alterations to the shell. It is also possible that there was some variation in environmental conditions, possible upwelling which would result in the need for a different ΔR value to analyze the samples. A more detailed discussion on the consequences of ΔR is discussed in Appendix B.

3.5 Summary

Three shells of *S. gigantea* from Comox and Deep Bay, British Columbia were analyzed for ^{14}C at three locations within the crossed lamellar portion of the shell: the hinge, the middle, and the ventral margin. Out of the three shells, only one showed a significant difference in the uncalibrated F14C measurements. Comparing the calibrated age ranges to understand intrashell variability is challenging because of the complicated non-uniform distribution of these age ranges and the possibility of the calibrated ranges being bimodal. However, using a simple illustrative example in which the age of a shell is already known, it is possible to compute expected F14C values for the samples. This demonstrated that a lack of intrashell variability is not unusual and is expected, especially when dealing with samples with a short ontogenetic age compared to that of the lifetime of carbon-14. The variation in one of the three samples could be due to undetected diagenesis, although more likely it is due to variable environmental conditions, particularly upwelling, which would necessitate a unique ΔR for that portion of the shell. More details on ΔR are presented in Appendix B.

Bibliography

[1] W. F. Libby. Radiocarbon Dating. *Science*, 133(3453):621–629, 1961.

[2] W. Kutschera. The Half-Life of ^{14}C—Why Is It So Long? *Radiocarbon*, 61(5):1135–1142, 2019.

[3] J. R. Arnold and W. F. Libby. Age Determinations by Radiocarbon Content : Checks with Samples of Known Age. *Science*, 110(2869):678–680, 1949.

[4] H. E. Suess. Bristlecone Pine Calibration of the Radiocarbon Time Scale from 4100 B.C. to 1500 B.C. In International Atomic Energy Agency, editor, *Radioac-*

tive Dating and Methods of Low-Level Counting, pages 143–151. International Atomic Energy Agency.

[5] M. Stuiver and G. W. Pearson. High-Precision Calibration of the Radiocarbon Time Scale, AD 1950-500 BC. *Radiocarbon*, 28(2B):805–838, 1986.

[6] G. W. Pearson and M. Stuiver. High-Precision Calibration of the Radiocarbon Time Scale, 500-2500 BC. *Radiocarbon*, 28(2B):839–862, 1986.

[7] J. van der Plicht, C. Bronk Ramsey, T. J. Heaton, E. M. Scott, and S. Talamo. Recent Developments in Calibration for Archaeological and Environmental Samples. *Radiocarbon*, 4(62):1095–1117, 2020.

[8] T. J. Heaton, M. Blaauw, P. G. Blackwell, C. Bronk Ramsey, P. J. Reimer, and E. M. Scott. The intcal20 approach to radiocarbon calibration curve construction: A new methodology using bayesian splines and errors-in-variables. *Radiocarbon*, 62(4):821–863, 2020.

[9] P. J. Reimer, W. E. N. Austin, E. Bard, A. Bayliss, P. G. Blackwell, C. Bronk Ramsey, M. Butzin, H. Cheng, R. L. Edwards, M. Friedrich, P. M. Grootes, T. P. Guilderson, I. Hajdas, T. J. Heaton, A. G. Hogg, K. A. Hughen, B. Kromer, S. W. Manning, R. Muscheler, J. G. Palmer, C. Pearson, J. Van Der Plicht, Ron W. Reimer, D. A. Richards, E. M. Scott, J. R. Southon, C. S. M. Turney, L. Wacker, F. Adolphi, U. Büntgen, M. Capano, S. M. Fahrni, A. Fogtmann-Schulz, R. Friedrich, P. Köhler, S. Kudsk, F. Miyake, J. Olsen, F. Reinig, M. Sakamoto, A. Sookdeo, and S. Talamo. The IntCal20 Northern Hemisphere Radiocarbon Age Calibration Curve (0-55 cal kBP). *Radiocarbon*, 62(4):725–757, 2020.

[10] P. J. Reimer, E. Bard, A. Bayliss, J. W. Beck, P. G. Blackwell, C. Bronk Ramsey, C. E. Buck, H. Cheng, R. L. Edwards, M. Friedrich, P. M. Grootes, T. P. Guilderson, H. Haflidason, I. Hajdas, C. Hatté, T. J. Heaton, D. L. Hoffmann, A. G. Hogg, K. A. Hughen, K. F. Kaiser, B. Kromer, S. W. Manning, M. Nium, R. W. Reimer, D. A. Richards, E. M. Scott, J. R. Southon, R. A. Staff, C. S. M. Turney, and J. van der Plicht. Intcal13 and Marine13 Radiocarbon Age Calibration Curves 0–50,000 Years Cal BP. *Radiocarbon*, 55(4):1869–1887, 2013.

[11] P. J. Reimer, M. G. L. Baillie, E. Bard, A. Bayliss, J. W. Beck, P. G. Blackwell, C. Bronk Ramsey, C. E. Buck, G. S. Burr, R. L. Edwards, M. Friedrich, P. M. Grootes, T. P. Guilderson, I. Hajdas, T. J. Heaton, A. G. Hogg, K. A. Hughen, K. F. Kaiser, B. Kromer, F. G. McCormac, S. W. Manning, R. W. Reimer, D. A. Richards, J. R. Southon, S. Talamo, C. S.M. Turney, J. van der Plicht, and C. E. Weyhenmeyer. IntCal09 and Marine09 radiocarbon age calibration curves, 0-50,000 years CAL BP. *Radiocarbon*, 51(4):1111–1150, 2009.

[12] P. J. Reimer. 14 Chrono Marine Reservoir Correction Database. `http://calib.org/marine/`, 2020.

[13] P. K. Swart. The geochemistry of carbonate diagenesis: The past, present and future. *Sedimentology*, 62(5):1233–1304, 2015.

[14] T. A. McConnaughey and D. P. Gillikin. Carbon isotopes in mollusk shell carbonates. *Geo-Marine Letters*, 28(5-6):287–299, 2008.

[15] M. Stuiver, G. W. Pearson, and T. Braziunas. Radiocarbon Age Calibration of Marine Samples Back to 9000 Cal YR BP. *Radiocarbon*, 28(2B):980–1021, 1986.

[16] R. McNeely, A. S. Dyke, and J. R. Southon. Canadian marine reservoir ages, preliminary data assessment, Open File 5049:3. *Geological Survey Canada*, 2006.

[17] C. A. Crann, S. Murseli, G. St-Jean, Z. Xiaolei, C. D. Ian, and W. E. Kieser. First status report on radiocarbon sample preparation techniques at the A. E. Lalonde AMS Laboratory (Ottawa, Canada). *Radiocarbon*, 59(3):16–20, 2017.

[18] T. D. J. Knowles, P. S. Monaghan, and R. P. Evershed. Radiocarbon Sample Preparation Procedures and the First Status Report From the Bristol Radiocarbon AMS (BRAMS) Facility. *Radiocarbon*, 61(5):1–10, 2019.

[19] G. M. Santos, R. B. Moore, J. R. Southon, S. Griffin, E. Hinger, and D. Zhang. AMS C Sample Preparation At the KCCAMS / Uci Facility : Status. *Radiocarbon*, 49(2):255–269, 2007.

[20] C. B. Ramsey. Oxcal 4.4. `https://c14.arch.ox.ac.uk/oxcal.html`, 2021.

[21] R. Carlson, P. Szpak, and M. Richards. The Pender Canal Site and the Beginnings of the Northwest Coast Cultural System. *Canadian Journal of Archaeology*, 41(1):1–29, 2017.

[22] A. Martindale, G. T. Cook, I. Mckechnie, K. Edinborough, I. Hutchinson, M. Eldridge, K. Supernant, and K. M. Ames. Estimating marine reservoir effects in archaeological chronologies: Comparing Δr calculations in Prince Rupert harbour, British Columbia, Canada. *American Antiquity*, 83(4), 2018.

[23] Christopher Bronk Ramsey. *OxCal 4.4 Manual*. 1 South Parks Road.

[24] T.C. Hiebert. Saxidomus giganteus. In T. C. Hiebert, B. A. Butler, and A. L. Shanks, editors, *Oregon Estuarine Invertebrates: Rudys' Illustrated Guide to Common Species*. University of Oregon Libraries and Oregon Institute of Marine Biology, Charleston, OR, 3rd edition, 2015.

[25] K. Douka, T. F. G. Higham, and R. E. M. Hedges. Radiocarbon dating of shell carbonates: old problems and new solutions. *Munibe*, 31:18 – 27, 2010.

[26] R. J. Telford, E. Heegaard, and H. J. B. Birks. The intercept is a poor estimate of a calibrated radiocarbon age. *Holocene*, 14(2):296–298, 2004.

Chapter 4

Discussion

While the infrared (IR) spectroscopy and ^{14}C measurements probe two fundamentally different parts of the shell $CaCO_3$, using both methods in conjunction can provide some valuable insights. In this chapter I discuss the use of IR spectroscopy in screening biogenic $CaCO_3$ from the bivalve mollusk *S. gigantea* for diagenesis and some of the challenges associated with this. I then consider how to grapple with the relative intensity differences seen in the IR data and what implications this might have for the ^{14}C analysis. This is followed by a discussion of the limitations of sampling strategies for studying ^{14}C in marine shell.

4.1 Screening for Diagenesis

Prior to ^{14}C dating any sample, screening the sample for diagenesis is crucial to ensure that the sample is pristine and that no non-original carbon is present. This is necessary to ensure that the ^{14}C measurement truly reflects the age of the sample. Diagenesis, as mentioned earlier, is any process that results in a change in the sample, whether it may be on the atomic, microscopic, or macroscopic scale, after its formation process is completed. In the case of mollusk shells, this is any process that alters the shell

$CaCO_3$ after biomineralization is complete.

In this research, I am primarily concerned with detecting the form of diagenesis that results in the recrystallization of aragonite into calcite. Recrystallized calcite is easily detected by IR spectroscopy. The presence of calcite is confirmed by the presence of only a single ν_4 peak (opposed to a doublet ν_4 peak, which indicates aragonite) and a shift in the ν_2 peak toward a higher wavenumber. The ν_1 peak is absent in pure calcite samples, but since diagenetically altered samples often end up being a mixture of calcite and aragonite, a ν_1 peak is usually present. Although I consider the possibility of recrystallization of the original aragonite as an aragonite with different crystallinity or more subtle changes in the lattice, I cannot confidently detect this type of diagenesis using only IR spectroscopy. However, previous work has shown that this aragonite-aragonite recrystallization only occurs in aquatic environments with exceptionally high Mg to Ca or Sr to Ca ratios [1, 2] - both high magnesium and high strontium would be detectable in IR spectra by shifts in the ν_2 and ν_4 peaks. Thus, it seems unlikely that this type of recrystallization affects my samples.

When aragonite is dissolved and recrystallized as calcite, this may affect the ^{14}C measurement [3, 4]. It is not the difference in polymorph (aragonite vs. calcite) that directly affects the ^{14}C signature, but rather the fact that the presence of calcite indicates the dissolution of the original $CaCO_3$ and the recrystallization of new $CaCO_3$ that may incorporate new carbon, and thus a ^{14}C signature that does not reflect the age of the shell. However, even if we know that diagenesis has affected a sample, this does not mean that we know how it affects the F14C. For example, Lindauer et al. [5] study the effect of heating and cooking on the ^{14}C content of mollusk shells from the United Arab Emirates. The authors confirmed the resulting diagenesis using Raman spectroscopy and analyzed the microstructures using scanning electron microscopy. Both experimental techniques showed evidence of heating. However, even in shells

that visually appear burnt and display mineralogical conversions of aragonite to calcite, the effects on the ^{14}C measurements were minuscule.

In using IR spectroscopy to detect changes in our samples apart from the presence of calcite, we used an approach similar to that of other studies that relied heavily on analyzing peak positions to detect changes in the composition of the aragonite. In a study by Guzman et al. [6], the authors interpret diagenesis as changes in ionic substitutions in the crystal lattices of calcite and aragonite from fossil *Concholepas* shell. Their approach utilizes Diffuse Reflectance Infrared Fourier Transform Spectroscopy (DRIFTS) and stable isotope measurements to study geochemical signatures of diagenesis. The authors find that the concentrations of strontium and magnesium in their samples seem to be correlated with shifts in the ν_2 peak. But the relationship between the concentrations of ions in their samples and their stable isotope measurements is less clear. Small variations in Guzman et al.'s stable isotope measurements are attributed to environment and/or diagenetic changes, but it is difficult to attribute the fluctuations to one or the other. Although the study by Guzman et al. [6] does not directly discuss ^{14}C measurements, they do emphasize that diagenesis can be vastly unpredictable. I face a similar problem in the interpretation of my ^{14}C data: it is often challenging to determine if changes in F14C are indeed due to diagenesis or to environmental factors.

Thus, diagenetic changes, in whatever form, whether it be changes in polymorph or changes in composition, do not always correlate with a change in the ^{14}C measurements or other geochemical measurements. Conversely, unexpected ^{14}C measurements may not be fully explained by the data obtained using methods that are usually used to detect diagenesis, such as scanning electron microscopy, infrared spectroscopy, or x-ray diffraction. This presents a challenge in predicting when ^{14}C dates will not accurately reflect age. However, because it can be difficult to determine whether or

not the presence of calcite may indicate a change in ^{14}C, for archaeological purposes it may be best to err on the side of caution and discard any aragonite shell sample that displays calcite.

4.1.1 IR Grinding Curves and Diagenesis

Only searching for recrystallized calcite is simply not enough to fully understand how diagenetic processes affect the mollusk shell $CaCO_3$. As mentioned above, there are cases when a change from aragonite to calcite may not produce a change in ^{14}C measurement, for example if the presence of calcite is a result of heating [5]. The heating simply induces a change in polymorph of the biomineralized aragonite, but no new carbon is being incorporated into the $CaCO_3$, and thus the age of ^{14}C would remain unchanged. It is not strictly true that heating never has an effect on the ^{14}C signatures. For example, Toffolo and Boaretto [7] show that above about 600 degrees Celsius, the CO_3 moiety breaks down and incorporates new CO_2 from the air. Similarly, recrystallization, which is the result of dissolution and reprecipitation, will also result in either new, more modern carbon, or old, dead carbon being incorporated and will affect the ^{14}C measurements.

The variation in relative IR peak intensity changes that I investigated using the IR grinding curve method may somehow be linked to diagenesis, however I cannot make a clear link between the two using only IR spectroscopy data. While the IR spectroscopy data, and particularly the IR grinding curve data, does show that there is certainly a difference in the relative peak intensities within the shell $CaCO_3$, IR spectroscopy cannot directly inform us if the carbon has been altered. The consistent difference in relative peak intensities that I record is valuable, as it provides a starting point for studying these differences with other experimental techniques that could help determine the cause of the patterns in relative IR peak intensities.

Previous research has shown that IR grinding curves can excel in detecting calcites and aragonites of different origins (geogenic, pyrogenic, and biogenic) based on their distinct grinding curves [8]. Perhaps in the future this method could be useful for distinguishing unaltered biomineralized aragonite from that which has been recrystallized. For biogenic carbonates, using relative IR peak intensities to study diagenesis is even more challenging because of the natural variability of the aragonite within a mollusk shell.

Diagenesis vs. natural variation

Our samples of *S. gigantea* from British Columbia show significant variation in relative IR peak intensities within a single shell and between samples. It is not clear how much of the variability, if any, is due to diagenesis and how much is due to natural variation. For marine bivalve shells like *S. gigantea*, when studying diagenesis it is necessary to be mindful of the natural variability that may be misinterpreted as diagenesis.

The consistent differences in the relative IR peak intensities between the inner and outer portions of the shell displayed by the IR grinding curves in this research are likely due to the natural differences in the aragonite. These two portions of the shell have different microstructures, as the inner shell is nacre and the outer shell is crossed lamellar aragonite, and [9]. Suzuki et al. [9] recorded a similar difference in these grinding curves for these microstructures, and suggested that this may be because of different aragonite crystal sizes within each of the microstructures. My grinding curve data alone cannot confirm the reason for this difference. However, it seems very unlikely that the shift in the grinding curves between the inner and outer portions of the shells is due to diagenesis because it is consistent in both archaeological and live-collected samples [9, 10].

In this thesis work, my samples were only analyzed for ^{14}C using material from

the outer crossed-lamellar portion of the shell. However, there is a study by Berger et al. [11] from the 1960's that demonstrated there is indeed a difference between the ^{14}C signatures of the inner and outer components of marine shell. More recent studies confirm that the reason for this difference is because of different sources of carbon and different hierarchical organization of the inner $CaCO_3$ layers [11–13]. In that sense, it seems that the ^{14}C variation between the inner and outer portion of the shell, as demonstrated in the literature, is primarily a result of natural intrashell differences. The consistent shift between inner and outer shell in my IR grinding curve data also shows what is likely a natural intrashell difference. Just as the difference in ^{14}C between the inner and outer components of the shell recorded by Berger et al. [11] likely has little to do with diagenesis, the differences in the grinding curves may also have little to do with diagenesis.

While the relative IR peak intensity differences between the inner and outer shell are likely linked to the different aragonite microstructures, there is some variability in the grinding curves within each of those microstructures. The variability of both the inner and outer grinding curves between the shells we sampled may be linked to diagenesis, but it may also be linked to natural, intraspecies variation. While the relative difference between the inner and outer shell grinding curves of a single shell is predictable, if we were to compare two outer shell samples from two different individual shells, there is no way to predict how the curves will be positioned with respect to one another. This highlights that screening for diagenesis using IR grinding curves is in its early stages of development, and decoding which samples are pristine based on the IR grinding curve method would require studying many completely pristine unaltered archaeological shell aragonite samples to determine the natural variability in the grinding curves. The patterns and variation that are present in my data need to be corroborated by other experiments, such as x-ray diffraction measurements, to

determine the reason for the relative intensity changes and the extent of individual and interspecies variation.

4.2 Considerations for sampling

Even with the most rigorous diagenetic screening protocols, and even if it were possible to determine how the diagenetic processes effect the $CaCO_3$ in the shell, there are still some key limitations in sampling for ^{14}C. The first is that time averaging is almost always unavoidable because the required size of samples for ^{14}C analysis necessitates averaging over multiple growth lines in the shell. Because of the low concentration of ^{14}C atoms in nature, and thus in samples submitted for ^{14}C dating, the Lalonde AMS Laboratory requires that $CaCO_3$ samples submitted to the lab be several mg, so that at least 1 mg of carbon can be obtained from the sample [14]. The abundance of ^{14}C in nature is 0.0000000001%, and thus for a sample of carbon of about 1 mg, this corresponds to only about 10^7 ^{14}C atoms. Older samples - those with very little modern carbon (^{14}C) - have an even smaller amount of ^{14}C and so a larger amount of carbon, and a larger $CaCO_3$ sample mass would be needed. To obtain a suitable amount of carbon for measurement from *S. gigantea*, a portion of the shell about 1 cm by 1 cm is needed. We estimated that each of these portions represents about 5-7 years of growth. When the ^{14}C analysis is conducted, all of the $CaCO_3$ in the 1 cm by 1 cm portion is pooled together and measured, so we end up with a measurement that averages over all the carbon in that sample. Thus, the ^{14}C measurement will average over those 5-7 years of ontogenetic growth and any fluctuations in the marine carbon reservoir that may have occurred in those years.

Averaging over several years of growth skews our ability to detect variability and cyclic variations in ^{14}C at a high resolution. There are theoretical studies that use

programs like ShellCorr [15], which is based on an analogous program for tree ring data [16], which can produce a theoretical shell ^{14}C profile based on shell growth rate information and regular marine upwelling patterns. This theoretical approach can be useful for analyzing intrashell data outside of the confines of the AMS sample size requirements and for exploring how varying marine conditions, mollusk shell growth patterns, and sampling strategies all play a role in understanding intrashell ^{14}C variation [17].

Without a doubt sampling strategies are an important factor in understanding intrashell ^{14}C variation. Some considerations of sampling are specific to the portion of the shell that is being studied, so I split the remainder of this section of the discussion into two subsections: considerations specific to the crossed lamellar portion and considerations specific to the remineralized portion.

4.2.1 Sampling Strategies and Growth Patterns: Crossed Lamellar Portion

Based on our basic understanding of how bivalve mollusks grow, we know that the different layers of aragonite in the crossed lamellar layer of the mollusk shell were not deposited at the same time. Specifically, we know that the $CaCO_3$ at the hinge was deposited before the $CaCO_3$ at the ventral margin. If we were to assume no environmental effects, contamination, or diagenesis, then we would expect that measurements at different locations on the shell should report different F14C values. Depending on the ontogenetic age of the mollusk and whether it happened to live during a time when the marine carbon levels were highly variable, this variation in F14C may not be significant enough to be detected by an AMS ^{14}C measurement (see Figure 3.6).

Considering again the variability in the DiSe7_1 shell (see Table 3.1). This shell displays a slightly older ^{14}C age at the hinge and a younger ^{14}C age at the ventral

margin. As both ontogenetic growth and variation in the local marine reservoir can affect the intrashell ^{14}C, it is possible that both of these factors may play a role in the observed variability in the DiSe7_1 shell. At first glance, we might assume that the ^{14}C variation reflects ontogenetic age of the shell - with the most recently deposited carbonate material being located at the ventral margin and the least recent located at the the hinge. However, if this were the only factor contributing to the shell ^{14}C then I would expect to see a similar pattern in the other shell samples.

To study this further in the future, the stratigraphy of the growth layers of the shell can be used to constrain the ^{14}C dates in a technique called wiggle matching. By incorporating knowledge of the mollusk's growth patterns, specifically which layers or portions of the shell were biomineralized before others, this can constrain calibrated ^{14}C ranges [18,19]. By applying wiggle matching, we can incorporate yet another check on our ^{14}C measurements to explore how "real" the F14C differences are. Where we see no intrashell variation, wiggle matching could be done to impose boundaries on the measurements and eliminate some uncertainty in the calibrated age ranges. Wiggle matching, however, is still limited by the amount of sample that must be submitted for analysis and is still subject to the issues associated with averaging. Additionally, wiggle matching functions on the basis that the F14C measurements are not affected by contamination, diagenesis, or any other external factors.

In order to confidently use the wiggle matching approach, it is necessary to fully understand where the carbon in the shell $CaCO_3$ is coming from and what the expected ^{14}C profile is. A variable ΔR in the local marine environment can complicate this wiggle matching approach. Temporal and spatial variability in the local marine carbon reservoir can result in ΔR varying over time and space. As bivalves grow and incorporate the resulting upwelling signatures into their $CaCO_3$, there may be regions of the shell where ^{14}C dates seem to fluctuate in unpredictable ways when really they

are only reflecting the variability in ΔR. Previous works by Jones et al. [13, 17] highlight how this variability in local ΔR overlaps with shell growth patterns. In many bivalve species, *S. gigantea* included, there are periods of slower growth in the winter, when less $CaCO_3$ is deposited, and faster growth in the summer, when more $CaCO_3$ is deposited, leading to an over-representation of "spring $CaCO_3$" in the shell compared to "winter $CaCO_3$." Combining this with fluctuating ΔR means that certain ΔR values are also overrepresented and it may be more difficult to choose a "correct" ΔR.

In the crossed lamellar portion, considering sampling strategies only gets us so far. We sampled all three shells in Chapter 3 in a similar way, but there are still unanswered questions about growth patterns and the local marine environment that are necessary to understand the ^{14}C variation.

4.2.2 Remineralized Carbonate in Shell: Sampling Strategies in the Inner Remineralized Portion

In this subsection, I briefly discuss considerations of ^{14}C in the inner remineralized (nacreous) aragonite portion of the shell. To clarify, the term remineralized can sometimes refer to organic carbon that has been freed into the ocean reservoir by biological pathways and is reincorporated into mineral deposits, sometimes shell [20], but here we use the term remineralized to refer to the innermost layer of the shell. This layer is formed as the mollusks digestive fluids dissolve and remineralize the aragonite in the outer crossed lamellar layer, depositing a smooth layer of nacre that does not contain growth lines like the unaltered crossed lamellar layer does.

Because this remineralized portion does not have the same connection to temporality that the crossed lamellar does, we do not have a clear idea of how the ^{14}C signatures or patterns in the relative IR peak intensities are linked to the environment,

if at all. I have shown in Chapter 2 that the IR grinding curves do show fluctuations in this portion of the shell, but I am currently unable to link this to ^{14}C measurements because the samples I used for the IR spectroscopy analysis and the ^{14}C analysis did not come from the exact same portions of the shell. We hope that in future studies we will be able to investigate how the variation, or lack thereof, differs in the remineralized portion from the crossed lamellar portion. Details on directions for future studies are discussed in Chapter 5.

There are two ways that the ^{14}C measurements are useful: 1) that the ^{14}C is an environmental measurement and 2) that all the ^{14}C in one portion of the shell is an average age of the shell. We have indeed shown that ^{14}C measurements in the crossed lamellar portion are not only useful as temporal measurements, but they also provide valuable information about the links between the material of the shell and its environmental conditions. Analyzing the ^{14}C signature of the remineralized portion may not be useful for temporal measurements in the same way that the crossed lamellar is, but it may be useful for studying how the remineralization process occurs and if there are any environmental signatures contained in this portion of the shell. We may also find the ^{14}C measurements useful for the purpose of comparing this portion of the shell with the outer crossed lamellar portion.

4.3 Sample Preparation: Addressing Diagenesis in ^{14}C Sample Preparation

The steps for sample preparation followed by the Lalonde AMS laboratory and those followed at other ^{14}C laboratories [21] focus primarily on removing contaminating $CaCO_3$ by doing an acid etch, which removes the outermost 20% of the sample. Some novel laboratory procedures ensure that, for aragonite samples, all contaminating cal-

cite is removed by a density separation procedure [21,22]. The acid etch only removes the outermost exposed portion of the sample, whereas more involved procedures like the density separation procedure would remove all calcite, regardless of the location of the contamination.

None of the above methods are done with the purpose of ensuring that the protein matrix which surround both the crossed lamellar and nacre crystals in the shell is eliminated. However, the protein portion is very small to begin with (on the order of 1%) and is typically considered to not have an effect on the ^{14}C measurements as most, if not all of the protein is removed during the acid etch. After the acid etch is completed, the shell material is reacted with H_3PO_4 and the resulting CO_2 is collected, which is then graphitized. The CO_2 gas that is collected at this stage is derived only from the $CaCO_3$ and not the organics.

However, the small protein portion that is removed when the protocol followed by the Lalonde AMS lab is followed has been analyzed for ^{14}C separately in previous studies. Berger et al. [11] measure ^{14}C dates on the mineral and organic portions of bivalve shells and find good agreement between the measurements. The findings of Gillespie et al. [23] do not concur; they report differences in the ^{14}C measurements on the order of thousands of years among $CaCO_3$, and amino acids and humic acids. Gillespie et al. postulate that this may be related to deamination of the acids, but they say it is not clear how this would affect the dates.

4.4 Summary: Relation Between Diagenesis, IR Spectroscopy, and ^{14}C

Because of limitations on lab work during the ongoing COVID-19 pandemic, we were not able to obtain and analyze the same samples (from the same location on the same

shell) for both IR data and ^{14}C data. However, the data we do have, which comes from several shells, can still help answer some questions about correlating variation in composition and structural properties with ^{14}C variation.

Bivalve mollusks are challenging to work with because of the presence of both individual variation and interspecies variation. Environmental variation further prevents us from making generalizations - for example we are unable to say that a sample taken at the hinge will always result in an older date than a sample taken at the ventral margin because of the variability in the global carbon reservoir. It is also challenging to make generalizations about the IR data. While all shell samples are aragonite, there is a distinct separation in the IR grinding curves between the inner and outer portions of the shells. In addition to this distinct separation, there is also variation among the curves that group together. We do not have a systematic way of predicting the variations among the IR grinding curves that group together.

Both ^{14}C and IR spectroscopy data reinforce the intrashell variation for *S. gigantea* and these results provide a starting point for new discussions about intrashell variability and diagenesis. The differences in the relative IR peak intensities display intrashell differences with unclear links as of yet to diagenesis and to the ^{14}C measurements.

In the previous sections, I have demonstrated that there is detectable variation in the relative IR peak intensities between the inner and outer portions of shells, as well as variation in F14C within the outer, crossed lamellar portion of the shells. When considering the variability in hierarchical samples like the bivalve mollusks studied here, both the F14C and the calibrated values are important because, while the F14C measurements may appear the same within their uncertainties, they may not necessarily reflect a real temporal overlap. According to Table 3.1 in Chapter 3, only one shell displays a significant difference in the intrashell F14C measurements, and the other two shells do not display a significant variation in F14C. This discrepancy

does cause issues for the interpretation of the calibrated ranges and may be due to a combination of factors including fluctuations in the atmospheric and marine reservoirs on the global scale (which is incorporated in the calibration curves), fluctuations in the marine reservoir on the local scale (ΔR), and issues regarding contamination and diagenesis of the shell carbonate.

The variety of factors that can affect intrashell ^{14}C variation raises questions about how we can account for and understand the variation in F14C without having other measurements to anchor our data to a specific point on the calibration curve and methods like IR spectroscopy can inform us about systematic differences that may be linked to either environment or diagenetic effects. In one sense, the IR spectroscopy data serves to eliminate severe doubt about the dates by ensuring that the variation in the ^{14}C does not appear because of contamination by non original carbon in the form of recrystallized calcite. On the other hand, even if no diagenesis has occurred there can still be a complex and unexplained intrashell ^{14}C profile.

Evidently, ontogenetic age, growth patterns, specific marine environment conditions, and larger scale oceanography conditions can all affect the ^{14}C signatures within the shells. Untangling all these factors individually is beyond the scope of this project, but the first and most crucial step in ^{14}C analysis is to screen for diagenesis. Diagenesis is a broad term that is often quite ambiguous. In archaeological contexts it refers to any process that occurs after the sample has been deposited in its archaeological context. The most important questions to me were whether or not these changes are detectable by IR spectroscopy and if they reduce the confidence in the ^{14}C measurement. Screening for diagenesis ensures that the carbonate being analyzed for ^{14}C is pristine and has no post-depositional signatures. The screening process should include considering both the chemical composition and the structural order of the sample. Sampling strategies also need to be considered. They raise questions

of how the resolution of sampling and the sampling locations can impact the ^{14}C measurements obtained. Mindful sampling strategies should entail a consideration of growth patterns and the ontogenetic age of the shell samples as these patterns may amplify changes in apparent ^{14}C age when they are combined with fluctuating local marine reservoir effects.

Additionally, focusing only on ^{14}C measurements does not leave space to explore the links to structural and compositional changes of the $CaCO_3$ and prevents us from being able to see if these variations manifest themselves in other ways and could be detectable by other methods. In my research, I used infrared spectroscopy, a method which does not require significant amounts of time and money, and which gives us the ability to obtain spectra in a matter of minutes, but it does necessitate thoughtful sampling strategies, data analysis, and contextualization. Because IR spectra are affected by composition, crystal structure, and crystallinity, it can be challenging to interpret the precise cause of different spectral features, however this method is still very useful for detecting differences between and within samples. Further, for this method to be used as a screening technique, the specific details behind the grinding curve shifts need not be understood for every sample to be screened. As long as the groundwork is laid to determine what the natural variability is in the grinding curves, then a simple check against this bracket of variability is all that is needed for screening.

Bibliography

[1] G. E. Webb, G. J. Price, L. D. Nothdurft, L. Deer, and L. Rintoul. Crytic meteoric diagenesis in freshwater bivalves: Implications for radiocarbon dating. *Geology*, 35(9):803–806, 2007.

[2] R. Enmar, M. Stein, M. Bar-Matthews, E. Sass, A. Katz, and B. Lazar. Diagenesis in live corals from the Gulf of Aqaba. I. The effect on paleo-oceanography tracers. *Geochimica et Cosmochimica Acta*, 64(18):3123–3132, 2000.

[3] K. Douka, T. F. G. Higham, and R. E. M. Hedges. Radiocarbon dating of shell carbonates: old problems and new solutions. *Munibe*, 31:18 – 27, 2010.

[4] G. Magnani, P. Bartolomei, F. Cavulli, M. Esposito, E. C. Marino, M. Neri, A. Rizzo, S. Scaruffi, and M. Tosi. U-series and radiocarbon dates on mollusc shells from the uppermost layer of the archaeological site of KHB-1, Ra's al Khabbah, Oman. *Journal of Archaeological Science*, 34(5):749–755, 2007.

[5] S. Lindauer, S. Milano, A. Steinhof, and M. Hinderer. Heating mollusc shells - A radiocarbon and microstructure perspective from archaeological shells recovered from Kalba, Sharjah Emirate, UAE. *Journal of Archaeological Science: Reports*, 21:528–537, 2018.

[6] N. Guzmán, Y. Dauphin, J. P. Cuif, A. Denis, and L. Ortlieb. Diagenetic changes in Concholepas concholepas shells (Gastropoda, Muricidae) in the hyper-arid conditions of Northern Chile - implications for palaeoenvironmental reconstructions. *Biogeosciences*, 6(2):197–207, 2009.

[7] M. B. Toffolo and E. Boaretto. Nucleation of aragonite upon carbonation of calcium oxide and calcium hydroxide at ambient temperatures and pressures : a

new indicator of fire-related human activities. *Journal of Archaeological Science*, 49:237–248, 2014.

[8] K. M. Poduska, L. Regev, F. Berna, E. Mintz, I. Milevski, H. Khalaily, S. Weiner, and E. Boaretto. Plaster Characterization At the PPNB Site of Yiftahel (Israel) Including the Use of ^{14}C: Implications for Plaster Production, Preservation, and Dating. *Radiocarbon*, 54(3):887–896, 2012.

[9] M. Suzuki, T. Kogure, S. Weiner, and L. Addadi. Formation of aragonite crystals in the crossed lamellar microstructure of limpet shells. *Crystal Growth and Design*, 11:4850–4859, 2011.

[10] M. Dusseault. Limits and Potential of FTIR Analysis in Archaeology. Bachelor's honours thesis, Memorial University of Newfoundland, 2019.

[11] R. Berger, A. G. Horney, and W. F. Libby. Radiocarbon Dating of Bone and Shell from Their Organic Components. *Science*, 144(3621):999–1001, 1964.

[12] T. A. McConnaughey and D. P. Gillikin. Carbon isotopes in mollusk shell carbonates. *Geo-Marine Letters*, 28(5-6):287–299, 2008.

[13] K. B. Jones, G. W. L. Hodgins, M. F. Etayo-Cadavid, C. F. T. Andrus, and D. H. Sandweiss. Centuries of Marine Radiocarbon Reservoir Age Variation Within Archaeological Mesodesma donacium Shells From Southern Peru. *Radiocarbon*, 52(2):1207–1214, 2010.

[14] C. A. Crann, S. Murseli, G. St-Jean, Z. Xiaolei, C. D. Ian, and W. E. Kieser. First status report on radiocarbon sample preparation techniques at the A. E. Lalonde AMS Laboratory (Ottawa, Canada). *Radiocarbon*, 59(3):16–20, 2017.

[15] J. Scourse, C. S. Richardson, G. Forsythe, I. Harris, J. Heinemeier, N. Fraser, K. Briffa, and P. Jones. First cross-matched floating chronology from the marine fossil record: Data from growth lines of the long-lived bivalve mollusc *Arctica islandica*. *Holocene*, 16(7):967–974, 2006.

[16] H. Grissino-Mayer. Evaluating Crossdating Accuracy: A Manual and Tutorial for the Computer Program COFECHA. *Tree-ring research*, 2001.

[17] K. B. Jones, G. W. L. Hodgins, C. F. T. Andrus, and M. F. Etayo-Cadavid. Modeling Molluscan Marine Reservoir Ages in a Variable-Upwelling Environment. *PALAIOS*, 25(2):126–131, 2010.

[18] C. B. Ramsey, J. van der Plicht, and B. Weninger. 'Wiggle matching' radiocarbon dates. *Radiocarbon*, 43(2A):381–389, 2001.

[19] S. Helama and B. C. Hood. Stone Age midden deposition assessed by bivalve sclerochronology and radiocarbon wiggle-matching of Arctica islandica shell increments. *Journal of Archaeological Science*, 38(2):452–460, 2011.

[20] J. E. Ferguson, K. R. Johnson, G. Santos, L. Meyer, and A. Tripati. Investigating δ^{13}C and Δ^{14}C within Mytilus californianus shells as proxies of upwelling intensity. *Geochemistry, Geophysics, Geosystems*, 14(6):1856–1865, 2013.

[21] F. Brock, T. Higham, P. Ditchfield, and C. Bronk. Current Pretreatment Methods for AMS Radiocarbon Dating at the Oxford Radiocarbon Accelerator Unit (ORAU). *Radiocarbon*, 52(1):103–112, 2010.

[22] K. Douka, R. E. M. Hedges, and T. F. G. Higham. Improved AMS ^{14}C dating of shell carbonates using high-precision X-ray diffraction and a novel density separation protocol (CarDS). *Radiocarbon*, 52(2):735–751, 2010.

[23] R. Gillespie, R. E. M. Hedges, and M. J. Humm. Routine AMS Dating of Bone and Shell Proteins. *Radiocarbon*, 28(2A):451–456, 1986.

Chapter 5

Conclusions and Future Work

5.1 Conclusions

In this thesis work, I have analyzed marine shell aragonite from the bivalve mollusk *Saxidomus gigantea* using both infrared spectroscopy (IR) and radiocarbon (^{14}C) measurements. Using IR, I screened for diagenesis and explored the extent of intrashell variation in the relative IR peak intensities. The shells of *S. gigantea* were analyzed for ^{14}C and I studied both the uncalibrated F14C measurements and the calibrated age ranges to investigate intrashell ^{14}C variation.

Using IR spectroscopy, I determined that calcite was only detected in certain parts of the shell, and the IR grinding curves showed a consistent difference in relative peak intensities between the inner and outer portions of the shell of *S. gigantea*. Through the IR analysis, I demonstrated that detecting diagenesis in the form of recrystallized calcite is straightforward, but understanding the variation in relative IR peak intensities throughout the shell, as displayed by the IR grinding curves, needs to be investigated further. A detailed explanation of what causes the variation in the grinding curves and how that variation links to inter- and intra-species variation

requires input from other experimental measurements that were beyond the scope of this project, such as scanning electron microscopy (SEM) and X-ray diffraction (XRD), and more detailed knowledge of the environment in which the sample was collected.

The ^{14}C analysis included sampling 3 shells of *S. gigantea* from the Salish Sea in British Columbia, with three different measurements taken from each shell. Analyzing the raw F14C measurements in conjunction with calibrated age ranges was insightful because it allowed me to study intrashell ^{14}C from two lenses: variation in the actual content of ^{14}C by looking at the F14C, and how the variation is intricately linked to environmental conditions by looking at the calibrated ages. Through this approach, I did not treat the ^{14}C measurements as only an age measurement, but rather as a tool to study another aspect of intrashell $CaCO_3$ variation.

The IR spectroscopy and ^{14}C measurements provided two different types of information about the shell material. The IR spectroscopy probed vibrational modes in the solid, and these vibrational modes were used to study the composition, crystal structure, and to detect more subtle variations in the $CaCO_3$ by analyzing relative IR peak intensities. The changes in the relative IR peak intensities may be linked to the crystallinity of the mollusk shell $CaCO_3$, but would need to be confirmed by other experimental methods. The ^{14}C provided information about the isotopic makeup of the carbon in the shell $CaCO_3$. Finding deeper, direct links between these two methods would be extremely useful, as AMS ^{14}C measurements are costly and time consuming while IR spectroscopy measurements are not, but in the case of biogenic aragonite samples this is a very difficult task and at present, the links are not clear. This study provides a preliminary look into where future research may start for studying the links between the relative IR peak intensities and ^{14}C variation. In future studies, focusing more on diagenetic factors and environmental factors that may affect the shell $CaCO_3$

will provide more insight.

Even though not all the links between the IR spectroscopy data and the ^{14}C data are fully understood, both methods continue to be useful to archaeologists and materials physicists alike. The remainder of this chapter will outline my recommendations for extracting usable ^{14}C dates from marine shells for archaeological purposes and my recommendations for future studies with a materials physics focus.

5.2 Recommendations for Extracting Usable Shell Dates

This section, intended specifically for archaeologists, focuses on the implications of the ^{14}C dates and their significance in archaeological contexts. In studies with an archaeological focus, an in-depth study of marine shell $CaCO_3$ and its ^{14}C is often not possible nor the goal of the research. There must be a balance between accounting for these complexities and variation in the $CaCO_3$ as much as we can, while still developing best practices for obtaining ^{14}C dates we trust.

In general, the more information that a researcher has about the shell sample and its archaeological context - growth patterns, potential cooking practices, and the environmental conditions in which the mollusk grew - the better. This information is not always available, and for this reason, it may be beneficial to consult other experts - geologists, sclerochronologists, biologists - who may have this information. However, it is still possible to work around these limitations. I outline below some suggestions for how to obtain trustworthy ^{14}C dates on archaeological marine shells.

1. I highly recommend that screening of samples be done prior to submission to a lab for ^{14}C analysis. Some possible screening techniques are listed below along

with useful sources that have previously used these techniques in archaeological contexts.

- Infrared spectroscopy probes the vibrational modes in both crystalline and amorphous solids, therefore allowing the researcher to study solids with differing degrees of crystalline order, as well as samples containing a mixture of polymorphs [1–3].
- X-ray diffraction provides crystallographic information, including the measurements of lattice constants.
- Scanning electron microscopy is useful for imaging aragonite microstructures and can also provide elemental composition data when used in conjunction with, for example, energy dispersive X-ray spectroscopy [4–7].
- Raman spectroscopy, similar to infrared spectroscopy, operates in the mid-infrared range, but detects the energy of scattered photons from a sample [8]. This technique has been used previously to detect aragonite to calcite diagenesis in marine shells [1].
- A combination of these methods may also be useful to study composition, particularly the presence of strontium, magnesium, and manganese, which may help in studying seawater conditions if that is of interest to the researcher.

2. I also suggest that researchers do as much of their own sample preparation as possible and are as involved and as informed as possible in the ^{14}C analysis processes, especially if there are specific parts of the shell that the researcher would like to sample or if multiple dates from the shell would like to be obtained. This includes carefully choosing the sampling location on the shell, meaning that chunks of shell or shell powder samples from intentionally sampled portions of

the shell are submitted to the lab rather than an entire shell. Some important points to consider in terms of sampling and sample preparation are outlined below.

- In general, sampling at the ventral margin should give a ^{14}C date that more closely reflects that of the time of deposition in archaeological context since it is the region of most recent growth of the mollusk.
- If the researcher would like to take multiple samples from the same shell, I refer them to the intentional and explorative sampling techniques modeled by [9–11] with insightful theoretical work from Jones et al. as well [12]. This may assist the researchers in determining a sampling technique appropriate for them and provide insight on the interpretation of the ^{14}C dates.
- If given the opportunity, I would recommend that researchers actively participate in the sample preparation process at the lab where the ^{14}C analysis takes place. The A.E. Lalonde AMS laboratory in Ottawa gives their clients the option to spend a week at the lab preparing their own samples. This is an excellent way to observe and understand all the details behind the preparation process and to work alongside the laboratory staff to make informed decisions about sampling. As different labs may have slightly different protocols, communication with the lab is crucial to understanding exactly what part of the sample is being measured for ^{14}C.

3. Most labs will report both F14C and calibrated dates and I suggest that the researcher considers both, especially when obtaining more than one measurement from a single shell. Considering the F14C values may help to determine if intrashell variability is larger than expected, as described in Chapter 3. The calibration should also be carefully analyzed by the researcher, so that the in-

dividual can make specific and intentional choices about choice of calibration curve and ΔR value.

5.3 Further Recommendations for Studies in Materials Physics that Focus on Marine Mollusk Radiocarbon and Other Material Properties

This section outlines considerations that would extend past archaeological studies and investigate the variability in ^{14}C and the biogenic aragonite itself from a condensed matter physics perspective. Here I will make some suggestions for interesting paths of investigation to try to reconcile the variation in the relative IR peak intensities and the variation in ^{14}C in marine shell.

To further enhance our understanding of how the patterns in relative IR peak intensities and ^{14}C signatures of mollusks are related, more controlled studies using infrared spectroscopy are required. While IR grinding curves are a technique that can provide interesting insight into the possible effects of diagenesis and the natural variation of marine shell $CaCO_3$, the IR grinding curve technique is not a well-established method for detecting diagenesis in archaeological shell. The grinding curves are influenced by the crystal domain size (the coherent crystalline regions within a solid), which is suspected to vary within a mollusk shell [13], but the individual and species variation make it difficult to standardize the grinding curve method. Looking at the research I have completed and the questions that it raises, it is apparent that a significant amount of research is yet to be done to standardize the grinding curve method as a technique to screen for diagenesis, but that the technique does have the potential to be used more widely in studies of biogenic aragonite.

To further explore the cause behind the differences in the relative IR peak intensities throughout the shell as evidenced by the grinding curve shifts, I recommend combining the IR grinding curve analysis with X-ray diffraction (XRD), which has been done in similar studies of non-biogenic $CaCO_3$ [14] and would be extremely beneficial for verifying and further critiquing the results and interpretations on diagenesis presented in this thesis work. This would serve as an additional check on the variation in crystallinity and can be used to obtain the lattice constants, which would give a quantitative method of comparison for intrashell variability.

I also recommend combining IR and XRD with scanning electron microscopy (SEM). SEM is used widely in the study of biogenic carbonates and is used alongside IR and XRD frequently [3, 15–18]. The shifts in the IR grinding curves that I recorded are likely linked to the aragonite microstructure. However, the IR grinding curve method is an indirect way of studying aragonite microstructure, and SEM can help confirm the microstructures and any changes to them by imaging the aragonite directly. Additional techniques like energy dispersive X-ray spectroscopy (EDS) can be used in conjunction with SEM to study the composition as well. Although most ionic substitutions in the aragonite lattice should be visible by peak shifts in the IR spectra, as discussed in Chapter 2, EDS could serve as an additional check on the composition of the aragonite.

Although the carbon in the crossed lamellar portion of the shell is considered to be primarily dissolved inorganic carbon, it may be valuable to complete a calculation to determine if the shell aragonite does indeed have a 100% marine signature. This calculation can be done by considering the ^{13}C isotopes from a known fully marine and fully atmospheric samples. The details for completing this calculation are outlined in Appendix B. Apart from confirming the correct choice of calibration curve, it is unclear if determining the source of carbon in the mollusk shell $CaCO_3$ would resolve

any other issues or correlate with the IR spectroscopy data in any way. However, these studies would, if nothing else, build confidence in the choice of calibration curve and help understand the extent of F14C variation.

In terms of sampling strategies, a promising and feasible next step to take the research presented in this thesis work a step further would be to increase the sampling resolution within a single shell. As we do not fully understand how complex the F14C variability is within *S. gigantea*, making measurements as precise as possible within the sample size limitations would make this picture more clear. Comparing ^{14}C measurements taken from the inner nacre layer with measurements from within the environmental crossed-lamellar layer, as well as studying the variation in the nacre layer itself are all possible future paths for exploration. Ideally, we would want to sample the crossed-lamellar aragonite and the remineralized aragonite at the same locations to see if there is a significant difference between the ^{14}C measurements. The size of the samples are still limited by the requirements set by the lab and the minimum amount of carbon needed to complete an AMS measurement, although new technologies like the Mini Carbon Dating System (MICADAS) may reduce the amount of sample needed and increase the measurement frequency possible within a shell [19].

The question of the local marine reservoir offset (ΔR) is quite involved and should certainly play a role in future studies focusing on intrashell F14C variation. This, however, requires more research that falls both within and outside the discipline of physics and the scope of this thesis. Both physiological factors of the mollusk and the physical oceanography of the Salish Sea could be considered in future studies to further assess the additional errors involved in the ΔR measurements and applications to ^{14}C calibration. Some key points of the issues surrounding ΔR are discussed in Appendix B.

It is worth noting that in some archaeological or geological contexts, there may be opportunities to date the age of the shell, or to compliment the date obtained for the shell, using other relative or chronometric dating techniques. For example laminar deposits (from lake sediment or marine sediment) or tephra (volcanic ash) layer counting may be valuable. These methods can be secure relative dating methods and under the right circumstances, within larger chronologies, can be used to obtain secure chronometric dates for layers and thus the samples within those layers [20–22].

The ideal experiment incorporates a combination of methods that can address ^{14}C and ^{13}C isotopic variation, elemental composition, and crystallinity. An outline of an ideal experiment for a future study is presented in the next subsection.

5.3.1 Ideal Sampling for Most Detailed Analysis

My thesis work explored ^{14}C variation in marine mollusk shell $CaCO_3$ in conjunction with infrared spectroscopy. Both types of analyses displayed variation, but the variation in the ^{14}C and the IR stem from different properties of the shell $CaCO_3$ (vibrational modes and the isotopic composition of the carbon) and any direct links between these two types of variability are by no means clear. Drawing from my results, I now outline an ambitious but ideal future experiment that would aim to address most of the considerations discussed in this thesis.

The key is to use samples that come from contexts where the age is already known so that the ^{14}C does not need to be used as an age measurement. By using samples where the age is already known, we can determine the extent of the variability in the F14C measurements and would be able to determine what variability is natural - can be explained by fluctuations in radiocarbon levels during the specific time period - and what is not, by comparing the F14C measurements to the known age. This comparison can be made by using the reverse calibration method that I explored in

Chapter 3. Ideally, we would analyze a shell that already comes from a securely dated context or from a marine shell chronology. Since no marine shell chronology currently exists on the coast of British Columbia, we would optimistically use an archaeological sample from this region that is anchored in time by a corresponding terrestrial ^{14}C measurement.

For each sample, the shell would be cut along the axis of growth, from the hinge to the ventral margin, to see a cross section of the entire growth of the shell. Then, for each of the desired portions to be analyzed for ^{14}C (one could sample at the hinge, middle, and ventral margin as we have done in this thesis work), the corresponding regions on the other half of the shell would be analyzed for growth patterns so the length of time contained in each section could be determined. In addition to studying growth lines using the half of the shell not used for ^{14}C analysis, that half of the shell could also be subjected to oxygen isotope analysis for the purpose of determining the corresponding sea surface temperatures. The oxygen isotopes can help to identify changes in upwelling patterns, as sea surface temperature tends to decrease as upwelling increases.

For each of the measurements taken from the outer crossed lamellar layer of the mollusk shell, where growth lines are visible, we would take sclerochronological approaches to determine the number of years of growth that are included in each radiocarbon sample to obtain a sense of how much time is being averaged over. For each intrashell ^{14}C measurement, ΔR can be calculated by comparing the shell measurements with the associated terrestrial measurement, allowing for the calculation of multiple ΔRs from the same shell. As ΔR is very closely linked with upwelling, this will be extremely useful to pair with oxygen isotope data.

The confidence in the variability of these intrashell ΔRs would be even stronger if, rather than a terrestrial radiocarbon date, we had a known collection date. This may

be feasible for more historical samples, but in the time frame of the samples used in this thesis (around 2000 years BP), that is more difficult because shell samples with a known collection year are likely few and far between.

It is important that prior to the ^{14}C analysis, IR and XRD would be used to screen samples for contamination and possible diagenesis. To avoid contamination by handling, the shell would need to be sectioned, with separate portions designated for ^{14}C analysis, oxygen isotope analysis, and IR spectroscopy and XRD. Only about $100\mu g$ of shell is needed per sample for oxygen isotope analysis [23], and only about 1 mg is needed for IR analysis, so it would likely not be an issue to complete both of these types of analysis on one half of a sectioned shell. For a powder XRD measurement, several grams of sample are needed, which would be a challenge to obtain at the same resolution of an oxygen isotope measurement or an IR spectroscopy measurement. With a large enough shell, it may be possible to reserve a large enough portion of the shell for XRD analysis, and divide up the remaining portion of the shell for oxygen isotope analysis, IR spectroscopy, and ^{14}C analysis. To complete all of these analyses on the same shell, the sampling resolution of the ^{14}C measurements may need to be sacrificed slightly, with the chunk of shell used for ^{14}C spanning a few growth lines.

This approach would allow for a more direct comparison between IR, XRD, ^{14}C, and isotopic measurements, like oxygen isotope measurements, that can help understand environmental conditions [24, 25]. Taken together, this experimental data can help to detect both diagenesis and environmental conditions that may affect the ^{14}C measurements of the mollusk shell $CaCO_3$. Pairing the experimental methods described above with the IR grinding curve method would be very insightful and allow for direct comparisons between crystallinity, possible diagenesis, and the ^{14}C measurements.

Analyzing several samples of the same species can help to determine the extent

of variation in the structure and composition of the aragonite between individuals of the same species. The carbon-13 analysis would build confidence in the calibration curves used for the ^{14}C analysis, and the oxygen isotopes would help determine the upwelling signatures within the shell $CaCO_3$, further building confidence in the ^{14}C.

While the focus on the crossed lamellar environmental layer is crucial for future work, completing corresponding measurements in the remineralized nacre layer is necessary to fully grasp the nature of the ^{14}C variation. To obtain these measurements, we would suggest isolating samples from the inner remineralized layer and the outer crossed lamellar layer at multiple (the more, the better) locations along the shell's axis of growth, meaning that at each position along the shell (from the direction of hinge to ventral margin), we have two measurements, one for the inner layer and one for the outer layer.

The approach outlined above would allow for variation in the ^{14}C to be studied in conjunction with variation in crystallinity by looking not only at the IR grinding curves but also at XRD and SEM. Additionally, any variation in F14C that may not correspond to the expected age could direct even more focused investigations into diagenesis.

5.4 Final Thoughts

In this thesis, I approached the study of marine shell calcium carbonate from samples of *S. gigantea* from British Columbia using two fundamentally different analysis methods: IR spectroscopy and ^{14}C analysis. While it is not uncommon for these two techniques to be used together for the purpose of identifying diagenesis and contamination prior to ^{14}C dating, here I did not concern myself directly with the archaeological implications of the ^{14}C data, but rather focused on investigating the extent

and significance of the ^{14}C variation and relative IR peak intensity variation within a shell. These techniques allow us to view the material variation within a shell from two different lenses.

Not only is this work necessary to untangle the intricacies of the ^{14}C variation in marine mollusk shells so that we can build confidence in ^{14}C measurements, but it also provides an opportunity to understand biogenic carbonates from a perspective that integrates multiple experimental approaches and enhances our understanding of the material itself. I have highlighted that there are many factors that can affect these measurements, and we are far from understanding the drivers behind the variability in these samples or from directly linking the systematic variations in IR peak intensities to the ^{14}C variation. However, continuing to study biogenic carbonates from this perspective will allow for a more holistic understanding of the material and will open up doors for other research to explore the environmental and oceanographic factors from new angles.

Bibliography

[1] S. Milano. *Unraveling the environmental record encoded in mollusk shell microstructures*. PhD thesis, University of Mainz, 2016.

[2] S. Milano, A. L. Prendergast, and B. R. Schöne. Effects of cooking on mollusk shell structure and chemistry: Implications for archeology and paleoenvironmental reconstruction. *Journal of Archaeological Science: Reports*, 7:14–26, 2016.

[3] S. Milano, S. Lindauer, A. L. Prendergast, E. A. Hill, C. O. Hunt, G. Barker, and B. R. Schöne. Mollusk carbonate thermal behaviour and its implications in understanding prehistoric fire events in shell middens. *Journal of Archaeological Science: Reports*, 20:443–457, 2018.

[4] M. F. Etayo-Cadavid, C. F. T. Andrus, K. B. Jones, G. W. L. Hodgins, D. H. Sandweiss, S. Uceda-Castillo, and J. Quilter. Marine radiocarbon reservoir age variation in Donax obesulus shells from northern Peru: Late Holocene evidence for extended El Niño. *Geology*, 41(5):599–602, 2013.

[5] S. Lindauer, S. Milano, A. Steinhof, and M. Hinderer. Heating mollusc shells - A radiocarbon and microstructure perspective from archaeological shells recovered from Kalba, Sharjah Emirate, UAE. *Journal of Archaeological Science: Reports*, 21(March):528–537, 2018.

[6] K. Knoll, N. H. Landman, J. K. Cochran, K. G. MacLeod, and J. A. Sessa. Microstructural preservation and the effects of diagenesis on the carbon and oxygen isotope composition of late Cretaceous aragonitic mollusks from the Gulf Coastal Plain and the Western Interior Seaway. *American Journal of Science*, 316(7):591–613, 2016.

[7] N. Guzmán, Y. Dauphin, J. P. Cuif, A. Denis, and L. Ortlieb. Diagenetic changes in Concholepas concholepas shells (Gastropoda, Muricidae) in the hyper-arid conditions of Northern Chile - implications for palaeoenvironmental reconstructions. *Biogeosciences*, 6(2):197–207, 2009.

[8] S. S. Mitra. Infrared and Raman Spectra Due to Lattice Vibrations. In Mitra S.S. Nudelman S., editor, *Optical Properties of Solids*, pages 333–451. Springer, Boston, MA, 1969.

[9] B. J. Culleton, D. J. Kennett, B. Lynn Ingram, J. M. Erlandson, and J. R. Southon. Intrashell radiocarbon variability in marine mollusks. *Radiocarbon*, 48(3):387–400, 2006.

[10] P. G. Butler, J. D. Scourse, C. A. Richardson, A. D. Wanamaker, C. L. Bryant, and J. D. Bennell. Continuous marine radiocarbon reservoir calibration and the ^{13}C Suess effect in the Irish Sea: Results from the first multi-centennial shell-based marine master chronology. *Earth and Planetary Science Letters*, 279(3-4):230–241, 2009.

[11] K. B. Jones, G. W. L. Hodgins, M. F. Etayo-Cadavid, C. F. T. Andrus, and D. H. Sandweiss. Centuries of Marine Radiocarbon Reservoir Age Variation Within Archaeological Mesodesma donacium Shells From Southern Peru. *Radiocarbon*, 52(2):1207–1214, 2010.

[12] K. B. Jones, G. W. L. Hodgins, C. F. T. Andrus, and M. F. Etayo-Cadavid. Modeling Molluscan Marine Reservoir Ages in a Variable-Upwelling Environment. *Palaios*, 25(2):126–131, 2010.

[13] M. Suzuki, Y. Dauphin, L. Addadi, and S. Weiner. Atomic order of aragonite crystals formed by mollusks. *CrystEngComm*, 13:6780–6786, 2011.

[14] B. Xu, M. B. Toffolo, E. Boaretto, and K. M. Poduska. Assessing Local and Long-Range Structural Disorder in Aggregate-Free Lime Binders. *Industrial and Engineering Chemistry Research*, 55(30):8334–8340, 2016.

[15] Y. Politi, R. A. Metzler, M. Abrecht, B. Gilbert, F. H. Wilt, I. Sagi, L. Addadi, S. Weiner, and P. U. P. A. Gilbert. Transformation mechanism of amorphous calcium carbonate into calcite in the sea urchin larval spicule. *Proceedings of the National Academy of Sciences*, 105(45):17362–17366, 2008.

[16] A. V. Radha, T. Z. Forbes, C. E. Killian, P. U. P. A. Gilbert, and A. Navrotsky. Transformation and crystallization energetics of synthetic and biogenic amor-

phous calcium carbonate. *Proceedings of the National Academy of Sciences of the United States of America*, 107(38):16438–16443, 2010.

[17] L. Addadi and S. Weiner. Biomineralization: Mineral formation by organisms. *Physica Scripta*, 89(9), 2014.

[18] R. Enmar, M. Stein, M. Bar-Matthews, E. Sass, A. Katz, and B. Lazar. Diagenesis in live corals from the Gulf of Aqaba. I. The effect on paleo-oceanography tracers. *Geochimica et Cosmochimica Acta*, 64(18):3123–3132, 2000.

[19] L. Wacker, G. Bonani, M. Friedrich, I. Hajdas, B. Kromer, M. Němec, M. Ruff, M. Suter, H. A. Synal, and C. Vockenhuber. Micadas: Routine and high-precision radiocarbon dating. *Radiocarbon*, 52(2):252–262, 2010.

[20] J. Beer and M. Sturm. Dating of lake and loess sediments. *Radiocarbon*, 37(1):81–86, 1995.

[21] C. Kuzucuoglu, J. F. Pastre, S. Black, T. Ercan, M. Fontugne, H. Guillou, C. Hatté, M. Karabiyikoglu, P. Orth, and A. Türkecan. Identification and dating of tephra layers from Quaternary sedimentary sequences of Inner Anatolia, Turkey. *Journal of Volcanology and Geothermal Research*, 85(1-4):153–172, 1998.

[22] A. D. Wanamaker, J. Heinemeier, J. D. Scourse, C. A. Richardson, P. G. Butler, J. Eiríksson, and K. L. Knudsen. Very long lived mollusks confirm 17th century AD tephra based radiocarbon reservoir ages for north Icelandic shelf waters. *Radiocarbon*, 50(3):399–412, 2008.

[23] M. Burchell, M. P. Stopp, A. Cannon, N. Hallmann, and B. R. Schöne. Determining seasonality of mussel collection from an early historic Inuit site, Labrador, Canada: Comparing thin-sections with high-resolution stable oxygen isotope analysis. *Journal of Archaeological Science: Reports*, 21(2018):1215–1224, 2018.

[24] M. Burchell, A. Cannon, N. Hallmann, H. P. Schwarcz, and B. R. Schöne. Refining Estimates for the season of shellfish collection on the pacific northwest coast: Applying high-resolution stable oxygen isotope analysis and sclerochronology. *Archaeometry*, 55(2):258–276, 2013.

[25] N. Hallmann, M. Burchell, N. Brewster, A. Martindale, and B. R. Schöne. Holocene climate and seasonality of shell collection at the Dundas Islands Group, northern British Columbia, Canada-A bivalve sclerochronological approach. *Palaeogeography, Palaeoclimatology, Palaeoecology*, 373:163–172, 2013.

Appendix A

Infrared Spectroscopy

A.1 Additional Grinding Curve Data

The infrared (IR) spectroscopy grinding curve method was used to study samples of not only *S. gigantea* from British Columbia, but also on samples of *M. arenaria* from Nova Scotia and samples of *Pomacea paludosa* (Florida Apple Snail) from Cuba. All of these samples, regardless of species and location, show the same shift in the grinding curve between the inner and outer shell. The grinding curves for the inner shells are consistently displaced below the curves for the outer shells.

More in-depth details about this preliminary study can be found in my archaeology undergraduate honours thesis [1], but I refer to it here to show that the difference in grinding curves is consistent across samples from multiple species and from multiple geographic locations. I will note that *M. arenaria* is another bivalve mollusk but *P. paludosa* is a gastropod with different growth patterns. Both of these samples are aragonitic as determined by the procedure outlined in Chapter 2.

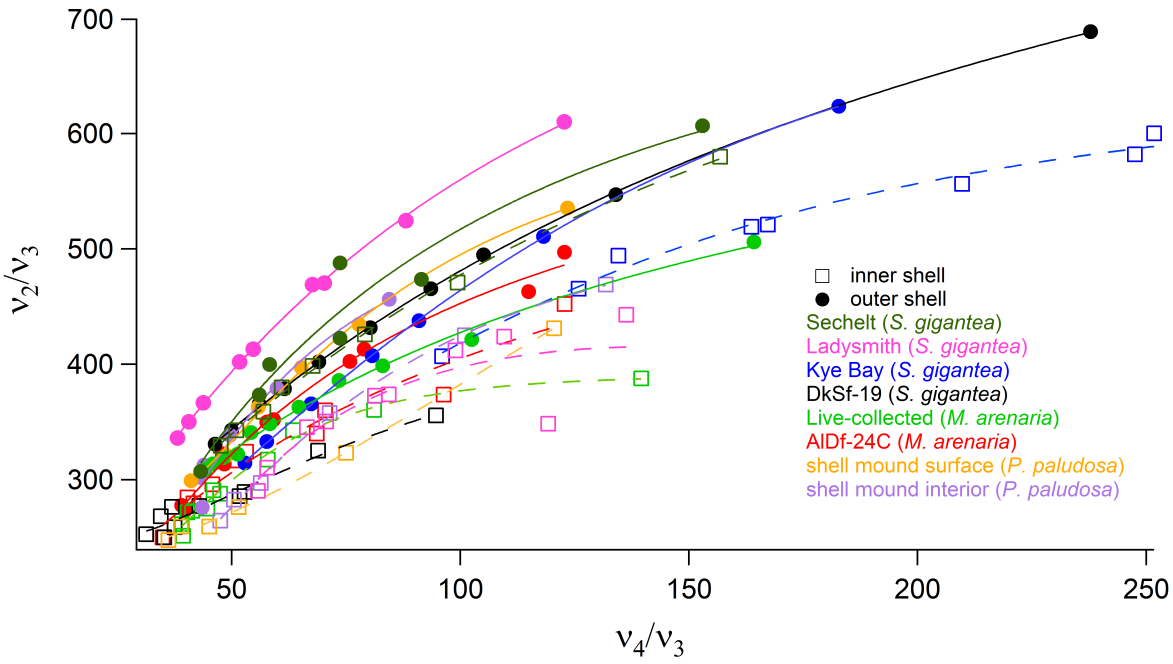

Figure A.1: Additional grinding curves from locations in British Columbia (Sechelt, Ladysmith, Kye Bay, and the DkSf-19 shell midden in Comox), Nova Scotia (AlDf-24C shell midden in Port Joli), and shells from Playa del Mango, Cuba (P. paludosa).

Bibliography

[1] M. Dusseault. Limits and Potential of FTIR Analysis in Archaeology. Bachelor's honours thesis, Memorial University of Newfoundland, 2019.

Appendix B

Radiocarbon

B.1 Additional details on fractionation calculations

The original publication that discusses standards for ^{14}C analysis is [1]. The standard used for ^{13}C and ^{14}C measurements is Pee Dee Belemnite (PDB) - a limestone ($CaCO_3$) from a Cretaceous fossil deposit of *Belemnitella americana* from South Carolina. This limestone is used as a standard because it is not subject to preferential uptake of the different carbon isotopes, which can occur in biological organisms.

The notation I use here follows that used by Stuiver and Robinson [2]. Fractionation is the process by which the ratios of isotopes (in this case $^{13}C/^{12}C$ and $^{14}C/^{12}C$) changes from its value in the atmosphere and/or oceans as it moves from the environment to the organism. For example, the fractionation factor α_{14} for ^{14}C corresponds to the ratio between the $^{14}C/^{12}C$ before a fractionation process (a measurement of atmospheric carbon for example) and after a fractionation process (a measurement from a tree ring for example) [3],

$$\alpha_{14} = \frac{(\frac{^{14}C}{^{12}C})_i}{(\frac{^{14}C}{^{12}C})_f} \tag{B.1}$$

To account for these changes in isotopic ratios during a fractionation process, a fractionation correction must be applied to the measured ^{14}C determination. This is done by considering the fractionation factor of carbon-13, which is related to that of carbon-14 by

$$\alpha_{14} = (\alpha_{13})^b \tag{B.2}$$

Where the value of b is usually taken to be 2 [4], while some recent studies have studied this more closely and obtained values slightly less than 2 [3].

The fractionation factor of the ^{13}C/^{12}C is denoted as α_{13}^2 and is used to normalize the sample activity (the ^{14}C/^{12}C measurements) by multiplying the measured sample activity by α_{13}^2 [3]. The fractionation factor of the carbon-13 ratio, α_{13}, can also be written as $(R_S(-25)/R_S)$, where $R_S(-25)$ is the $^{13}C/^{12}C$ ratio normalized to -25 parts per mil with respect to PDB, also referred to as R_{PDB},

$$A_{SN} = A_S(R_{PDB}/R_S)^2 = A_S\alpha_{13}^2 \tag{B.3}$$

By simplifying this equation and using

$$\delta^{13}C_S = \left[\frac{R_S}{R_{PDB}} - 1\right] 1000 \tag{B.4}$$

$$\delta^{13}C_S = \left[\frac{(^{13}C/^{12}C)_S}{(^{13}C/^{12}C)_{PDB}} - 1\right] 1000 \tag{B.5}$$

We get the normalized sample activity as described by Stuiver and Polach [4], or a normalized sample AMS measurement is calculated from the measured sample activity (or AMS measurement) by:

$$A_{SN} = A_S \left[1 - \frac{2(25 + \delta^{13}C_S)}{1000}\right] \tag{B.6}$$

The fractionation ratio, b, plays a direct role in the calculation of fractionation corrected dates. As shown in equation B.6, a δ^{13}C measurement is needed in order to correct ^{14}C measurements for fractionation. The second term in parentheses is the difference in parts per mil, between the measured δ^{13}C value from the sample and the value of -25 ‰.

It is apparent by looking at Equation B.6 that a measurement of ^{14}C that is corrected for fractionation is linked to a ^{13}C measurement. The ^{14}C value is normalized to a ^{13}C value of -25‰ with respect to the measured value of the standard Pee Dee Belemnite (PDB) [3, 4]. Carbon isotopes 13 and 14 are used together to correct for fractionation.

The oxalic acid is similarly corrected for fractionation, but normalized to -19 with respect to PDB and multiplied by 0.95 for convention as follows

$$A_{ON} = 0.95 A_{OX} \left[1 - \frac{2(19 + \delta^{13}C)}{1000}\right] \tag{B.7}$$

Finally, the fraction of modern carbon is calculated as

$$F^{14}C = \frac{A_{SN}}{A_{ON}} \tag{B.8}$$

B.2 Mixed Marine-Atmospheric Curves: How to calculate percent marine and percent atmospheric

In Chapter 3, I presented the ^{14}C measurements calibrated to both a marine curve and atmospheric curve and I briefly raised the question of whether or not the shell samples are purely marine or if they contain some signatures of atmospheric carbon.

My ^{14}C measurements are taken from the mineral portion of the crossed lamellar aragonite layer. Therefore, the carbon detected by these measurements is primarily dissolved inorganic carbon (DIC) originating from the dissolved CO_2 and HCO_3 in the seawater. It is possible that the ^{14}C contains traces of particulate organic carbon (POC) that make its way into the organism by food consumption and may contain a more prominent atmospheric carbon signature [5, 6].

There are several models used for calculating mixed marine-atmospheric models [7,8], but below I outline a basic model which calculates the percent marine signature by comparing the δ^{13}C values from a sample that is known to be fully terrestrial and a sample that is known to be fully marine using the following equation:

$$\%Marine = \frac{\delta^{13}C_{terrestrial} - \delta^{13}C_{sample}}{\delta^{13}C_{terrestrial} - \delta^{13}C_{marine}} \times 100 \tag{B.9}$$

Where $\delta^{13}C_{terrestrial}$, $\delta^{13}C_{marine}$, and $\delta^{13}C_{sample}$ are calculated in the same way as discussed in the previous section:

$$\delta^{13}C_S = \left[\frac{(^{13}C/^{12}C)_S}{(^{13}C/^{12}C)_{PDB}} - 1 \right] 1000 \tag{B.10}$$

Equation B.9 estimates the percent of carbon atoms that come from marine protein, thus with the appropriate samples we could determine which combination of

marine and atmospheric curves is the best for our sample and to give some insight into the effects of the carbon signatures of the protein matrix may have on ^{14}C dates.

B.3 Carbon fluctuations on the local scale: ΔR

The marine calibration curves map out the changes in the global ^{14}C reservoir over time, but similar records do not always exist on the local scale for the ΔR corrections. Even with the most detailed experiments and with a multidimensional materials science approach, we still need to either choose an appropriate ΔR, or calculate our own.

Most ΔR values used in archaeological contexts are calculated using shell-charcoal pairs and, as mentioned above, stratigraphy is not always easy to understand and can subsequently result in arbitrary choices needing to be made when either calculating ΔR or choosing which ΔR is appropriate to use to calibrate your sample. There are databases available to find ΔRs such as the 14CHRONO database, but the main challenge is that *time varying* ΔR is not readily available to researchers in an accessible format. This leads to the same ΔR values being used for time periods of hundreds or thousands of years.

Discussing the questions, and really the uncertainty around ΔR illustrates why we propose that looking at ^{14}C as an absolute time measurement is not sufficient for our samples. This is primarily because we do not know how the ΔR may vary throughout the mollusks lifetime - it may very well be insignificant - and without a clear answer to this question, we end up time averaging again. I refer to time averaging here not in the sense that the carbon lumped together in the measurement is averaged, but that we apply a blanket correction to all samples where it may not be the most accurate choice.

B.3.1 What is the correct ΔR?

Unless one has a complete knowledge of past upwelling patterns and those relevant to the period from which the samples are obtained, I argue that it is not possible to be 100% confident in a ΔR value from the literature and that the best option, if possible, is to calculate your own ΔR.

The ΔR of 226±70 was calculated in 2017 by Carlson et al. [9]. They used human bone that had a marine isotopic signature which can be attributed to their marine diet [10], and several terrestrial mammal bone burial artifacts. Despite the fact that humans are terrestrial mammals, their carbon signatures were marine because of their marine food source [9,10]. This value was calculated for Pender Island, which is on the southern shore of Vancouver Island. While this is not an ideal ΔR for our samples, there does not currently exist ΔR values for our specific sites. We highlight that using a non-local ΔR does add a level of uncertainty to the calibrated age ranges, and moreover it does not allow for accurate analysis of local carbon fluctuations.

The theory and method behind calculating ΔR values and their effects on calibrated dates is quite straightforward: measure the F14C of two samples from the same context, whether that be a known collection year (sample 1) and a measurement on a marine sample (sample 2), or archaeological charcoal (sample 1) and a marine sample (sample 2) from the same archaeological context. The terrestrial sample (either collection year or charcoal in this case) is taken to be the true calendar year, and that value is compared with the value measured for the marine sample and the difference is the ΔR. The greatest challenges come from determining which calculated ΔR values actually represent the local marine reservoir offsets for both the particular region of interest and the time frame of interest. For archaeologically determined ΔRs, you must trust that the context from which you find your marine and associated terrestrial sample is secure so that the terrestrial age can be used to model a marine age.

To illustrate what it would entail to calculate ΔR from a shell sample anchored in a chronology we refer to Butler et al [11]. Butler et al. [11] use a unique method to determine a local reservoir age from an *A. islandica* individual anchored in a chronology from the Irish Sea. The date of death of the individual was determined by its placement in the chronology, this date also corresponds to the "calibrated" age at the edge of the ventral margin. The sample that is ^{14}C dated is a portion of the shell from the ventral margin, so the age which is then used to determine the modelled marine age is taken from the center of that sample, roughly 20 years prior to the determined date of death. This modelled marine age is then substracted from the uncalibrated ^{14}C age of the shell sample to determine ΔR.

To use the most ideal approach exemplified by Butler et al. [11], we need a historically anchored marine shell chronology for the British Columbia Coast that extends back roughly 2000 years. No such chronology currently exists, but a good place to start would be to compile existing ^{14}C data and obtain new ^{14}C data from historically collected and archived mollusk shells from British Columbia. This would most likely involve a large amount of time and money but would be an invaluable resource for future studies.

B.3.2 Investigating ΔR: what effect does it have on calibrated dates?

The ΔR values are modelled as a normal distribution centered around the central value, in this case 226. Carlson et al. 2017 [9] assume that the measurements on human bone have a fully marine signature because of the prominence of marine resources in the diet. The authors analyzed 15 different burials, obtaining ^{14}C dates from both human bone and terrestrial mammal bone and calculated the difference, which gives the ΔR value.

For the ΔR values shown in the table, those are as reported by the Lalonde lab. The values are reported to be determined from the following database: http://calib.org/marine/. The 14CHRONO database exclusively includes data from the 2006 GEOSCAN database by McNeely, Southon, and Dyke [12] that reports ΔR values from across Canada. There is variation in the ΔR used in other studies [13], and this in turn will affect our understanding of material variation. This database reports a ΔR of 380 ± 50; specifically from Comox B.C. When DkSf20_C is calibrated as 100% marine with the Δ R for Comox, the date is 1510-1280 cal BP (95.4%). Comparing this date with the one reported in Table 3.2 reveals that these ranges overlap, but that the date with the larger ΔR is shifted to a slightly older age. In this specific case, a shift in the ΔR results only in a shift in the calibrated range, and no second region of probability appears. Results for calibration using different ΔR values are shown in Table B.1.

The application of a local ΔR value is applied directly to the F14C value (i.e. *before* the F14C value is corrected to the marine curve), as illustrated by the two gaussians shown in Figure 3.3. Because the local marine reservoir on the west coast of British Columbia has an older ^{14}C age than the global marine reservoir, applying a positive ΔR shifts our measured age to a slightly younger age so that it can be appropriately calibrated using the global marine curve. The local ΔR effectively determines which region of the calibration curve is applied to a measurement and because of this, use of an incorrect ΔR may cause not only a shift in the calibrated range of dates, but also the appearance of a second region of probability. Because the marine curve tends to be smoother than the atmospheric curve, this second range of probability does not appear.

Understanding how a local marine reservoir correction affects calibration is important because it directly shifts the uncalibrated measurement, and it indirectly shifts

sample name	F14C	ΔR = 226 $\pm$ 70	ΔR = 380 $\pm$ 50
DiSe7_1M	0.817(2)	1130-770 (95.4%)	901-680 (95.4%)
DiSe7_1C	0.812(2)	1175-824 (95.4%)	943-713 (95.4%)
DiSe7_1H	0.808(2)	1221-899 (95.4%)	987-739 (95.4%)
DiSe7_2M	0.851(2)	769-515 (95.4%)	625-450 (95.4%)
DiSe7_2C	0.852(2)	758-609 (95.4%)	621-442 (95.4%)
DiSe7_2H	0.849(2)	784-519 (95.4%)	634-466 (95.4%)
DkSf20_M	0.760(2)	1711-1346 (95.4%)	1504-1273 (95.4%)
DkSf20_C	0.759(2)	1735-1360 (95.4%)	1510-1280 (95.4%)
DkSf20_H	0.759(2)	1735-1360 (95.4%)	1510-1280 (95.4%)

Table B.1: Calibration using the Marine13 curve for the intrashell 14C measurements of *Saxidomus gigantea* bivalve mollusks from Deep Bay and Comox, British Columbia. ΔR values of 226$\pm$70 and 380$\pm$50 are used and compared.

the calibrated age range.

B.3.3 1σ vs. 2σ Calibration

When calibrating ^{14}C dates in a program like Oxcal [14], the user is given a choice of calibrating the dates to 1σ or 2σ. These calibrated ranges present the regions in which the probability of the actual age existing is 68.2% or 95.4% respectively. In archaeology publications, both 1σ and 2σ are used and in some cases it may not even be specified [**?**,9,15]. While it may be tempting to report 1σ dates because they often result in more confined age ranges, it is important to consider the 2σ range as well to see how different they are. We present our data calibrated to both ranges in Table B.2.

The result of calibration using 1σ or 2σ is similar to the differences seen between the marine and atmospheric curve calibrations in that it is highly dependent on how wiggly the calibration curve is in the region specified. In some cases, a choice between 1σ or 2σ can result in perhaps a single probability range for 2σ being 2 or more ranges for a 1σ calibration. Using a 2σ range means that a larger portion of the curve is

used in the calibration process, if expanding from a 1σ range to a 2σ range happens to capture a more wiggly portion of the calibration curve, then the calibrated range can be split into two or more ranges.

sample name	F14C	2σ	1σ
DiSe7_1M	0.817(2)	1130-770 (95.4%)	1045-871 (68.2%)
DiSe7_1C	0.812(2)	1175-824 (95.4%)	1078-913 (68.2%)
DiSe7_1H	0.808(2)	1221-899 (95.4%)	1125-953 (68.2%)
DiSe7_2M	0.851(2)	769-515 (95.4%)	686-557 (68.2%)
DiSe7_2C	0.852(2)	758-609 (95.4%)	677-554 (68.2%)
DiSe7_2H	0.849(2)	784-519 (95.4%)	716-590 (63.0%), 580-565 (5.2%)
DkSf20_M	0.760(2)	1711-1346 (95.4%)	1622-1426 (68.2%)
DkSf20_C	0.759(2)	1735-1360 (95.4%)	1660-1460 (68.2%)
DkSf20_H	0.759(2)	1735-1360 (95.4%)	1660-1460 (68.2%)

Table B.2: 1σ and 2σ calibration using the Marine13 curve for the intrashell 14C measurements of *Saxidomus gigantea* bivalve mollusks from Deep Bay and Comox, British Columbia. A ΔR of 226$\pm$70 is used for both calibrations.

B.4 Additional ^{14}C dates from the Salish Sea

The shell dates reported in table B.3 are all *S. gigantea* samples from British Columbia. The F14C measurements are reported with their uncertainties and dates are calibrated to both the Marine13 curve and the atmospheric IntCal13 curve. When calibrated to the marine curve, a ΔR of 226$\pm$72 is also applied [9]. We present both choices of calibration to illustrate the possible variation between age ranges that results from only the calibration curves. The majority of these samples happen to have F14C values that fall on a particularly variable, yet overall flat portion of the IntCal13 curve, which is why the calibrated ranges in the last column have multiple modes (multiple ranges where there is a statistically significant probability that the actual age of the sample falls within that range).

Calibrating these dates to the Marine13 calibration curve, with the ΔR from above (that is not highly localized), compared to calibrating to the IntCal13 atmospheric curve give calibrated age ranges that differ on average by about 400 years. Many of the atmospheric dates show a bimodality that is not present when calibrated using the marine curve. In fact, majority of the dates return at least two date ranges, some even return three.

sample name	lab ID	F14C	Marine13 (cal BP)*	IntCal13 (cal BP)
DfRu-13_1	3_DfRw13_1	0.808(4)	1231-890 (95.4%)	1706-1552 (95.4%)
DfRu-13_2	4_DfRw13_7	0.802(4)	1257-932 (95.4%)	1813-1601 (94.1%), 1581-1573 (1.3%)
DfSj-23A_1	5_DfSj23A_17	0.868(4)	655-376 (95.4%)	1174-1157 (5.1%), 1149-964 (90.3%)
DfSj-23A_2	5_DfSj23A_18	0.871(4)	632-334 (95.4%)	1172-1161 (1.2%), 1118-1114 (0.3%), 1082-932 (93.9%)
DfSj-23A_3	7_DfSj23A_1	0.878(4)	564-280 (95.4%)	1055-1022 (10.4%), 1010-916 (85.0%)
DfSj-23A_4	8_DfSj23A_3	0.882(4)	530-269 (95.4%)	980-895 (70.6%), 874-796 (24.8%)
DfSj-23A_5	9_DfSj23A_11	0.799(4)	1280-955 (95.4%)	1823-1686 (76.1%), 1678-1619 (19.3%)
DfSi-4_1	10_DfSi4_19	0.876(4)	601-301 (95.4%)	1056-1021 (20.9%), 1012-927 (74.5%)
DfSi-4_2	11_DfSi4_20	0.713(3)	2330-1945 (95.4%)	2877-2756 (95.4%)
DfSi-4_3	12_DfSi4_21	0.684(3)	2737-2351 (95.4%)	3360-3170 (95.4%)
DfSi-4_4	13_DfSi4_22	0.872(4)	626-329 (95.4%)	1072-931 (95.4%)
DgRs-1_1	14_DgRs1_1	0.629(3)	3570-3170 (95.4%)	4220-4208 (1.1%), 4156-3973 (94.3%)
DgRs-1_2	15_DgRs1_2	0.628(3)	3589-3188 (95.4%)	4226-4201 (4.1%), 4177-4172 (0.6%), 4160-3980 (90.7%)
DiSe-7_1	MB1_DiSe_7_1_1	0.836(2)	910-638 (95.4%)	1369-1297 (95.4%)
DiSe-7_2	MB2_DiSe_7_2_6	0.844(2)	859-550 (95.4%)	1313-1266 (95.4%)
DiSe-7_3	MB3_DiSe_7_3_3	0.850(2)	780-516 (95.4%)	1291-1230 (68.8%), 1209-1183 (26.6%)
DiSe-7_5	MB5_DiSe_7_5_20	0.848(2)	804-523 (95.4%)	1299-1237 (83.1%), 1209-1186 (12.3%)
DkSf-19_1	MB7_DkSf19_1_6	0.896(3)	465-103 (95.4%)	905-858 (20.3%), 830-810 (5.1%), 804-730 (70.0%)
DkSf-19_2	MB8_DkSf19_2_10	0.765(2)	1653-1304 (95.4%)	2303-2244 (28.7%), 2179-2168 (1.8%), 2162-2056 (64.8%)
DkSf-19_3	MB9_DkSf19_3_8	0.760(2)	1715-1346 (95.4%)	2310-2149 (95.4%)
DkSf-19_4	MB10_DkSf19_4_2	0.761(2)	1707-1342 (95.4%)	2310-2145 (95.4%)
DfRu-13_1	MB11_DfRu13_1_1	0.857(3)	712-489 (95.4%)	1267-1171 (75.3%), 1160-1082 (20.1%)
DfRu-13_2	MB12_DfRu13_2_6	0.698(2)	2613-2148 (95.4%)	3142-3092 (6.7%), 3080-2947 (20.1%)
DfRu-13_3	MB13_DfRu13_3_10	0.733(2)	2075-1690 (95.4%)	2721-2650 (22.7%), 2645-2489 (72.7%)
DfRu-20_1	MB14_DfRu_20_1_1	0.757(2)	1770-1385 (95.4%)	2335-2295 (21.7%), 2270-2155 (73.7%)
DkSf-20_1	MB16_DKSf_20_3_5	0.736(2)	2039-1640 (95.4%)	2714-2429 (94.4%), 2392-2382 (1.0%)
DgRr-1_1	MB17_DgRr-1_6	0.857(3)	712-487 (95.4%)	1265-1171 (72.1%), 1161-1081 (23.3%)
DgRr-2_1	MB18_DgRr2_2	0.864(3)	665-443 (95.4%)	1179-1055 (91.8%), 1023-1010 (3.6%)

Table B.3: Fraction of modern carbon (F14C) measurements, marine calibrated age ranges, and atmospheric calibrated age ranges to 2σ for *S. gigantea* bivalve mollusks from 11 different sites in British Columbia.
* all marine dates calibrated with a ΔR of 226 $\pm$ 72. Calibrated to 2σ.

Bibliography

[1] H. Craig. Isotopic standards for carbon and oxygen and correction factors for mass-spectrometric analysis of carbon dioxide. *Geochimica et Cosmochimica Acta*, 12(1-2):133–149, 1957.

[2] M. Stuiver and S. W. Robinson. University of Washington Geosecs North Atlantic carbon-14 results. *Earth and Planetary Science Letters*, 23(1):87–90, 1974.

[3] S. M. Fahrni, J. R. Southon, G. M. Santos, S. W. L. Palstra, H. A. J. Meijer, and X. Xu. Reassessment of the $^{13}C/^{12}C$ and $^{14}C/^{12}C$ isotopic fractionation ratio and its impact on high-precision radiocarbon dating. *Geochimica et Cosmochimica Acta*, 213:330–345, 2017.

[4] M. Stuiver and H. A. Polach. Discussion Reporting of ^{14}C Data. *Radiocarbon*, 19(3):355–363, 1977.

[5] T. A. McConnaughey and D. P. Gillikin. Carbon isotopes in mollusk shell carbonates. *Geo-Marine Letters*, 28(5-6):287–299, 2008.

[6] D. P. Gillikin, A. Lorrain, S. Bouillon, P. Willenz, and F. Dehairs. Stable carbon isotopic composition of Mytilus edulis shells: relation to metabolism, salinity, $\delta^{13}C_{DIC}$ and phytoplankton. *Organic Geochemistry*, 37(10):1371–1382, 2006.

[7] J. Arneborg, J. Heinemeier, N. Lynnerup, H. L. Nielsen, and N. Rud. Change of diet of the greenland vikings determined from stable carbon isotope analysis and ^{14}C dating of their bones. *Radiocarbon*, 41(2):157–168, 1999.

[8] O. E. Craig, L. Bondioli, L. Fattore, T. Higham, and R. Hedges. Evaluating marine diets through radiocarbon dating and stable isotope analysis of victims

of the AD79 eruption of vesuvius. *American Journal of Physical Anthropology*, 152(3):345–352, 2013.

[9] R. Carlson, P. Szpak, and M. Richards. The Pender Canal Site and the Beginnings of the Northwest Coast Cultural System. *Canadian Journal of Archaeology*, 41(1):1–29, 2017.

[10] B. S. Chisholm. *Reconstruction of prehistoric diet in British Columbia using stable-carbon isotopic analysis*. Phd, Simon Fraser University, 1986.

[11] P. G. Butler, J. D. Scourse, C. A. Richardson, A. D. Wanamaker, C. L. Bryant, and J. D. Bennell. Continuous marine radiocarbon reservoir calibration and the ^{13}C Suess effect in the Irish Sea: Results from the first multi-centennial shell-based marine master chronology. *Earth and Planetary Science Letters*, 279(3-4):230–241, 2009.

[12] R. McNeely, A. S. Dyke, and J. R. Southon. Canadian marine reservoir ages, preliminary data assessment, Open File 5049:3. *Geological Survey Canada*, 2006.

[13] A. Martindale, G. T. Cook, I. Mckechnie, K. Edinborough, I. Hutchinson, M. Eldridge, K. Supernant, and K. M. Ames. Estimating marine reservoir effects in archaeological chronologies: Comparing Δr calculations in Prince Rupert harbour, British Columbia, Canada. *American Antiquity*, 83(4), 2018.

[14] P. J. Reimer. 14 Chrono Marine Reservoir Correction Database. `http://calib.org/marine/`, 2020.

[15] Jason Nesbitt. El Niño and second-millennium BC monument building at Huaca Cortada (Moche Valley, Peru). *Antiquity*, 90(351):638–653, 2016.